



UNIVERSIDAD DE INVESTIGACIÓN DE TECNOLOGÍA EXPERIMENTAL YACHAY

Escuela de Ciencias Biológicas e Ingeniería

TÍTULO: Human Gait Analysis in Biometric Identification Profiles Using Artificial Intelligence

Trabajo de integración curricular presentado como requisito para la
obtención del título de Ingeniero Biomédico

Autor:

Angel Isaac Arias Serrano

Tutor:

PhD. Fernando Villalba

Co-Tutor:

PhD. Diego Almeida

Urcuquí, Julio 2023

AUTORÍA

Yo, **ARIAS SERRANO ANGEL ISAAC**, con cédula de identidad 131175132-3, declaro que las ideas, juicios, valoraciones, interpretaciones, consultas bibliográficas, definiciones y conceptualizaciones expuestas en el presente trabajo; así como, los procedimientos y herramientas utilizadas en la investigación, son de absoluta responsabilidad de el/la autora (a) del trabajo de integración curricular. Así mismo, me acojo a los reglamentos internos de la Universidad de Investigación de Tecnología Experimental Yachay.

Urcuquí, Julio 2023.

Angel Isaac Arias Serrano

CI:131175132-3

AUTORIZACIÓN DE PUBLICACIÓN

Yo, **ARIAS SERRANO ANGEL ISAAC**, con cédula de identidad 131175132-3, cedo a la Universidad de Investigación de Tecnología Experimental Yachay, los derechos de publicación de la presente obra, sin que deba haber un reconocimiento económico por este concepto. Declaro además que el texto del presente trabajo de titulación no podrá ser cedido a ninguna empresa editorial para su publicación u otros fines, sin contar previamente con la autorización escrita de la Universidad.

Asimismo, autorizo a la Universidad que realice la digitalización y publicación de este trabajo de integración curricular en el repositorio virtual, de conformidad a lo dispuesto en el Art. 144 de la Ley Orgánica de Educación Superior

Urququí, Julio 2023.

Angel Isaac Arias Serrano

CI:131175132-3

Dedicatoria

A mi madre, por enseñarme que la grandeza está en todos nosotros, sin importar lo humilde de nuestros orígenes y lo ambiciosos de nuestros inquebrantables sueños.

A mi padre, por brindarme sabiduría a través de sus experiencias, dotándome de la visión de que todo es alcanzable mediante el trabajo constante y sin miedo a empezar de cero.

A mi hermano, por ser el hombre más noble que he conocido.

A mi familia, por brindarme su apoyo en las horas más oscuras, cuando siendo apenas un niño mi vida se vio afectada por una enfermedad catastrófica.

Finalmente, a mis amigos y todas aquellas personas con las que compartí un espacio de mi vida, esto va por ustedes.

Agradecimiento

Mis agradecimientos totales a todos y cada uno de los docentes de la Universidad Yachay Tech que ayudaron no solo en mi formación profesional, sino también en mi formación personal como un ser humano con vocación de servicio a los demás.

Así mismo, a todas aquellas personas que conocí en estos años de formación, pues algo de ustedes está conmigo, y algo de mi está con ustedes.

Resumen

La marcha humana es un proceso de locomoción intrínseco y único para cada individuo, que se caracteriza generalmente por el movimiento del sujeto en posición erguida, logrado mediante la compleja coordinación combinada de la interfaz cerebro-nervio-músculo. Por otro lado, el análisis de la marcha humana se ha convertido en una herramienta poderosa para describir los patrones de marcha individuales, y los datos obtenidos se aplican en áreas como la medicina, la biomecánica y la robótica mediante el procesamiento de señales. Sin embargo, el análisis de la marcha humana ha demostrado ser una característica biométrica suave que permite la identificación de personas, ya que la individualidad del patrón de marcha persiste con el tiempo. Por lo tanto, la marcha puede detectarse y medirse a baja resolución y, en consecuencia, puede utilizarse en circunstancias en las que los datos faciales o retinales no son accesibles con suficiente resolución para la identificación.

Este proyecto de investigación propone la creación de perfiles de identificación biométrica a través del análisis de la marcha humana como una alternativa innovadora a los sistemas de seguridad tradicionales (basados en conocimiento y tokens). El análisis de la "Smart Gait" (SG) se realiza mediante el uso de bases de datos abiertas, que contienen videos de personas caminando en condiciones reales y controladas. De esta manera, se lleva a cabo la extracción de características del cuerpo humano, centrándose en el comportamiento del cuerpo en las áreas de interés biomecánico. Las fases de entrenamiento y validación para el sistema de identificación de la marcha se llevan a cabo a través de la Inteligencia Artificial (IA), previa a la agregación de datos y al preprocesamiento de las imágenes de desplazamiento relacionadas con el ciclo de marcha.

Palabras Clave:

Marcha humana, Identificación, Perfil Biométrico, Inteligencia Artificial.

Abstract

The human gait is a process of locomotion intrinsic and unique to each individual. This is generally characterized by the movement of the subject in an upright position, achieved by the complex combined coordination of the brain, nerve and muscle interface. Conversely, the human gait analysis has become a powerful tool for describing individual gait patterns, with the data obtained being applied in areas such as medicine, biomechanics, and robotics through signal processing. However, human gait analysis has evidencing to be a soft biometric feature that able the identification of people since the individuality of the gait pattern persists over time. Therefore, gait can be detected and measured at low resolution, and consequently it can be used in circumstances where face or retinal data is not accessible in high enough resolution for identification.

This research project proposes the creation of biometric identification profiles through the analysis of human walking as an innovative alternative to traditional security systems (knowledge-based and token-based). Smart Gait (SG) analysis is performed through the use of open databases, which contain videos of people walking in real and controlled conditions. In this way, the extraction of characteristics of the human body is carried out, focused on the behaviour of the body in the areas of biomechanical interest. The training and validation phases for the gait identification system are carried out through Artificial Intelligence (AI), prior to data aggregation and pre-processing of the displacement images related to the gait cycle.

Key Words:

Human Gait, Identification, Biometric Profile, Artificial Intelligence.

Contents

CHAPTER I: General Introduction	1
INTRODUCTION	2
1.1 Problem Statement	3
1.2 Justification	4
1.3 Objectives	6
1.3.1 General Objective	6
1.3.2 Specific Objectives	6
CHAPTER II: State-of-the-Art	7
STATE-OF-THE-ART	8
2.1 The Human Gait.....	8
2.1.1 Basis of the Human Gait	8
2.1.2 The Evolution of the Human Gait.....	9
2.1.3 The Human Gait Cycle	11
2.1.4 Parameters and Applications in Gait Analysis.....	14
2.2 The Human Gait Biometrics	17
2.2.1 Basis of Gait Biometrics	17
2.2.2 Former Biometrics Modalities	18
2.2.3 The Gait Signature	21
2.2.4 Gait Biometric Approaches.....	22
2.2.5 Artificial Intelligence Based Algorithms	24
2.3 Databases for Gait Biometrics	27
2.3.1 The Significance of Reliable Gait Database	27
2.3.2 CASIA-B Dataset: A Gold Standard in Gait Biometrics	29
2.4 Feature Extraction for Gait Biometrics	33
2.4.1 Basis of the Feature Extraction	33
2.4.2 The Geometric Moments Method	34
2.4.3 The Euclidean Distances	35
2.4.4 Classifiers for Features Extraction.....	37
2.5 Artificial Neural Networks (ANNs) for Gait Biometrics.....	37
2.5.1 Basis of Artificial Neural Networks.....	37
2.5.2 Architecture of Artificial Neural Networks	38
2.5.3 Training Process of Artificial Neural Networks	39
2.6 MATLAB for Gait Biometrics.....	41
2.6.1 Basis of MATLAB.....	41

2.6.2	Graphical User Interface App Designer	43
CHAPTER III: Materials and Methods		46
MATERIALS AND METHODS		47
3.1	Analysis.....	47
3.1.1	Performance criteria for the Gait Biometric System.....	47
3.1.2	Operational Resources – Software	49
3.1.3	Operational Resources – Hardware Selection.....	49
3.2	Design and Implementation	49
3.2.1	User-Written and Built-in Function for a Gait Biometrics System.....	49
3.2.2	Data Reading.....	50
3.2.3	Feature Extraction.....	52
3.2.4	Storage of the Obtained Data	54
3.2.5	Integration of Functions for Gait Data	55
3.2.6	Artificial Neural Network Classifier Gait Biometrics.....	57
3.2.7	Gait Biometrics Identification.....	61
3.3	Dataset Preparation	62
3.3.1	Dataset Selection.....	62
3.4	Parameter Settings	63
3.4.1	Configurable Parameters.....	63
3.4.2	Hyperparameters Selection	64
3.5	User Interface (UI) Prototype	65
3.5.1	User Interface Implementation – App Designer	65
3.6	Experimental Setup.....	67
3.6.1	Experiment 1: Dataset 1 – Configuration Tag A	67
3.6.2	Experiment 2: Dataset 1 – Configuration Tag B.....	67
3.6.3	Experiment 3: Dataset 2 – Configuration Tag A	68
3.6.4	Experiment 4: Dataset 2 – Configuration Tag B.....	68
3.6.5	Experiment 5: Dataset 3 – Configuration Tag A	68
3.6.6	Experiment 6: Dataset 3 – Configuration Tag B.....	69
3.7	Validation.....	69
3.7.1	Assessment Process.....	69
3.7.2	Metrics Calculation.....	70
CHAPTER IV: Results		76
RESULTS		77
4.1	Results for Experimental Setups	77
4.1.1	Results – Experimental Setup 1	77

4.1.2	Results – Experimental Setup 2	78
4.1.3	Results – Experimental Setup 3	79
4.1.4	Results – Experimental Setup 4	80
4.1.5	Results – Experimental Setup 5	81
4.1.6	Results – Experimental Setup 6	82
4.2	Results for User Interface (UI) Prototype	83
4.2.1	Inserting Individual Biometric Profile – Function	83
4.2.2	Adding Multiple Biometric Profiles – Function	85
4.2.3	Training Model – Function	87
4.2.4	Profile Identification – Function	87
4.3	Biometric Software – Executable (.exe)	89
CHAPTER V: Discussion		92
DISCUSSION		93
5.1	Discussion of Results	93
CHAPTER VI: Conclusions and Future Work		105
CONCLUSIONS AND FUTURE WORKS		106
6.1	Conclusions	106
6.2	Future Works	107
REFERENCES		109
Appendix A		116
Experimental Setup 1 – Confusion Matrices & Metrics Tables		116
Appendix B		122
Experimental Setup 2 – Confusion Matrices & Metrics Tables		122
Appendix C		128
Experimental Setup 3 – Confusion Matrices & Metrics Tables		128
Appendix D		134
Experimental Setup 4 – Confusion Matrices & Metrics Tables		134
Appendix E		140
Experimental Setup 5 – Confusion Matrices & Metrics Tables		140
Appendix F		151
Experimental Setup 6 – Confusion Matrices & Metrics Tables		151

List of Figures

Figure 1. Bipedal Locomotion – Broad Movements and Postural Supports in Human Gait.	9
Figure 2. The Normal Gait Cycle - Stance and Swing Phases in Motion.	11
Figure 3. Stride Length - Measuring the Distance Between Contact Points in Human Gait.	14
Figure 4. Key Parameters in Gait Analysis: Anthropometric, Spatial-Temporal, Kinematic, Kinetic, and Electromyographic Measures.....	15
Figure 5. Diverse Applications of Human Gait Analysis: From Traditional Assessments to Innovative Gait Biometrics.	17
Figure 6. Gait Signature: Comprehensive Extraction and Association for Biometric Identification...	22
Figure 7. Key Components in a Model-Based Gait Recognition System.	23
Figure 8. Key Components in an Appearance-Based Gait Recognition System.	24
Figure 9. Approximate Number of Open-Access Papers Mentioning the Dataset in the Last Five Years, Retrieved from (Code, 2023).	30
Figure 10. Gait Angles at CASIA-B, modified from (Yu et al., 2006).	31
Figure 11. Gait Under Different Status at CASIA-B, modified from (Yu et al., 2006).	31
Figure 12. Gait Labeling Format at CASIA-B.	32
Figure 13. Elemental Image Representation and Storage.	33
Figure 14. Schematic Representation for Centre of Mass Calculation in Gait Silhouette.	35
Figure 15. Schematic of Euclidean Distance Calculation in Gait Silhouette Pixels.	36
Figure 16. Elemental Exemplification for the Architecture of Artificial Neural Network.	39
Figure 17. General Training Structure of an Artificial Neural Network.	40
Figure 18. Schematic Overview of Key MATLAB Features.....	42
Figure 19. General Key Components Involved for User Interface (UI) at App Designer.	44
Figure 20. Key Components in the Material and Methods Framework.	47
Figure 21. Flowchart for Multiple Raw Data Loading, 1A.	51
Figure 22. Flowchart for Solo Raw Data Loading, 1B.	51
Figure 23. Flowchart for Feature Extraction Subprocess, 2A.	53
Figure 24. Flowchart for Feature Extraction Complete Process, 2B.	54
Figure 25. Main Database Storage Capacity, 3.	55
Figure 26. Integration of Functions for Multiple Gait Data, 1 UI.	56
Figure 27. Integration of Functions for Solo Gait Data, 2 UI.	57
Figure 28. Artificial Neuronal Network (ANN) Designed for Gait Biometrics, 4.	58
Figure 29. Complete Artificial Neuronal Network (ANN) Classifier Model, 3UI.	60
Figure 30. Gait Biometric Identification Schematic Function, 4UI.	61
Figure 31. Final “BIOMETRIA DE LA MARCHA” User Interface.	66
Figure 32. Schematic Representation for a Primary Confusion Matrix.	72
Figure 33. User Interface Inserting Individual Biometric Profile – Function.	83
Figure 34. Selecting the Individual Folder for Image Sequence Addition.	83

Figure 35. Providing Class Number for New and Existing Biometric Profiles.	84
Figure 36. Final LED Indicators for Function Progress and Database Management.	85
Figure 37. User Interface Adding Multiple Biometric Profiles – Function.	85
Figure 38. Selecting CASIA-B Folder Structure for Multiple Biometric Profiles.	86
Figure 39. Specifying Number of Subjects, Sequences, and Camera Angle.	86
Figure 40. User Interface Training Model – Function.	87
Figure 41. User Interface Profile Identification – Function.	88
Figure 42. Selection of Individual Folder Containing the Image Sequence for Identification.	88
Figure 43. Selection of Individual Folder Containing the Image Sequence for Identification.	89
Figure 44. App Designer Interface and Application Compiler Tool.	90
Figure 45. Application Installer Information.	90
Figure 46. Application Installer Information.	91
Figure 47. Final Software Installer .exe Information.	103
Figure 48. Installation of the Gait Biometric Software.	103
Figure 49. Main User Interface Window for the Gait Biometric Software.	104
Figure 50. User Interface Testing Process for the Gait Biometric Software.	104

List of Tables

Table 1. Evolution of Human Gait with Age.	10
Table 2. Biometric Identifiers: A Visual Overview.	19
Table 3. Principal Gait Biometrics Systems Reported in Literature.	25
Table 4 Principal Gait Biometrics Databases Reported in Literature.	28
Table 5. Fixed Hyperparameters for ANN Training.	64
Table 6. Variable Hyperparameter for ANN Training.	64
Table 7. Key Variables for ANN Classifier Training in Experiment 1 with Configuration Tag A and Dataset 1.	67
Table 8. Key Variables for ANN Classifier Training in Experiment 2 with Configuration Tag B and Dataset 1.	67
Table 9. Key Variables for ANN Classifier Training in Experiment 3 with Configuration Tag A and Dataset 2.	68
Table 10. Key Variables for ANN Classifier Training in Experiment 4 with Configuration Tag B and Dataset 2.	68
Table 11. Key Variables for ANN Classifier Training in Experiment 5 with Configuration Tag A and Dataset 3.	69
Table 12. Key Variables for ANN Classifier Training in Experiment 6 with Configuration Tag B and Dataset 3.	69
Table 13. Linear Regression (R-Value) and Mean Square Error Metrics (MSE) for All Camera View Angle, Dataset 1 – Configuration Tag A.	77
Table 14. Total Accuracies Summarised for All Camera View Angle, Dataset 1 – Configuration Tag A.	77
Table 15. Linear Regression (R-Value) and Mean Square Error Metrics (MSE) for All Camera View Angle, Dataset 1 – Configuration Tag B.	78
Table 16. Total Accuracy Summarised for All Camera View Angle, Dataset 1 – Configuration Tag B.	78
Table 17. Linear Regression (R-Value) and Mean Square Error Metrics (MSE) for All Camera View Angle, Dataset 2 – Configuration Tag A.	79
Table 18. Total Accuracy Summarised for All Camera View Angle, Dataset 2 – Configuration Tag A.	79
Table 19. Linear Regression (R-Value) and Mean Square Error Metrics (MSE) for All Camera View Angle, Dataset 2 – Configuration Tag B.	80
Table 20. Total Accuracy Summarised for All Camera View Angle, Dataset 2 – Configuration Tag B.	80
Table 21. Linear Regression (R-Value) and Mean Square Error Metrics (MSE) for All Camera View Angle, Dataset 3 – Configuration Tag A.	81
Table 22. Total Accuracy Summarised for All Camera View Angle, Dataset 3 – Configuration Tag A.	81
Table 23. Linear Regression (R-Value) and Mean Square Error Metrics (MSE) for All Camera View Angle, Dataset 3 – Configuration Tag B.	82

Table 24. Total Accuracy Summarised for All Camera View Angle, Dataset 3 – Configuration Tag B.	82
Table 25. Total Accuracies for CASIA-B at 24-subjects Identification.....	99

CHAPTER I: General Introduction

INTRODUCTION

Human gait represents an intrinsic and distinctive locomotion process for each individual (Horst et al., 2017; Huang et al., 2021). Throughout the years, it has been generally characterized as a cyclical movement that takes place when a person moves in an upright position while standing (Alharthi et al., 2019). Gait unfolds in phases defined by specific movements of various body regions, resulting from a complex coordination among the brain, nerve, and muscular interfaces (Huang et al., 2021). Owing to its functional nature, gait can be measured, categorized, and described, leading to what is known in biomechanics as gait analysis (Alharthi et al., 2019; Huang et al., 2021; Khera & Kumar, 2020). This human gait analysis can be applied in fields such as disease detection, sports performance evaluation, prosthetic design, rehabilitation, biometrics, among others (Cicirelli et al., 2022; Klöpfer-Krämer et al., 2020; Rathor et al., 2020).

Then, biometrics can effectively utilize human gait analysis as a soft biometric feature for identification purposes, owing to its distinctive and hard-to-imitate characteristics (Alharthi et al., 2019; Horst et al., 2017). In security applications, gait analysis has demonstrated success in recognizing individuals from a distance, typically captured via closed circuit television (CCTV) cameras, without necessitating active cooperation from the subject (Battistone & Petrosino, 2019; Yan et al., 2016). Similarly, ground reaction force also plays a significant role in identifying individuals based on their footstep patterns and walking behavior (Klöpfer-Krämer et al., 2020). Additionally, gait recognition has a wide range of applications, including person identification and authentication, gender recognition, age estimation, occupancy detection, crowd density estimation, and video surveillance monitoring (Harris et al., 2022).

Additionally, gait recognition is an innovative technology that increases security and reliability in recognition tasks, due to the operational principle of the biometric method (Alharthi et al., 2019; Cicirelli et al., 2022; Harris et al., 2022; Horst et al., 2017). Thus, a system implementing this technology offers protection to users before accessing information. Currently, numerous computational biometric solutions have been presented to refine the identification process and address potential vulnerabilities (Harris et al., 2022). Utilizing this knowledge, it is feasible to create a gait recognition system employing artificial intelligence, specifically through deep neural network algorithms (Wu et al., 2017). In this way, a new smart gait (SG) identification system based on gait biometrics can be developed, providing accessibility with low resources as a supporting tool to be used with existing identification systems.

1.1 Problem Statement

Unauthorized access to sensitive information represents a security risk for users and services, affecting aspects such as data integrity, privacy, and digital signatures. Once identification is compromised, the damage produced to the user or service is proportional to the level of information that was accessed. Despite the effectiveness of traditional biometrics, their security systems have demonstrated vulnerabilities. In contrast, human gait cannot be easily imitated or falsified. Nowadays, literature presents applicable approaches for gait biometrics and identification algorithms based on deep learning. Nevertheless, most prevailing works presents complex deep neural networks lacking accessibility for users without specialized programming knowledge, limiting the growth and development of these technologies. Moreover, current works are focused on classification tasks and not on providing additional tools that make it possible to generate a reusable biometric profile once the recognition algorithms is executed. This thesis project aims to address this issue by

creating a straightforward artificial neural network for identifying individuals through gait analysis, incorporating a user interface (UI) and generating biometric profiles to facilitate its use.

1.2 Justification

The identification of individuals through human gait analysis is an innovative approach in the field of identification technologies (Chao et al., 2019; Chen et al., 2018; Fan et al., 2020; Y. He et al., 2019; Hernandez-de-Menendez et al., 2021; Kukreja et al., 2021; Parashar et al., 2023; Sayed, 2018; Sokolova & Konushin, 2019; Yan et al., 2016; Y. Zhang et al., 2019). The advantages of this method have been clearly highlighted in the literature, surpassing other types of biometrics in controlled scenarios (Alharthi et al., 2019; Harris et al., 2022). Moreover, the future potential of gait biometrics has underscored the need for further research in this area by experts and enthusiasts of this technology (Harris et al., 2022; Khera & Kumar, 2020; Klöpfer-Krämer et al., 2020; Kukreja et al., 2021).

However, gaps for its proper and widespread implementation exist in most cases. Initially, the correct execution of algorithms focused on identification through gait requires prior knowledge in programming and artificial intelligence (Cao et al., 2018; Chao et al., 2019; Chen et al., 2018; Costilla-Reyes et al., 2021; Fan et al., 2020; Harris et al., 2022; Y. He et al., 2019; Luo et al., 2020; Martinho-Corbishley et al., 2019; Sokolova & Konushin, 2019; Vandersmissen et al., 2018; Zou et al., 2018). Thus, the techniques employed for extremely precise gait recognition primarily rely on Convolutional Neural Networks (CNN) given the investment in high computer resources (Kukreja et al., 2021; Song et al., 2019; Takemura et al., 2018; Vandersmissen et al., 2018; Wu et al., 2017; Y. Zhang et al., 2019).

This complicates the growth, replicability, and repeatability of these studies for non-specialized users.

Beyond that, the execution of many of these *state-of-the-art* studies not only requires advanced prior knowledge but also significant computational resources, such as the use of Graphics Processing Units (GPUs) for their operation (Cao et al., 2018; Chao et al., 2019; Costilla-Reyes et al., 2021; Fan et al., 2020; Y. He et al., 2019; Liu et al., 2018; Parashar et al., 2023; Sokolova & Konushin, 2019; Song et al., 2019; Y. Zhang et al., 2020).

In particular, although many studies have focused on improving gait biometric methods by making them increasingly complex, they do not provide a simple and reusable system, thereby neglecting to make them available to a broader audience (Harris et al., 2022; Kukreja et al., 2021; Parashar et al., 2023). Several articles have emphasized the need to make technology accessible and easy to understand for the public by including a user interface (UI) (Amershi et al., 2019; S. He & Li, 2020; Ratcliffe & Puthusserypady, 2020; Silistre et al., 2020). Furthermore, current research focuses solely on classifying individuals rather than creating a biometric identification profile that allows, in addition to labeling, the assignment of new gait-related information when desired (Harris et al., 2022). According to (Harris et al., 2022), studies focusing on gait biometrics principally present only the proposed model along with the utilized databases and the achieved performance.

Therefore, it would be ideal to obtain a software that enables the identification of individuals through gait biometrics in a practical manner. In other words, not only propose deep learning algorithms for gait biometrics identification but also a gait biometric identification system that allows to identify individuals through generated profiles with UI. This approach aims to enhance the accessibility of these technologies to a broader audience,

thereby fostering an environment that facilitates increased research opportunities in gait biometrics.

1.3 Objectives

1.3.1 General Objective

To implement a neural network for classifying features extracted from the gait cycle while maintaining low complexity for limited-computing resources. Then, provide a user interface that allows non-specialized users to interact with the functionalities of the identification system managing the information as biometric profiles.

1.3.2 Specific Objectives

To develop an elemental artificial neural network for individual identification through human gait analysis by formerly applying fundamental computer vision techniques for feature extraction.

To propose an accessible user interface that enables non-expert users to engage with the identification capabilities of the gait biometric system, while concurrently managing the relevant data as biometric profiles.

To acquire a validated gait cycle image database, adhered to clear protocols and operably accessible. Besides, prioritize a database that have previously demonstrated validity in gait biometric studies in order to ensure a model grounded in the existing literature.

To prepare several experiments that compare the final model with each other, making variations in the hyper parameters of the proposed artificial neural network architecture to cover a varied range of different models for prediction.

CHAPTER II: State-of-the-Art

STATE-OF-THE-ART

This chapter addresses the concepts necessary to understand the theoretical components of this thesis project. Thus, concepts such as human gait, biometrics, and database repositories are defined, highlighting principles, evolution over the years based on authors and areas of study as needed. Subsequently, more specific concepts such as feature extraction techniques and artificial neural networks are discussed, emphasizing geometric moment methods, Euclidean distances, artificial neural networks, learning algorithms, and hyperparameters. Finally, the primary programming environment and user interface tools are presented. Definitions are provided in a descriptive manner and with a systematic analysis. In this way, studies are described as a comparative assessment between authors along with a rigorous analysis to reduce biases in the *state-of-the-art*. For the proper development of this work, specialized academic search engines such as Google Scholar, PubMed, and Scopus were used. The documents were selected based on their relevance and contribution to the elaboration and understanding of this thesis project.

2.1 The Human Gait

2.1.1 Basis of the Human Gait

Human gait can be described as a locomotion process that enables an individual to move in a bipedal position (Horst et al., 2017; Huang et al., 2021; Stenum et al., 2021). This process involves alternating rhythmic movements of the limbs and trunk, with both bipedal and monopodial support, generating forward displacement relative to a center of gravity (Huang et al., 2021). At the neurological level, gait is the outcome of a coordination of environmental signals received by the cerebral cortex and the limbic system of the subject, which in turn execute voluntary and corrective motor movements (Cicirelli et al., 2022;

Isvoranu et al., 2021; Rayner et al., 2020). Bipedal locomotion, along with its typical stance phases and supports, is depicted in Figure 1.

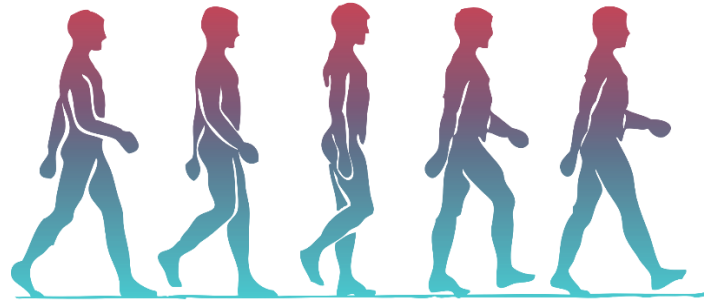


Figure 1. Bipedal Locomotion – Broad Movements and Postural Supports in Human Gait.

2.1.2 The Evolution of the Human Gait

Two approaches have been proposed concerning the principles of gait (Frigon et al., 2022; Kabbaligere & Layne, 2019; Kuiper et al., 2019; Russo et al., 2021; Thiele et al., 2021; S. Xu & Mok, 2022). In studies examining human gait as an automatic process, several authors have concluded that it is an innate trait of human beings. Its evolution over time suggests that it is acquired through imitation and learning via a trial-and-error system in the individual (Frigon et al., 2022; Kabbaligere & Layne, 2019; Russo et al., 2021). Another academic approach posits that walking, rather than being the development of a reflex, is the result of a learned process throughout the growth of an individual (Kuiper et al., 2019; Thiele et al., 2021; S. Xu & Mok, 2022).

Irrespective of the underlying principle, literature on gait analysis and artificial intelligence (AI) demonstrates that each individual displays distinct characteristics in their gait, which is ultimately influenced by factors such as their environment, limb dimensions, or body volume (Gupta, 2021; Harris et al., 2022; Horst et al., 2017, 2019; Huang et al., 2021; Sayed, 2018).

Moreover, human gait serves as a survival tool (Senut et al., 2018). For infants, its impact is evident in psychomotor development, granting autonomy to move through space, expand their field of vision, and grasp and manipulate objects that were previously inaccessible (Badihian et al., 2017; Thiele et al., 2021).

However, the development of human gait is delayed compared to other quadrupeds, which can acquire this ability within days or weeks (Albeshar et al., 2019; Frigon, 2017). Instead, this process occurs over various developmental stages in babies, such as holding the head up (6 weeks), maintaining a bipedal position (4-5 months), and independent gait (>1 year) (Malloggi et al., 2021; Mani et al., 2021).

Therefore, gait evolves with the age of the individual, as demonstrated by the automatic gait reflexes present in babies when they are held by the armpits and placed in an upright position while their feet touch the ground (Rose & Arellano, 2021). From this point, the automatic gait reflex develops and transitions into the distinct normal adult gait cycle are summarized in Table 1.

Table 1. Evolution of Human Gait with Age.

<i>Reference</i>	<i>Stage</i>	<i>Development</i>
(Albeshar et al., 2019; S. Xu & Mok, 2022)	2 mo	Automatic Gait
(Kuiper et al., 2019; Thiele et al., 2021)	7 mo	Tracking
(Thiele et al., 2021)	8 mo	Upright Position with Support
(Thiele et al., 2021; S. Xu & Mok, 2022)	10 mo	Crawling (Abdomen in Close Proximity to the Ground)
(Albeshar et al., 2019; Rose & Arellano, 2021)	11-12 mo	Assisted Gait
(Rose & Arellano, 2021)	13-15 mo	Independent Gait

(Albesher et al., 2019; Malloggi et al., 2021)	5-7 years	Adult-like Gait
---	-----------	-----------------

Legend: Months (mo).

As a result, a person recognition system must be delimited in the age of the users to identify. Although literature in Table 3 suggests that the range is applicable from 7-years-old to more advanced ages (Horst et al., 2017), the decision to restricted the user-age could be ideal to establish a more reliable age range for correct user recognition. In this way, a biometric recognition task for subjects between 18-years-old to 60-years-old is able to carry a correct performance in different scenarios.

2.1.3 The Human Gait Cycle

The normal gait cycle begins with the contact of the foot on the ground, and concludes upon the subsequent contact of the same foot with the ground (Bach et al., 2021; Cicirelli et al., 2022; Horst et al., 2019; Malloggi et al., 2021; Rathor et al., 2020). This cycle is characterized by two primary phases: the stance phase and the swing phase (Alharthi et al., 2019; Huang et al., 2021; Jung & Yeop, 2016; Russo et al., 2021). A leg is deemed to be in the stance phase as long as it remains in contact with the ground. Conversely, the same leg is considered to be in the swing phase when it is not in contact with the ground (Figure 2).

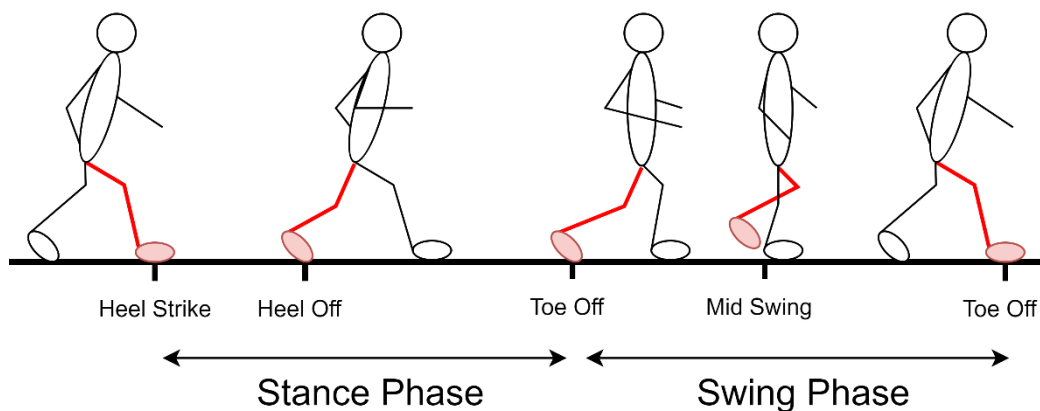


Figure 2. The Normal Gait Cycle - Stance and Swing Phases in Motion.

As a result, the time spent completing a gait cycle at a normal speed is unique to each individual. However, this can be measured in a relative manner, resulting in a stance phase comprising 60% of the cycle and a swing phase comprising 40% of the cycle (Alharthi et al., 2019; Huang et al., 2021; Russo et al., 2021). During double support, the front of one foot and the back of the other foot touch the ground for a brief period. The significance of this distinction lies in the fact that the absence of double support in the locomotion of an individual differentiates running from walking (Huang et al., 2021). The classical model divides the gait phases into five events for the stance phase and three events for the swing phase, concluding in eight events:

- Event 1 - Initial Contact (IC): This occurs when the heel of a reference foot touches the ground. From this point, the loading response phase begins, encompassing 0% to 2% of the total gait cycle.
- Event 2 – Load Response (LR): This begins when the reference foot contacts the ground and lasts until the other foot is lifted for its respective swing. During this period, the individual's weight is entirely transferred to the extremity of the reference foot, encompassing 2% to 10% of the total gait cycle.
- Event 3 – Mid-Stance (MS): This occurs from the contralateral swing of the toe and ends once the center of mass is repositioned on the reference foot. The tibia of the swinging limb (contralateral) is vertical to the ground, encompassing 10% to 30% of the total gait cycle.
- Event 4 – Terminal Stance (TS): This is characterized by the extension of the limb from the hip on the reference foot, ending just before the pre-swing when the

contralateral foot touches the ground in parallel. This phase encompasses 30% to 50% of the total gait cycle.

- Event 5 – Pre-Swing (PS): This begins when the contralateral toe is in the initial contact phase, while the reference foot is about to leave the ground. It encompasses 50% to 60% of the total gait cycle.
- Event 6 – Initial Swing (IS): At this point, the swing stage commences. The extremity corresponding to the reference foot leaves the ground as the knee flexes, encompassing 60% to 73% of the total gait cycle.
- Event 7 – Mid-Swing (MS): The swing of the limb is extended and displaced, reaching maximum knee flexion. This phase encompasses 73% to 87% of the total gait cycle.
- Event 8 – Terminal Swing (TS): In this phase, the movement of the limb concludes, causing the tibia to form a perpendicular angle to the ground, and the reference foot is positioned to touch the ground. This phase encompasses 87% to 100% of the total gait cycle before another complete cycle begins.

Similarly, stride length is another component of human gait, defined as the distance between the contact points created by one-foot relative to the distance of the other foot (Bach et al., 2021; Malloggi et al., 2021; Rathor et al., 2020). The full stride length is considered the distance traversed in the plane by a specific foot from one point to another, that is, the progression between the contact points of the same foot (Figure 3).

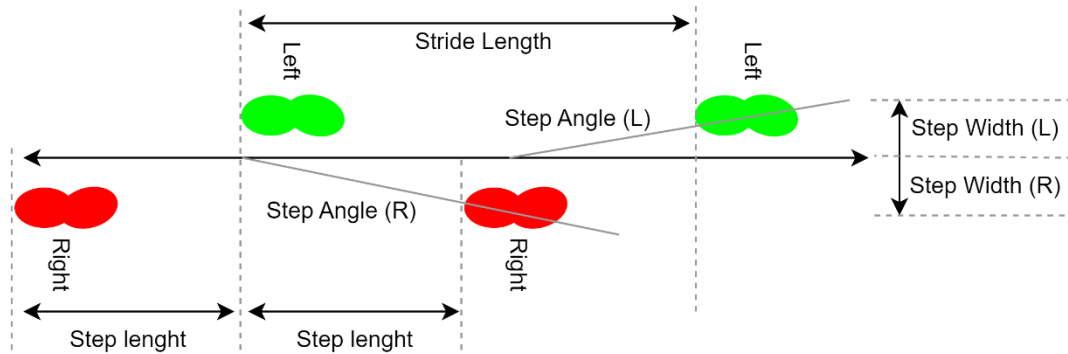


Figure 3. Stride Length - Measuring the Distance Between Contact Points in Human Gait.

2.1.4 Parameters and Applications in Gait Analysis

As a cyclical biomechanical process, gait can be measured and recorded, enabling an analysis that describes its forms and performance as a gait analysis (Alharthi et al., 2019; Huang et al., 2021; Jung & Yeop, 2016; Kabbaligere & Layne, 2019). Health professionals such as physiotherapists and orthopedists utilize gait analysis as a tool to monitor the variables that compose it (Horst et al., 2019; Jung & Yeop, 2016; Khera & Kumar, 2020; Malloggi et al., 2021).

The literature indicates that gait analysis involves the measurement of anthropometric (Bach et al., 2021; Harris et al., 2022; Horst et al., 2017; Klöpfer-Krämer et al., 2020; Malloggi et al., 2021; Mani et al., 2021), spatial-temporal (Battistone & Petrosino, 2019; Filipi Gonçalves Dos Santos et al., 2021; Gupta, 2021; Kabbaligere & Layne, 2019; Rayner et al., 2020; Sayed, 2018), kinematic (Harris et al., 2022; Kabbaligere & Layne, 2019; Klöpfer-Krämer et al., 2020; Rathor et al., 2020; Rayner et al., 2020; Russo et al., 2021; Stenum et al., 2021; S. Xu & Mok, 2022), kinetic (Bach et al., 2021; Frigon et al., 2022; Gupta, 2021; Harris et al., 2022; Klöpfer-Krämer et al., 2020; Malloggi et al., 2021; Russo et al., 2021), and electromyographic parameters (Alharthi et al., 2019; Frigon et al., 2022; Harris et al., 2022; Huang et al., 2021; Kabbaligere & Layne, 2019; Khera & Kumar, 2020; Malloggi et al., 2021; Rayner et al., 2020; Russo et al., 2021).

Once these parameters are recorded, it becomes possible to draw conclusions regarding the age, size, weight, or vitality of an individual (Harris et al., 2022). Furthermore, the spatial-temporal parameter is highly applicable to gait biometrics tasks because it stores elemental variables of motion (Fan et al., 2020; Liu et al., 2018; Sayed, 2018; Y. Zhang et al., 2020), making it applicable to the several gait scenarios presented in literature. Figure 4 summarizes the essential parameters used in the literature for gait analysis.

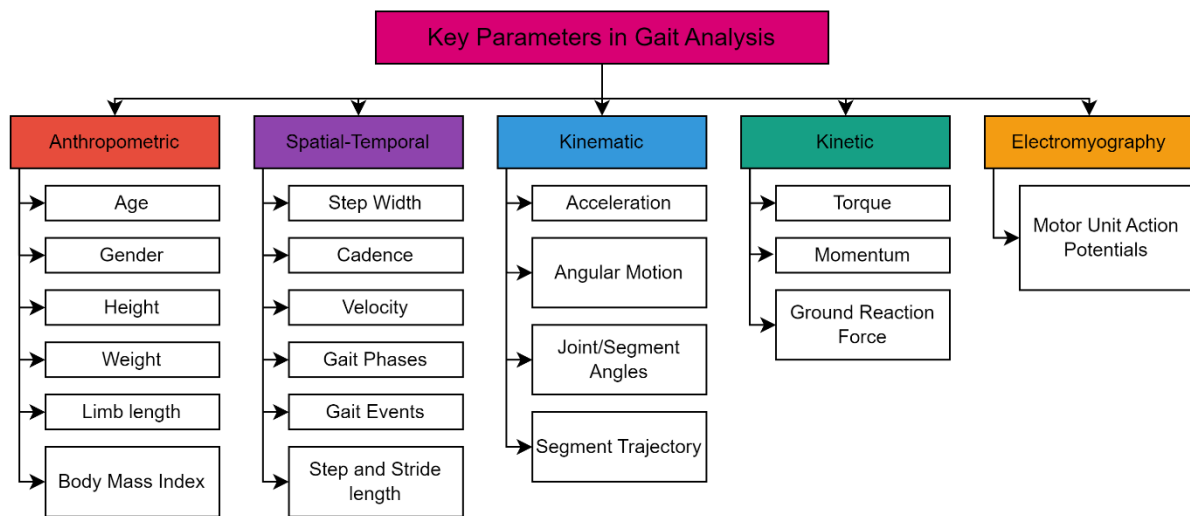


Figure 4. Key Parameters in Gait Analysis: Anthropometric, Spatial-Temporal, Kinematic, Kinetic, and Electromyographic Measures

Consequently, the analysis of the human gait through the description of its phases done by the different parameters and approaches for its registration has allowed the generation of applications related to the process and its performance (Harris et al., 2022; Marin et al., 2020; Marín et al., 2019, 2020; Prakash et al., 2018; Stenum et al., 2021). Hence, traditional applications related to analysis, artificial gait, control, and the now innovative gait biometrics have been described.

Thus, applications in the area of analysis related to the identification of standard gait, clinical gait assessment, geriatric care, and sport performance have been achieved (Alharthi et al., 2019; Cicirelli et al., 2022; Harris et al., 2022; Isvoranu et al., 2021; Kabbaligere & Layne, 2019; Khera & Kumar, 2020; Mani et al., 2021; Rayner et al., 2020).

Similarly, in applications related to artificial gait, advances have been made in rehabilitation and humanoid robots (Cicirelli et al., 2022; Frigon, 2017; Harris et al., 2022; Kabbaligere & Layne, 2019; Khera & Kumar, 2020; Rathor et al., 2020; Senut et al., 2018; S. Xu & Mok, 2022).

Equally, in applications related to control, areas such as animation and simulation, computer interfaces, and industrial applications have been developed (Alharthi et al., 2019; Filipi Gonçalves Dos Santos et al., 2021; Harris et al., 2022; S. Xu & Mok, 2022).

Lastly, the applications of gait biometrics, being the area of study relevant to this thesis project, have recently presented innovative advancements related to the monitoring of cognitive activity and surveillance for population groups and citizens (Albesher et al., 2019; Alharthi et al., 2019; Badihian et al., 2017; Battistone & Petrosino, 2019; Cicirelli et al., 2022; Filipi Gonçalves Dos Santos et al., 2021; Gupta, 2021; Harris et al., 2022; Horst et al., 2017; Kabbaligere & Layne, 2019; Khera & Kumar, 2020; Mani et al., 2021; Parashar et al., 2023; Senut et al., 2018; Thiele et al., 2021; Wu et al., 2017; C. Xu et al., 2019; Yan et al., 2016). Figure 5 recaps the essential applications reported in literature.

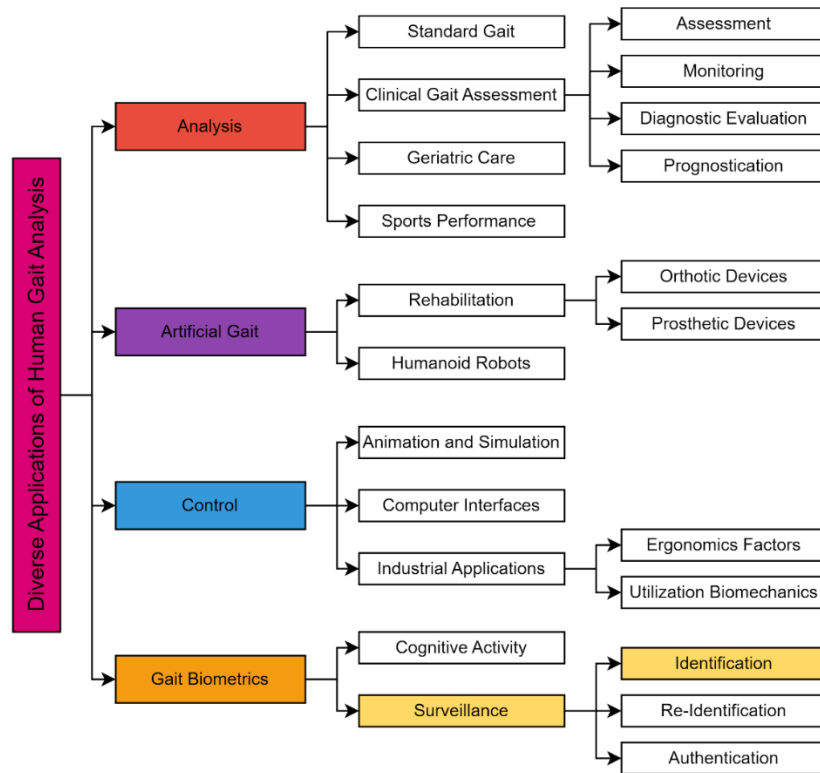


Figure 5. Diverse Applications of Human Gait Analysis: From Traditional Assessments to Innovative Gait Biometrics.

Among gait biometrics, there are identification, re-identification, and authentication of individuals through their gait (Alharthi et al., 2019; Amershi et al., 2019; Battistone & Petrosino, 2019; Cicirelli et al., 2022; Filipi Gonçalves Dos Santos et al., 2021; Gupta, 2021; Harris et al., 2022; Horst et al., 2017; Kabbaligere & Layne, 2019; Khera & Kumar, 2020; Parashar et al., 2023; Wu et al., 2017; C. Xu et al., 2019; Yan et al., 2016). However, the subsequent reviewed literature on gait biometrics is specially focus on the tasks of person identification.

2.2 The Human Gait Biometrics

2.2.1 Basis of Gait Biometrics

Gait biometrics is a soft biometric feature, as gait possesses several unique characteristics that enable the identification of individuals based on their movement patterns

during the gait cycle (Battistone & Petrosino, 2019; Filipi Gonçalves Dos Santos et al., 2021; Gupta, 2021; Harris et al., 2022; Khera & Kumar, 2020; Parashar et al., 2023; Wu et al., 2017; C. Xu et al., 2019; Yan et al., 2016). As previously mentioned, this individuality in gait patterns persists over time and across various pathologies, making gait biometric analysis both reliable and enduring (Cicirelli et al., 2022; Horst et al., 2017; Kabbaligere & Layne, 2019). Furthermore, gait biometric data is practical to record, as it is represented by raw data in the form of video sequences that capture and process individuals walking in uncontrolled and long-distance scenarios (Alharthi et al., 2019; Harris et al., 2022). Consequently, the widespread presence of surveillance cameras in various locations, such as streets, stations, airports, shopping malls, office buildings, and even private residences, has facilitated the integration of gait recognition technology as a valuable tool (Stenum et al., 2021).

2.2.2 Former Biometrics Modalities

Gait biometrics is non-intrusive in nature, functioning without the need for subject cooperation, which, in conjunction with its capture by cameras, allows for remote evaluation without requiring the prior consent of the observed subject (Filipi Gonçalves Dos Santos et al., 2021; Harris et al., 2022; Yan et al., 2016). Additionally, gait is considered an advanced behavioural biometric, as it is linked to individual performance, making its biometric features particularly difficult to hide, steal, or fake (Filipi Gonçalves Dos Santos et al., 2021; Harris et al., 2022). In contrast to other non-behavioural physiological biometric modalities, such as DNA, fingerprints, irises, and facial features, which, although not less important, require direct cooperation from the individual (Adamović et al., 2020; B. Mazumdar, 2018; Bours & Ellingsen, 2018; Hernandez-de-Menendez et al., 2021; Ibrahim et al., 2017; Israa, 2015; Khan & Naaz, 2020; Mitchell & Shing, 2018). The main biometric identifiers reported in literature are summarized on Table 2.

Table 2. Biometric Identifiers: A Visual Overview.

<i>Reference</i>	<i>Biometric</i>	<i>Description</i>	<i>Disadvantages</i>	<i>Principle</i>	
(B. Mazumdar, 2018; Israa, 2015)		Retina	Pattern of blood vessels in the retina, located at the back of the eye.	Complexity in obtaining high-quality images of images of finger patterns	Physiological
(Adamović et al., 2020; B. Mazumdar, 2018; Israa, 2015)		Iris	Analysis of the unique pattern present in the irides (colored portion of the eyes).	Inability to reduce false acceptance rates without introducing additional false rejection rates	Physiological
(B. Mazumdar, 2018; Israa, 2015; Mitchell & Shing, 2018)		Fingerprint	Examination of the friction ridge and valley patterns on fingertips.	Unreadable when the skin is damaged or injured	Physiological
(B. Mazumdar, 2018; Ibrahim et al., 2017)		DNA	Assessment of genetic code, which is unique to an individual	Identical twins share the same DNA	Physiological
(B. Mazumdar, 2018; Israa, 2015; Mitchell & Shing, 2018)		Voice	Voice print identification, based on the unique sound, pattern, and rhythm	Scammers will call and ask certain questions, and record the answers given to them by the victim	Behavioral
(B. Mazumdar, 2018; Israa, 2015; Mitchell & Shing, 2018)		Ear	Evaluation of ear symmetry and shape for identification purposes.	Low circumvention resistance	Physiological
(B. Mazumdar, 2018; Bours & Ellingsen, 2018; Israa, 2015)		Keystroke dynamics	Analysis of dwell time (keystroke duration) and flight time (time between keystrokes)	Hand or arm injuries may impact the rhythm of keystroke dynamics.	Behavioral

(B. Mazumdar, 2018; Israa, 2015; Mitchell & Shing, 2018)		Signature	Examination of writing characteristics, including pen pressure, duration, spatial coordinates, azimuth, inclination, and direction.	Fails to differentiate between actual signature and skilled forged one	Behavioral
(B. Mazumdar, 2018; Israa, 2015; Mitchell & Shing, 2018)		Hand/finger geometry	Analysis of the shape and dimensions of hands and fingers	Requires a special hardware device for scanning the hand geometry	Physiological
(Hernandez-de-Menendez et al., 2021; Khan & Naaz, 2020)		Odor	Identification based on the unique and distinguishable body odor pattern	Body odor can vary due to illness, food, mood swings, etc.	Physiological
(B. Mazumdar, 2018; Ibrahim et al., 2017; Israa, 2015)		Facial recognition	Assessment of facial geometry, focusing on distinguishing features	Facial aging may affect identification accuracy.	Physiological
(B. Mazumdar, 2018; Harris et al., 2022; Israa, 2015; Klöpfer-Krämer et al., 2020)		Gait	Gait analysis, focused on the way a person walks	Post-injury changes may affect identification accuracy	Behavioral

Legend: Deoxyribonucleic acid (DNA).

Therefore, gait biometrics in their smart gait (SG) identification systems encounter challenges stemming from variable parameters that impact the size and quality of video and image inputs, including camera viewpoint, lighting, occlusion, image resolution, and the

attire and carrying conditions of the subjects (Gupta, 2021; Harris et al., 2022; Khera & Kumar, 2020; Malloggi et al., 2021). Consequently, numerous research papers have sought to address one or more of these difficulties by enhancing previously studied and implemented algorithms (Gupta, 2021; Harris et al., 2022; Khera & Kumar, 2020). As a result, gait recognition methods are diverse, with most gait biometrics works reported in literature handling cases in which gait data is extracted from video (Battistone & Petrosino, 2019; Harris et al., 2022; Ibrahim et al., 2017; Khera & Kumar, 2020).

2.2.3 The Gait Signature

One of the several notions behind the methods for gait biometrics is to obtain a trustable discriminatory gait signature (Gupta, 2021; Harris et al., 2022; Sayed, 2018). A gait signature is a distinctive feature vector capable of differentiating individuals, incorporating invariant properties embedded within a person, such as stride length, height/width, gait cycle, and self-occlusion, as well as those related to the imaging system, such as translation, rotation, scale, noise, and occlusion by other objects (Gupta, 2021; Hadjkacem et al., 2020; Zou et al., 2018). In a given SG identification system, from the extracted gait characteristics, a unique gait signature for each person in the corresponding database is derived (Harris et al., 2022; Sayed, 2018). Subsequently, extracted gait signatures from video are compared to the stored gait signatures of known individuals for identification purposes, allowing the opportunity to generate biometric profiles per subject (Figure 6).

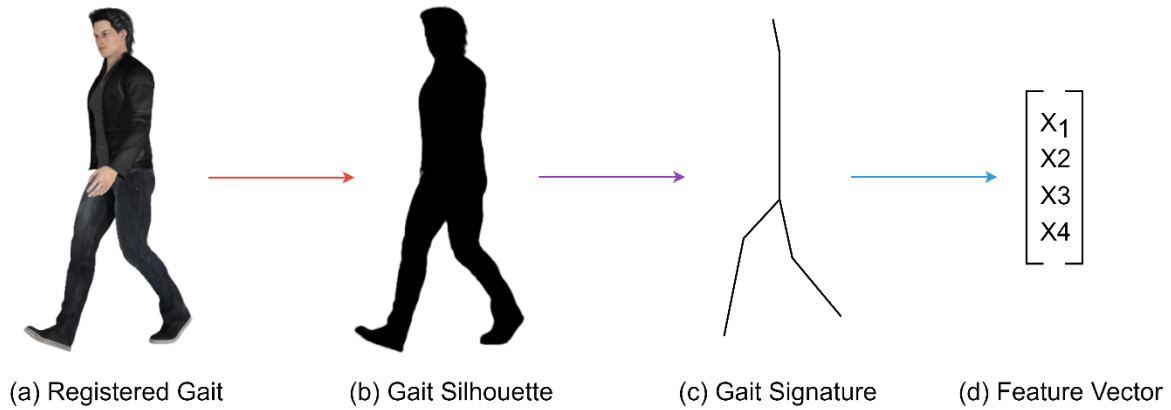


Figure 6. Gait Signature: Comprehensive Extraction and Association for Biometric Identification.

2.2.4 Gait Biometric Approaches

Primarily, gait biometrics methods can be classified based on the approach of gait feature extraction for classification, falling into two broad categories: model-based approaches and appearance-based approaches (Battistone & Petrosino, 2019; Chen et al., 2018; Fan et al., 2020; Filipi Gonçalves Dos Santos et al., 2021; Gupta, 2021; Harris et al., 2022; Khera & Kumar, 2020; Sokolova & Konushin, 2019). These distinct methodologies allow for the efficient extraction and analysis of gait features, providing various lines according to the needs and resources in the field of biometric identification.

In this sense, model-based gait recognition involves identification through underlying mathematical constructs representing discriminatory gait characteristics, whether static or dynamic, characterized by a set of parameters and logical, quantitative relationships between them (Cao et al., 2018; Chen et al., 2018; Luo et al., 2020; Sokolova & Konushin, 2019; Vandersmissen et al., 2018; Zou et al., 2018). These approaches fit 3D body models or intermediate body representations to body limbs to extract key parameters describing gait dynamics (Cao et al., 2018; Vandersmissen et al., 2018). Particularly, model-based approaches align sequences of features with a physical model of the human body and its inherent dynamics, such as a feature extraction process principally guided by biomechanical

analysis for gait-based person identification (Chen et al., 2018; Luo et al., 2020; Sokolova & Konushin, 2019; Zou et al., 2018). The primary advantages of the model-based approach include reliable handling of occlusion (particularly self-occlusion), noise, scale, and rotation (Cao et al., 2018; Sokolova & Konushin, 2019; Zou et al., 2018). Figure 7 summarizes the main elements comprising model-based gait biometrics.

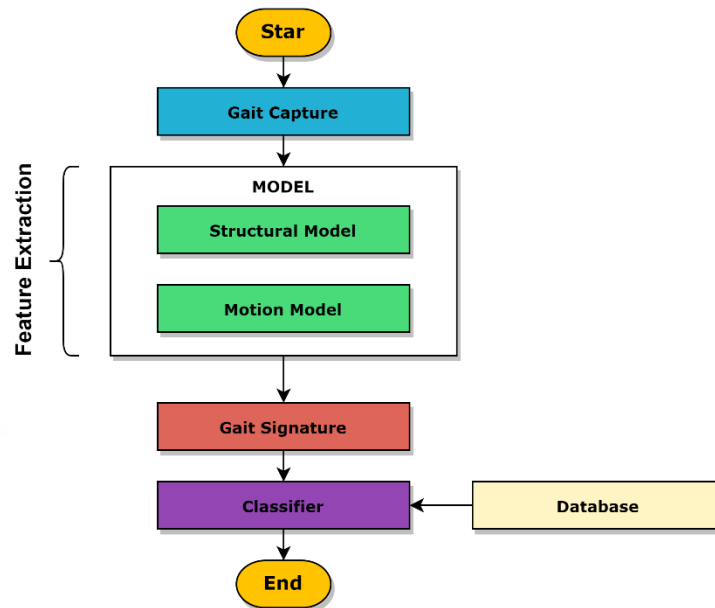


Figure 7. Key Components in a Model-Based Gait Recognition System.

In contrast, appearance-based approaches for gait recognition aim to capture spatiotemporal gait characteristics directly from input sequences without fitting a body model (Chao et al., 2019; Costilla-Reyes et al., 2021; Fan et al., 2020; Y. He et al., 2019; Liu et al., 2018; Martinho-Corbishley et al., 2019; Song et al., 2019; Y. Zhang et al., 2020). These approaches do not require high-resolution subjects, making them more applicable in outdoor surveillance applications where subjects may be at significant distances from the camera (Chao et al., 2019; Fan et al., 2020; Song et al., 2019; Y. Zhang et al., 2020). By extracting a gait signature from the spatial and temporal distribution of features on a tracked subject without needing to fit a body model or locate limbs, appearance-based approaches have proven successful in gait recognition and are suitable for scenarios where gait biometric

features must be extracted from a distance (Costilla-Reyes et al., 2021; Fan et al., 2020; Y. He et al., 2019; Liu et al., 2018; Martinho-Corbishley et al., 2019).

Besides, there are limitations to current gait recognition systems, such as achieving invariance to viewing conditions like viewpoint invariance (Fan et al., 2020; Liu et al., 2018; Vera-Rodriguez et al., 2013; Y. Zhang et al., 2020). However, even the model-based approaches are often affected by changes in appearance (Harris et al., 2022). Then, the appearance-based approach relies on binary sequences of human gait silhouette images allowing a low computational cost (Sayed, 2018). Figure 8 summaries the main elements comprising appearance-based gait biometrics.

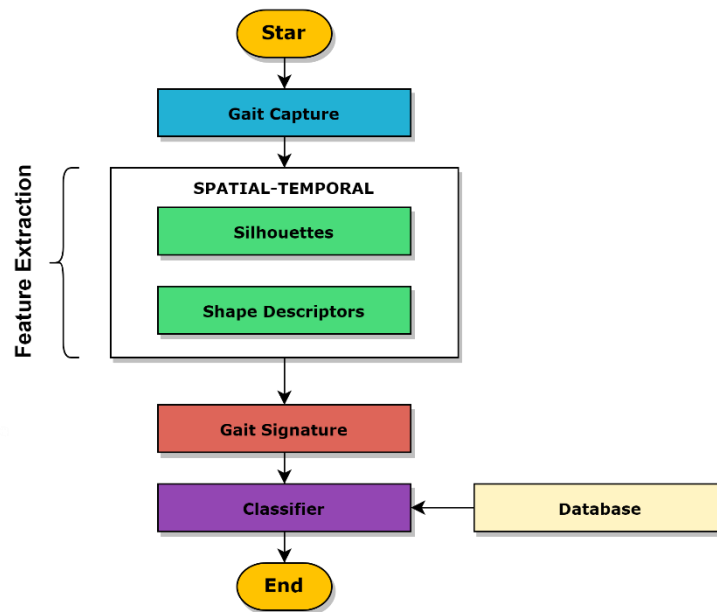


Figure 8. Key Components in an Appearance-Based Gait Recognition System.

2.2.5 Artificial Intelligence Based Algorithms

Artificial intelligence (AI)-based algorithms in deep learning models have emerged as an elegant solution for tackling image, video, and sequential information related to both model-based and appearance-based approaches (Gupta, 2021; Harris et al., 2022). Deep learning models surpass in tasks such as classification, labelling, object detection and recognition,

decision making, machine learning, natural language processing, and computer vision, among others (Gupta, 2021; Harris et al., 2022).

Consequently, deep learning architectures have proven to be powerful tools for gait recognition when employing various techniques. For example, convolutional neural networks (CNN) (Cao et al., 2018; Chao et al., 2019; Chen et al., 2018; Fan et al., 2020; Liu et al., 2018; Martinho-Corbishley et al., 2019; Sayed, 2018; Sokolova & Konushin, 2019; Song et al., 2019; Vandersmissen et al., 2018; Y. Zhang et al., 2020), artificial neural networks (ANN) (Sayed, 2018), recurrent neural networks (RNN) (Fan et al., 2020), auto-encoders (Sokolova & Konushin, 2019), capsule networks (CN), generative adversarial networks (GAN) (Y. He et al., 2019), and deep belief networks (DBN) have all been reported in the literature (Harris et al., 2022). Table 3 summarizes the most relevant gait biometrics research conducted in recent years, with a particular emphasis on the methodologies employed to achieve the recognition assignments.

Table 3. Principal Gait Biometrics Systems Reported in Literature.

<i>Reference</i>	<i>Proposed Method For Person Identification</i>	<i>Hardware</i>	<i>UI</i>
(Fan et al., 2020; Liu et al., 2018)	GaitPart: Extracts frame-level spatial features and local short-range temporal features for each body part, creating unique spatial-temporal representations.	GPU	
(Y. Zhang et al., 2020)	Introduction of angle center loss, a gait-specific loss function, incorporating horizontal partitions of gait templates and a temporal attention model.	GPU	
(Luo et al., 2020)	GRaaS: An RFID-based wireless gait recognition system employing DRL tag selection algorithm and attention-based LSTM model.	N/A	

(Chao et al., 2019, 2022)	GaitSet: Utilizes Set Pooling to aggregate silhouettes into a single set for deep set-based person identification.	GPU	✗
(Y. He et al., 2019; Song et al., 2019)	Multi-task GANs: Learns view-specific gait feature presentations and proposes PEI, a new multi-channel gait template.	GPU	✗
(Costilla-Reyes et al., 2021)	Biometric Footstep Recognition: Combines ResNet and SVM ensemble with floor-only sensor data.	GPU	✗
(Martinho-Corbishley et al., 2019)	Crowd Prototyping: Recognizes age, gender, and ethnicity using ResNet-152 CNN.	N/A	✗
(Sokolova & Konushin, 2019)	Pose-based deep person identification employing WideResNet with OpenPose.	GPU	✗
(Zou et al., 2018)	AutoID: Implements WiFi-Based person identification using C3SL.	N/A	✗
(Cao et al., 2018)	RadarId: Develops a deep CNN architecture based on raw radar micro-Doppler signatures.	GPU	✗
(Vandersmissen et al., 2018)	Indoor person identification utilizing Deep CNN with radar data for privacy-preserving, intruder detection, and identification in the dark.	N/A	✗
(Chen et al., 2018)	A model-based multi-gait recognition method employing the L-CRF model.	N/A	✗

Legend: User Interface (UI), Graphics Processing Unit (GPU), Central Processing Unit (CPU), No Answer (N/A), Gait Recognition as a Service (GRaaS), Radio Frequency Identification (RFID), Deep Reinforcement Learning (DRL), Long Short-term Memory (LSTM), Generative Adversarial Network (GAN), Residual Neural Network (ResNet), Support Vector Machine (SVM), Artificial, Neural Network (ANN), Convex Clustered Concurrent Shapelet Learning (C3SL), Convolutional Neural Network (CNN), Latent Conditional Random Field (L-CRF).

Additionally, Table 4 includes a section dedicated to describing the selected hardware for recognition tasks. It is observed that due to the complexity of the recognition tasks, the use of a GPUs is predominant in conducting new-paradigm-studies (Harris et al., 2022). Furthermore, it is concerning to note in Table 4 that the major studies reported in the literature lack a UI, which allow non-specialized users to utilize these studies (Amershi et al., 2019). Consequently, the replicability and reproducibility of the literature is reduced due to limitations in the requirements of prior knowledge and computer resources before employing these biometric identification studies based on gait.

2.3 Databases for Gait Biometrics

2.3.1 The Significance of Reliable Gait Database

The importance of having a valid and reliable database in the literature for gait biometrics tasks and achieving trustable metrics cannot be misplaced. A well-structured and representative database is crucial for several reasons in the context of scientific research (Harris et al., 2022). First, it ensures that the developed algorithms and methodologies are tested and validated on a wide range of samples, encompassing various gait patterns, demographics, and environmental conditions (Fan et al., 2020; Gupta, 2021; Harris et al., 2022; Liu et al., 2018; Luo et al., 2020). This diversity in data helps enhance the generalizability and robustness of the proposed models, making them applicable in real-world scenarios (Liu et al., 2018; Luo et al., 2020; Vandersmissen et al., 2018; Wu et al., 2017; Zou et al., 2018).

Second, a valid database enables fair comparisons and benchmarking between different gait recognition approaches (Costilla-Reyes et al., 2021; Martinho-Corbishley et al., 2019; Sayed, 2018; Sokolova & Konushin, 2019; Song et al., 2019; Zou et al., 2018). By providing a common ground for evaluation, researchers can objectively assess the

performance of their methods, identify strengths and weaknesses, and foster innovation by building on previous works (Harris et al., 2022).

Furthermore, the availability of a reliable and comprehensive database contributes to the replicability and reproducibility of research findings (Fan et al., 2020; Harris et al., 2022; Y. He et al., 2019). As a fundamental pillar of scientific integrity, reproducibility allows other researchers to confirm the validity of the results and corroborate the claims made in the literature (Harris et al., 2022). This process helps establish trust and confidence in the research community, ultimately driving the field forward.

Lastly, having an general and valid database expedites the development of more efficient and varied gait biometrics systems (Cao et al., 2018; Chao et al., 2019; Gupta, 2021; Y. He et al., 2019; Khera & Kumar, 2020; Luo et al., 2020; Parashar et al., 2023; Sayed, 2018; Wu et al., 2017; Yan et al., 2016; Zou et al., 2018). By continuously working gait recognition models based on the same dataset, researchers can compare performance metrics, leading to enhanced precision, recall, mean square error (MSE) or accuracy analysis of performances (Cao et al., 2018; Chao et al., 2019; Gupta, 2021; Y. He et al., 2019; Khera & Kumar, 2020; Luo et al., 2020; Parashar et al., 2023; Sayed, 2018; Wu et al., 2017; Yan et al., 2016; Zou et al., 2018).

Consecutively, this ensures that gait recognition systems are prepared to meet the growing demands of various applications, such as security, healthcare, and human-computer interaction (Harris et al., 2022). The primary gait biometrics databases based on gait sequences reported in the literature are summarized in Table 4.

Table 4 Principal Gait Biometrics Databases Reported in Literature.

<i>Database</i>	<i>Source</i>	<i>Original Study</i>
<i>Reference</i>	<i>Data/Input</i>	

(Yu et al., 2006)	CASIA-B	A Framework for Evaluating the Effect Of View Angle, Clothing and Carrying Condition on Gait Recognition
(Iwama et al., 2012)	OULP	The OU-ISIR Gait Database Comprising the Large Population Dataset and Performance Evaluation of Gait Recognition
(Takemura et al., 2018)	OU-MVLP	Multi-View Large Population Gait Dataset and its Performance Evaluation for Cross-View Gait Recognition
(Iwama et al., 2012)	OU-ISIR	The OU-ISIR Gait Database Comprising the Large Population Dataset and Performance Evaluation of Gait Recognition
(Vera-Rodriguez et al., 2013)	SfootBD	Comparative Analysis and Fusion of Spatiotemporal Information for Footstep Recognition
(Hofmann et al., 2014)	TUM-GAID	The Tum Gait From Audio, Image and Depth (GAID) Database: Multimodal Recognition of Subjects and Traits
(Sarkar et al., 2005)	USF	The HumanID Gait Challenge Problem: Data Sets, Performance, and Analysis
(Bossard et al., 2013)	PEC	Event recognition in photo collections with a stopwatch HMM
(Barbosa et al., 2012)	IIT PAVIS	Re-Identification With RGB-D Sensors
(Barbosa et al., 2012)	IASLab	Re-Identification With RGB-D Sensors
(Frank et al., 2011)	McGill University Gait Dataset	Activity Recognition With Mobile Phones
(Ngo et al., 2014)	Osaka University Gait Dataset	The Largest Inertial Sensor-Based Gait Database And Performance Evaluation Of Gait-Based Personal Authentication

2.3.2 CASIA-B Dataset: A Gold Standard in Gait Biometrics

In this sense, the CASIA-B dataset is a multi-view gait database created in January 2005 (Yu et al., 2006), this database has been a gold standard in gait biometrics research,

enabling a reliable assessment of the performance of a recognition system, providing a clear visualization of the effectiveness for proposed gait biometric approach (Alharthi et al., 2019; Chen et al., 2018; Filipi Gonçalves Dos Santos et al., 2021; Harris et al., 2022; Sayed, 2018; Sokolova & Konushin, 2019; Y. Zhang et al., 2020). These characteristics make this database the ideal choice for feature extraction and classification tasks, due to its credibility and accessibility previously demonstrated in the literature (Figure 9).

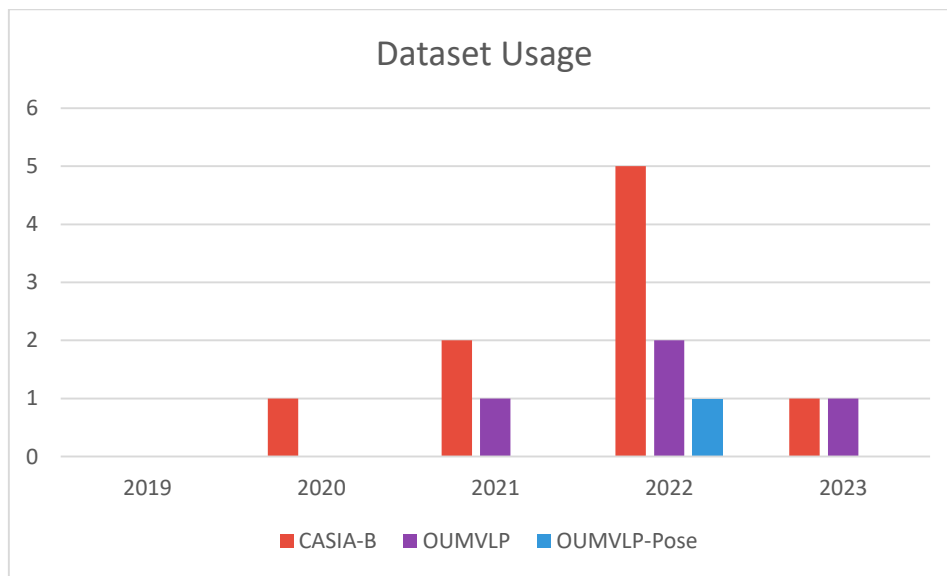


Figure 9. Approximate Number of Open-Access Papers Mentioning the Dataset in the Last Five Years, Retrieved from (Code, 2023).

CASIA-B contains 124 subjects and there are 110 sequences per subject, labeled from 001 to 124. For instance, the gait data was captured from 11 different views. The 11 views are labeled from 0° to 180° , with increments of 18° (see Figure 10). The grayscale human silhouettes with semantic extraction from the videos are able for free download. In addition, the original video files are provided if required prior request.

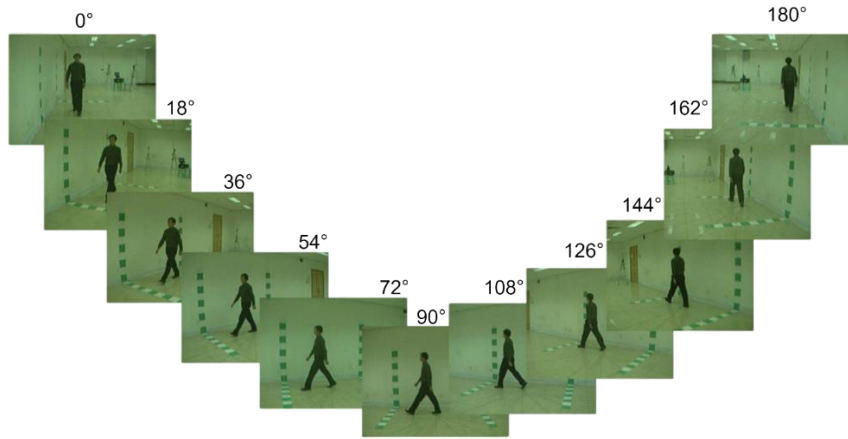


Figure 10. Gait Angles at CASIA-B, modified from (Yu et al., 2006).

Additionally, the database include three gait status for the assessment per subject: normal gait (nm) status with 6 sequences, coat (cl) status with 2 sequences, and bag status (bg) with 2 sequences (Yu et al., 2006) (see Figure 11).



Figure 11. Gait Under Different Status at CASIA-B, modified from (Yu et al., 2006).

To calculate the total number of sequences per subject in the CASIA-B dataset, we have that each subject has $(6 + 2 + 2) = 10$ gait status, and each gait status has 11 views ($0^\circ, \dots, 180^\circ$). Consequently, the total number of sequences per subject is $10 \times 11 = 110$ sequences as previously mentioned (Yu et al., 2006). Additionally, each sequence may contain between 50 to 100 images, since each gait recording depends solely on the gait pattern and duration of the subject. Thus, the number of frames contained in the different sequences is not uniform and may vary. The labeling format for the images in the CASIA-B dataset is “xxx-mm-nn-ttt.PNG”, where:

- xxx: subject id, ranging from 001 to 124.

- mm: gait status, can be “nm” (normal), “cl” (in a coat), or “bg” (with a bag).
- nn: series number.
- ttt: view angle, can be “000”, “018”, ..., “180”.

The image file name format in CASIA-B is easy to understand and allows users to quickly access relevant information for each image (See Figure 12).

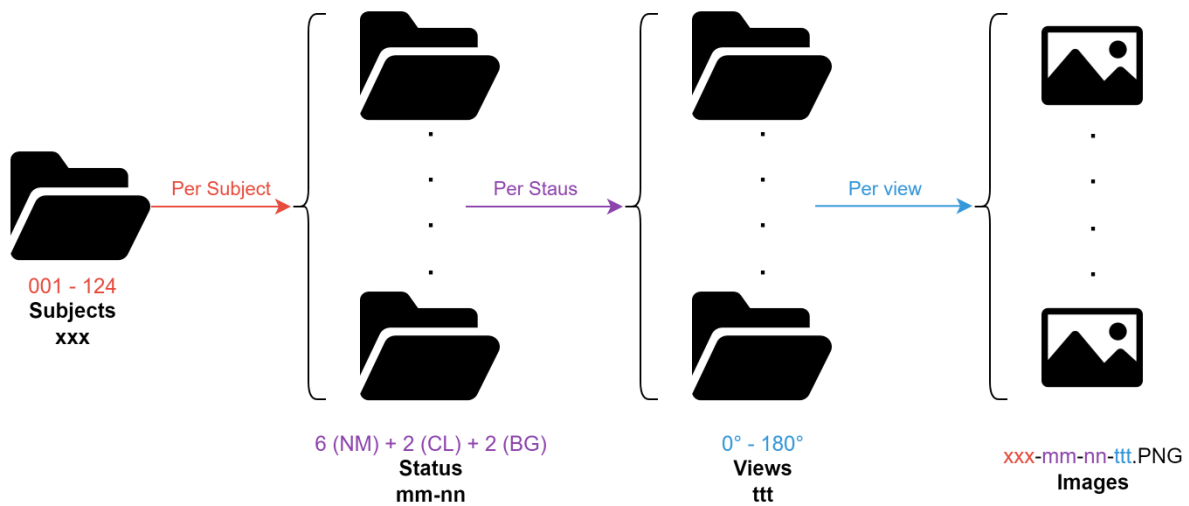


Figure 12. Gait Labeling Format at CASIA-B.

The first part of the file name, “xxx”, refers to the subject identification and enables users to easily identify who each image sequence belongs to. The second part, “mm”, refers to the gait status. The third part, 'nn', is the sequence number and allows users to identify the sequence within a specific subject. Lastly, the fourth part, 'ttt', refers to the view angle and enables users to identify the specific view of each sequence. Together, this labeling format allows users to quickly access to each gait sequence in the CASIA-B dataset and able the opportunity to develop a biometric profile per subject as desired.

2.4 Feature Extraction for Gait Biometrics

2.4.1 Basis of the Feature Extraction

Image processing focused on feature extraction is a crucial component in the literature of identification systems using images (Chao et al., 2019; Chen et al., 2018; Harris et al., 2022; Y. He et al., 2019; Liu et al., 2018; Y. Zhang et al., 2020). In this way, gait biometric systems have implemented a variety of approaches in accordance with their computational requirements (Filipi Gonçalves Dos Santos et al., 2021; Hadjkacem et al., 2020; Harris et al., 2022; Parashar et al., 2023; Sayed, 2018).

The fundamental element of an image is the pixel, which serves as the basis for applications related to feature extraction (Harris et al., 2022; Sayed, 2018). The image is represented as a matrix, where each element corresponds to a pixel of information. Consequently, the image representation is matrix-based, and the collection of all pixels is referred to as a grid. In the case of a binary image that stores information, only two possible values will be considered for a pixel: 1 or 0, representing on and off, respectively (Chen et al., 2018; Klöpfer-Krämer et al., 2020; Martinho-Corbishley et al., 2019; More & Deore, 2018; Sokolova & Konushin, 2019; Song et al., 2019) (See Figure 13).

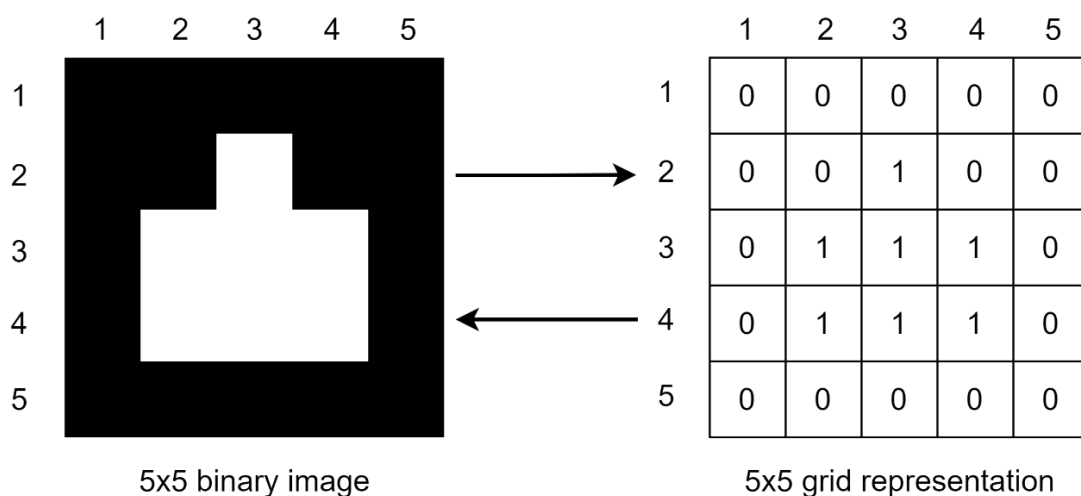


Figure 13. Elemental Image Representation and Storage.

2.4.2 The Geometric Moments Method

The Geometric Moments (GM) method is a technique employed for feature extraction from images, which relies on the utilization of geometric moments (Bach et al., 2021; Harris et al., 2022; Kukreja et al., 2021; Sayed, 2018). Geometric moments are numerical properties that can be derived from a given image. The use of moments enables the acquisition of substantial information from an image and offers the advantage of not only considering the edges of a shape but also taking into account all the pixels within it (Harris et al., 2022; Kukreja et al., 2021; Sayed, 2018). They are primarily used for recognizing a shape within an image but the principle is applicable to gait shape images. The equations for the GM calculation of the centre of mass point (\bar{x}, \bar{y}) is defined as follows:

$$\bar{x} = \frac{1}{N} \sum_{i=1}^l \sum_{j=1}^m j * f(i, j), \quad (1)$$

$$\bar{y} = \frac{1}{N} \sum_{i=1}^l \sum_{j=1}^m i * f(i, j) \quad (2)$$

Where:

$$N = \sum_{i=1}^l \sum_{j=1}^m f(i, j), \quad (3)$$

Represents the area of the figure in binary images and is the sum of the values of all the pixels.

The most useful application of the geometric moments method lies in the information that can be extracted from them, which are invariant to geometric transformations such as translation, scaling, and rotation (Harris et al., 2022; Sayed, 2018). Consequently, the geometric moments are utilized for recognizing the centre of mass for a given shape in an image, regardless of its position on a coordinate axis (Hadjkacem et al., 2020; Harris et al.,

2022; Sayed, 2018). Figure 14 summarizes the practical application of the GM method in gait silhouette shape, notice that the threshold is inverted for an optimal visualization.

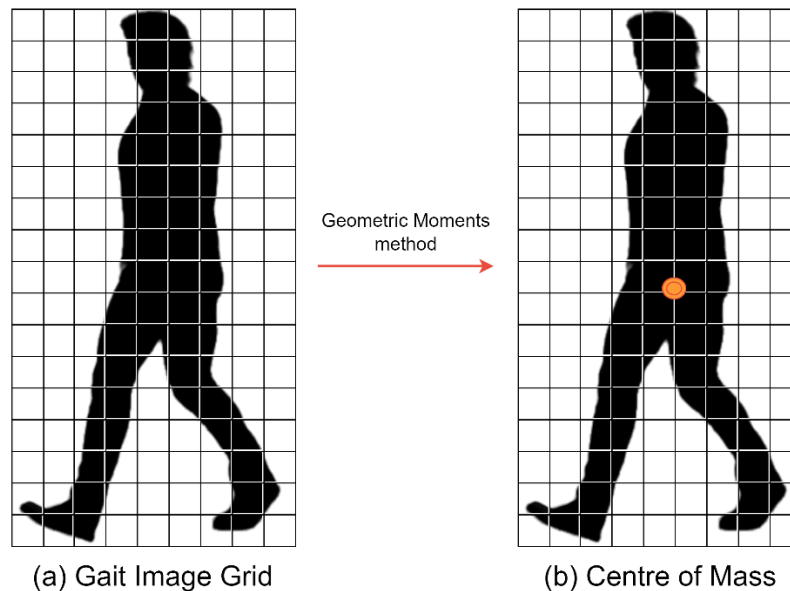


Figure 14. Schematic Representation for Centre of Mass Calculation in Gait Silhouette.

The calculated centre of mass centroids can then be used for classifying and recognizing objects, as well as identifying patterns in gait image sequences. Moreover, this method is computationally efficient and easy to implement (Harris et al., 2022; Sayed, 2018). Then, various studies in the literature have reported the calculation of centre of mass for centroid identification as an essential component in recognition algorithms for gait-based biometric identification of individuals (Hadjkacem et al., 2020; Mansouri et al., 2018; More & Deore, 2018; Wang et al., 2018; Y. Zhang et al., 2019).

2.4.3 The Euclidean Distances

The Euclidean distance, is a widely used metric for measuring the straight-line distance between two points in Euclidean space (Harris et al., 2022). In the context of geometry and data analysis, Euclidean distance is often employed to determine the similarity or dissimilarity between two points or objects, particularly when working with multidimensional data (B. Mazumdar, 2018; Harris et al., 2022; More & Deore, 2018; Sayed,

2018; Wang et al., 2018). Mathematically, the Euclidean distance between two points, “ P_1 ” and “ P_2 ”, with coordinates (x_1, y_1) and (x_2, y_2) respectively in a two-dimensional plane, is calculated using the following formula:

$$\text{Euclidean Distance } (d) = \sqrt{(x_2 - x_1)^2 + (y_2 - y_1)^2} \quad (4)$$

In this context, Euclidean distance emerges as a widely reported measure in the gait biometric recognition literature for comparing the gait patterns of various individuals (Harris et al., 2022; More & Deore, 2018; Sayed, 2018; Wang et al., 2018; Yu et al., 2006). This is grounded in the understanding that each person possesses a distinct gait pattern, referred to as their gait signature, as previously discussed (Gupta, 2021; Harris et al., 2022; Sayed, 2018). Consequently, when implementing the Euclidean distance in a gait biometric recognition system, this method quantifies the distance between pixels containing information of interest (Barbosa et al., 2012; Battistone & Petrosino, 2019; Chen et al., 2018; Harris et al., 2022; Sayed, 2018; C. Xu et al., 2019; Yu et al., 2006). Figure 15 exemplifies the calculation of the Euclidean Distances for a given set of pixel of interest.

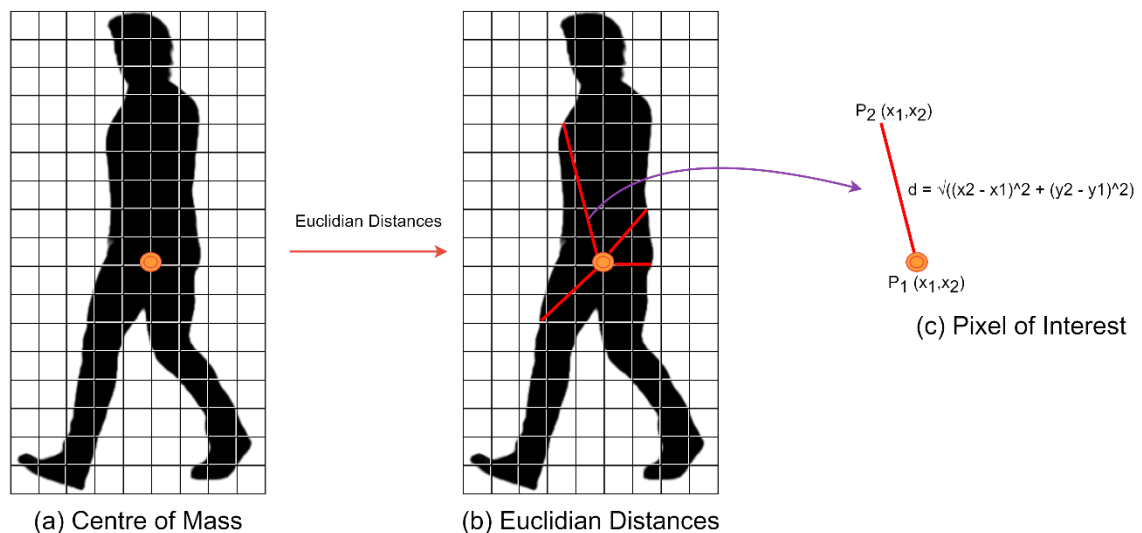


Figure 15. Schematic of Euclidean Distance Calculation in Gait Silhouette Pixels.

2.4.4 Classifiers for Features Extraction

The spatial-temporal approach, is commonly employed for feature extraction in gait recognition systems, as binary sequences of gait silhouettes captured encompass stride length, stride duration, step height, and gait speed of an individual (Barbosa et al., 2012; Battistone & Petrosino, 2019; Chen et al., 2018; Harris et al., 2022; Prakash et al., 2018; Sayed, 2018; C. Xu et al., 2019). Once the gait signatures for two individuals have been extracted, a classifier such as Artificial Neural Networks (ANN), Support Vector Machine (SVM), k-Nearest Neighbors (k-NN), among others, is utilized to ascertain their similarity or dissimilarity (Alharthi et al., 2019; Chen et al., 2018; Hadjkacem et al., 2020; Harris et al., 2022; Horst et al., 2019; Khera & Kumar, 2020; Liu et al., 2018; Sayed, 2018; Wang et al., 2018). If the gait signatures exhibit considerable differences, it is probable that the individuals are distinct. Conversely, if the gait signatures demonstrate similarity, it is plausible that the individuals are the same person.

2.5 Artificial Neural Networks (ANNs) for Gait Biometrics

2.5.1 Basis of Artificial Neural Networks

Artificial Neural Networks (ANNs), also known as Feedforward Neural Networks, are an elemental and simple class of deep learning models that operate within the supervised learning paradigm (Alharthi et al., 2019; Cicirelli et al., 2022; Horst et al., 2019; Khera & Kumar, 2020; Sayed, 2018; Vandersmissen et al., 2018). In the context of gait biometrics, ANNs can be employed for feature extraction, classification, and identification tasks (Adamović et al., 2020; Cicirelli et al., 2022; Harris et al., 2022; Hernandez-de-Menendez et al., 2021; Liu et al., 2018; Sayed, 2018). By processing input data in the form of vectors of numbers from gait-related extracted features, such as stride length, stride duration, step

height, and gait speed in the spatial-temporal approach (Alharthi et al., 2019; Harris et al., 2022; Sayed, 2018). As a result, ANNs can identify distinctive patterns that represent the unique gait signature of an individual, owing to their ability to learn complex, non-linear relationships between inputs and outputs (Filipi Gonçalves Dos Santos et al., 2021; Gupta, 2021; Harris et al., 2022; Kukreja et al., 2021; Sayed, 2018).

By applying an ANN to gait biometric recognition, researchers can leverage the architecture of the network to ably process gait-related features due a low-resource demand, ultimately facilitating the classification and identification of individuals based on their unique gait patterns for reduced tasks (Harris et al., 2022; Sayed, 2018). The unidirectional flow of information through the network ensures that the model effectively learn and adapt to the inherent variability in gait data, contributing to the robustness and reliability of gait biometric recognition systems (Alharthi et al., 2019; Cicirelli et al., 2022; Horst et al., 2019; Khera & Kumar, 2020; Sayed, 2018; Vandersmissen et al., 2018).

2.5.2 Architecture of Artificial Neural Networks

The primary structure of an ANN consists of an input layer, one or more hidden layers, and an output layer (Filipi Gonçalves Dos Santos et al., 2021; Harris et al., 2022; Khera & Kumar, 2020; Kukreja et al., 2021; Sayed, 2018; Yan et al., 2016; Y. Zhang et al., 2020). Each layer is composed of interconnected neurons, also known as nodes, which are responsible for performing mathematical operations on the input data (Filipi Gonçalves Dos Santos et al., 2021; Gupta, 2021; Harris et al., 2022; Sayed, 2018). The input layer receives the raw data, whereas the hidden layers perform intermediate transformations on the data. The output layer generates the final predictions or classifications (Battistone & Petrosino, 2019; Harris et al., 2022; Khera & Kumar, 2020; Kukreja et al., 2021; Sayed, 2018; Yan et al., 2016).

As a result, the architecture of an ANN is characterized by the absence of cycles, which means that the information flows in a unidirectional manner from the input layer to the output layer, passing through the hidden layers without looping back (Battistone & Petrosino, 2019; Harris et al., 2022; Kukreja et al., 2021; Sayed, 2018; Vandersmissen et al., 2018; Yan et al., 2016; Y. Zhang et al., 2020). This unique architectural feature differentiates ANNs from other types of neural networks, such as Recurrent Neural Networks (RNNs) and Long Short-Term Memory (LSTM) networks, which possess feedback loops that enable them to maintain internal states for processing sequential data (Battistone & Petrosino, 2019; Luo et al., 2020; Y. Zhang et al., 2019, 2020) (See Figure 16).

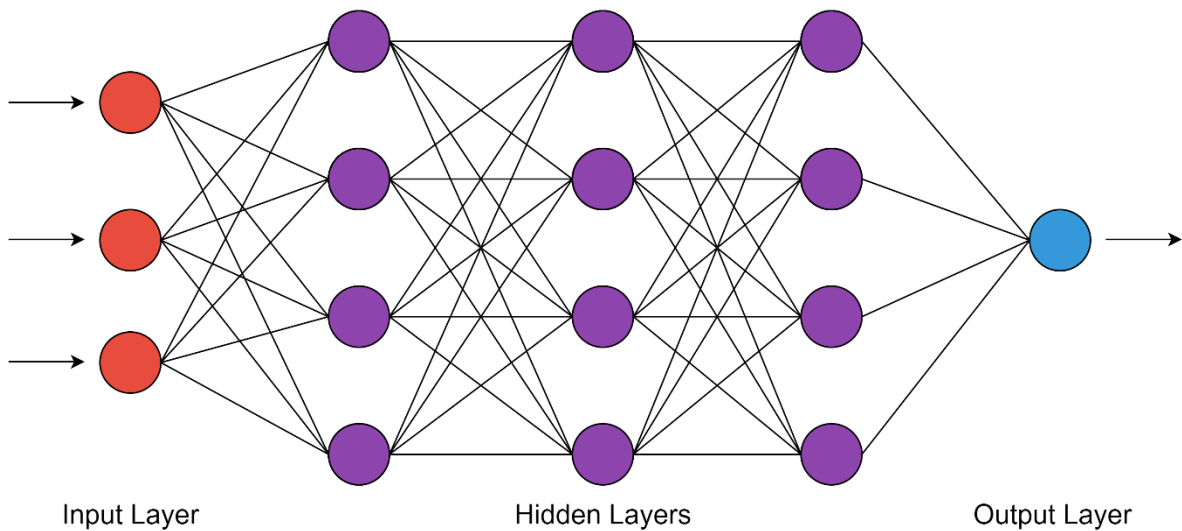


Figure 16. Elemental Exemplification for the Architecture of Artificial Neural Network.

2.5.3 Training Process of Artificial Neural Networks

In the context of the training process, the input layer of an ANN receives raw data in the form of feature vectors representing gait characteristics (Alharthi et al., 2019; Horst et al., 2019; Khera & Kumar, 2020; More & Deore, 2018; Sayed, 2018). Each neuron in this layer corresponds to a specific feature of the input data. The role of the input layer is to distribute the input data to the subsequent hidden layers for further processing, such as identifying unique gait patterns associated with individuals (Alharthi et al., 2019; Horst et al., 2019;

Khera & Kumar, 2020; Malloggi et al., 2021; More & Deore, 2018; Sayed, 2018). The number of neurons in the input layer is determined by the dimensionality of the input data.

Then, ANNs learn to minimize the error between the predicted outputs and the ground truth labels by adjusting the weights and biases of the network connections (Alharthi et al., 2019; Harris et al., 2022; Horst et al., 2019; Khera & Kumar, 2020; More & Deore, 2018; Sayed, 2018). This is typically achieved using the backpropagation algorithm, which computes the gradients of the loss function with respect to the weights and biases, followed by an optimization algorithm, such as stochastic gradient descent (SGD) or adaptive moment estimation (Adam), to update the parameters (Filipi Gonçalves Dos Santos et al., 2021; More & Deore, 2018; Sayed, 2018; Sokolova & Konushin, 2019) (See Figure 17).

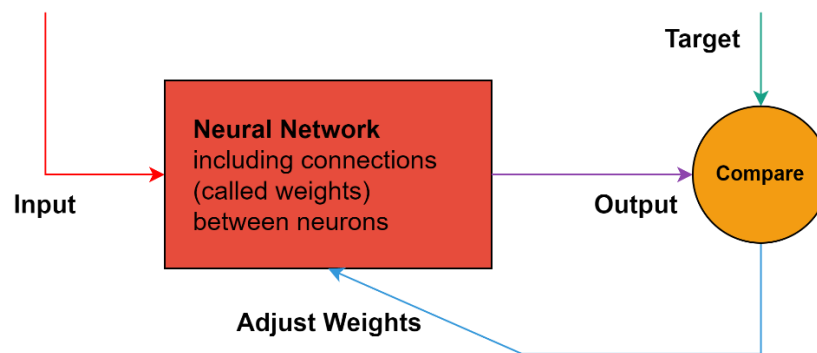


Figure 17. General Training Structure of an Artificial Neural Network.

To avoid overfitting and improve generalization, various regularization techniques can be employed during the training of ANNs for gait biometric recognition (Alharthi et al., 2019; Horst et al., 2019; Khera & Kumar, 2020; More & Deore, 2018). Some common methods include dropout, weight decay, early stopping, and hyper parameters modification (Fan et al., 2020; More & Deore, 2018; Sayed, 2018; Vandersmissen et al., 2018; C. Xu et al., 2019). These techniques help prevent the network from relying too heavily on specific features in the training data, thus promoting better performance on unseen gait data and enhancing the robustness of the gait biometric recognition system.

2.6 MATLAB for Gait Biometrics

2.6.1 Basis of MATLAB

MATLAB is a versatile high-level software for numerical computing and data visualization that is widely used in various fields (Gupta, 2021; Harris et al., 2022; Huang et al., 2021; Malloggi et al., 2021; Mani et al., 2021; MathWorks, 2023b; More & Deore, 2018; Rose & Arellano, 2021; Sayed, 2018). The cross-platform compatibility represents an advantage for research to work seamlessly on multiple operating systems and devices (Windows, Mac OS X and Linux) (Harris et al., 2022; MathWorks, 2015, 2023b). This allows researchers to collaborate more effectively and to easily share their work, without having to worry about compatibility issues (MathWorks, 2015, 2023b). Its programming language offers a wide range of functions and tools for resolving complex mathematical problems, data analysis, and visualization (Gupta, 2021; Harris et al., 2022; Malloggi et al., 2021; Mani et al., 2021; MathWorks, 2023b; Rose & Arellano, 2021; Sayed, 2018; S. Xu & Mok, 2022) (See Figure 18).

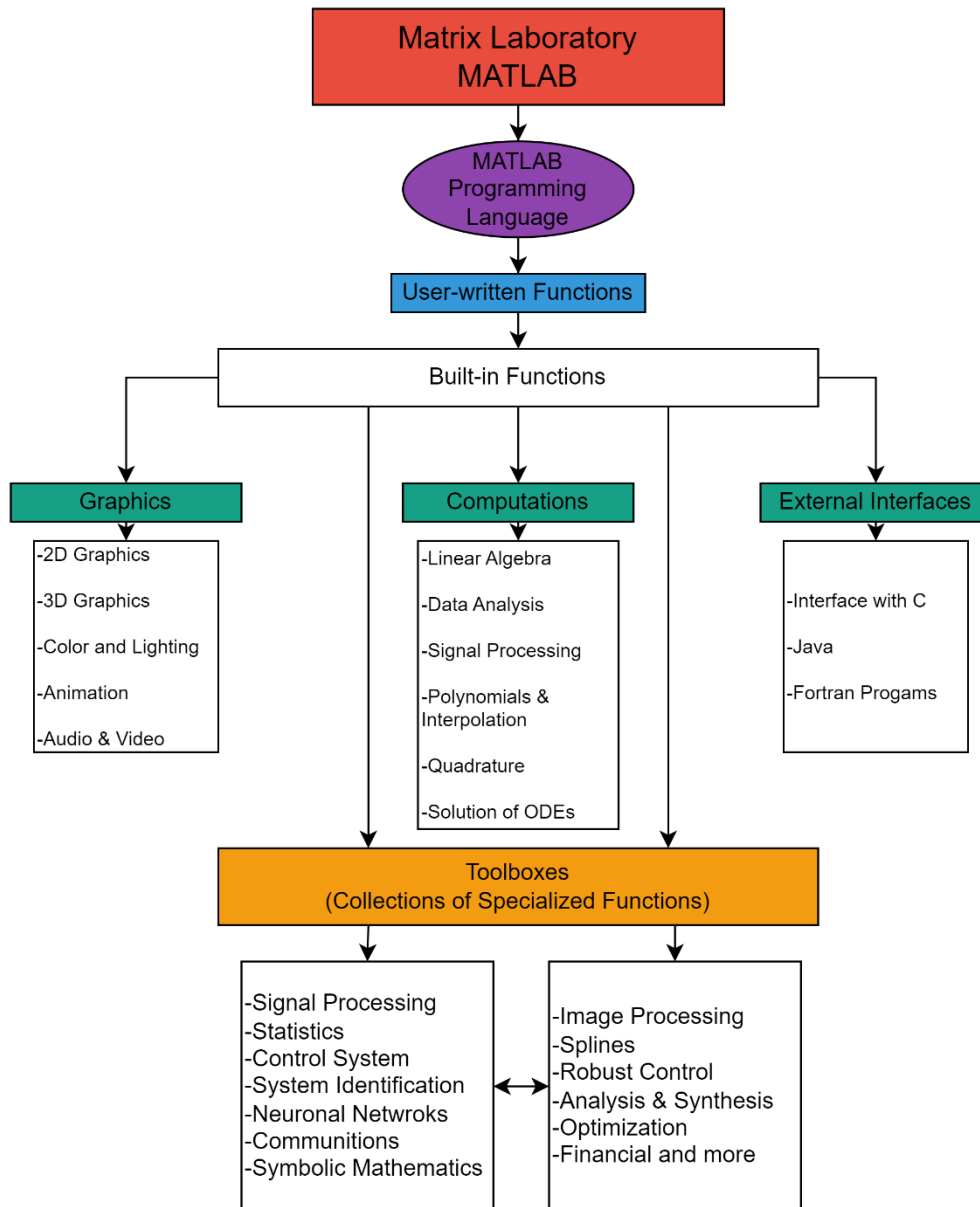


Figure 18. Schematic Overview of Key MATLAB Features.

In the gait biometrics field, MATLAB is particularly useful for the analysis and visualization of gait data, such as gait videos sequences, feature gait data, and signal gait records (Gupta, 2021; Harris et al., 2022; Huang et al., 2021; Malloggi et al., 2021; Mani et al., 2021; MathWorks, 2023b; More & Deore, 2018; Rose & Arellano, 2021; Sayed, 2018). As a result, the functionalities from MATLAB are able to be apply in the recognition of individuals through gait images by feature extraction, pattern analysis, data classification, and data visualization (Gupta, 2021; Harris et al., 2022; Huang et al., 2021; Malloggi et al., 2021; MathWorks, 2023b; More & Deore, 2018; Prakash et al., 2018; Rose & Arellano, 2021;

Sayed, 2018; S. Xu & Mok, 2022). These techniques can enhance the clarity and precision of the underlying structures and patterns of gait images.

2.6.2 Graphical User Interface App Designer

The Graphical User Interface (GUI) development environment, App Designer, serves as a potent instrument that streamlines the process of crafting user interfaces (UIs) for MATLAB applications (S. He & Li, 2020; MathWorks, 2015, 2023b, 2023a). App Designer furnishes an extensive array of UI components, encompassing buttons, text boxes, drop-down lists, and graphical displays, which can be seamlessly integrated into the design workspace. Furthermore, users can assign tasks to these components, such as executing code or invoking MATLAB functions, thereby fostering the development of interactive and user-friendly applications (Amershi et al., 2019; MathWorks, 2015, 2023b; Ratcliffe & Puthusserypady, 2020). App Designer also incorporates debugging and testing utilities to pinpoint and rectify code errors prior to public release (see Figure 19).

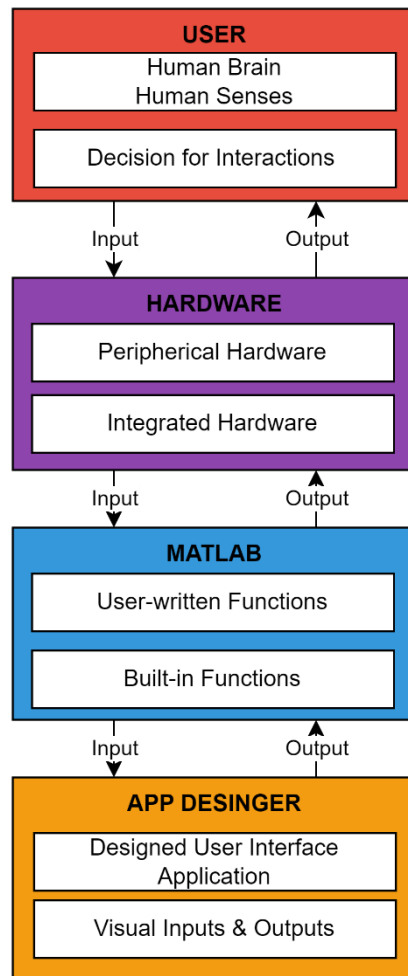


Figure 19. General Key Components Involved for User Interface (UI) at App Designer.

In the realm of biometrics, gait recognition necessitates the analysis of information embedded within gait images. Upon devising requisite functions, users can employ App Designer to establish a comprehensive system that incorporates a graphical interface for capturing and visualizing gait images, in addition to executing recognition functions grounded in subject-specific biometric profiles (MathWorks, 2015, 2023b, 2023a). The capacity of App Designer to generate .exe executable files, which can be shared and executed on MATLAB-free computers, offers a distinct advantage (MathWorks, 2015, 2023b, 2023a). The culmination is a secure, protected executable file amenable to distribution and utilization across diverse environments.

In summation, App Designer represents a user-friendly tool that expedites the creation of customized UIs for MATLAB applications. Its compatibility with MATLAB code, capacity to assign tasks to UI components, and template reusability render it a versatile instrument for crafting interactive, accessible applications (S. He & Li, 2020; MathWorks, 2015, 2023b, 2023a; Ratcliffe & Puthusserypady, 2020). App Designer proves particularly advantageous in the biometrics domain, where it can be deployed to construct gait recognition systems comprising graphical interfaces for capturing and visualizing gait images. The ability of App Designer to create secure, protected executable files facilitates the distribution and application of MATLAB programs across an array of environments and circumstances.

CHAPTER III: Materials and Methods

MATERIALS AND METHODS

In this chapter, the materials and methodological frameworks are presented for the development of an individual identification system based on gait analysis. The subsequent steps in this process are considered as: Analysis, Design and Implementation, Dataset Preparation, Hyperparameters, User Interface (UI) Prototype, Experimental Setup and Validation (See Figure 20).

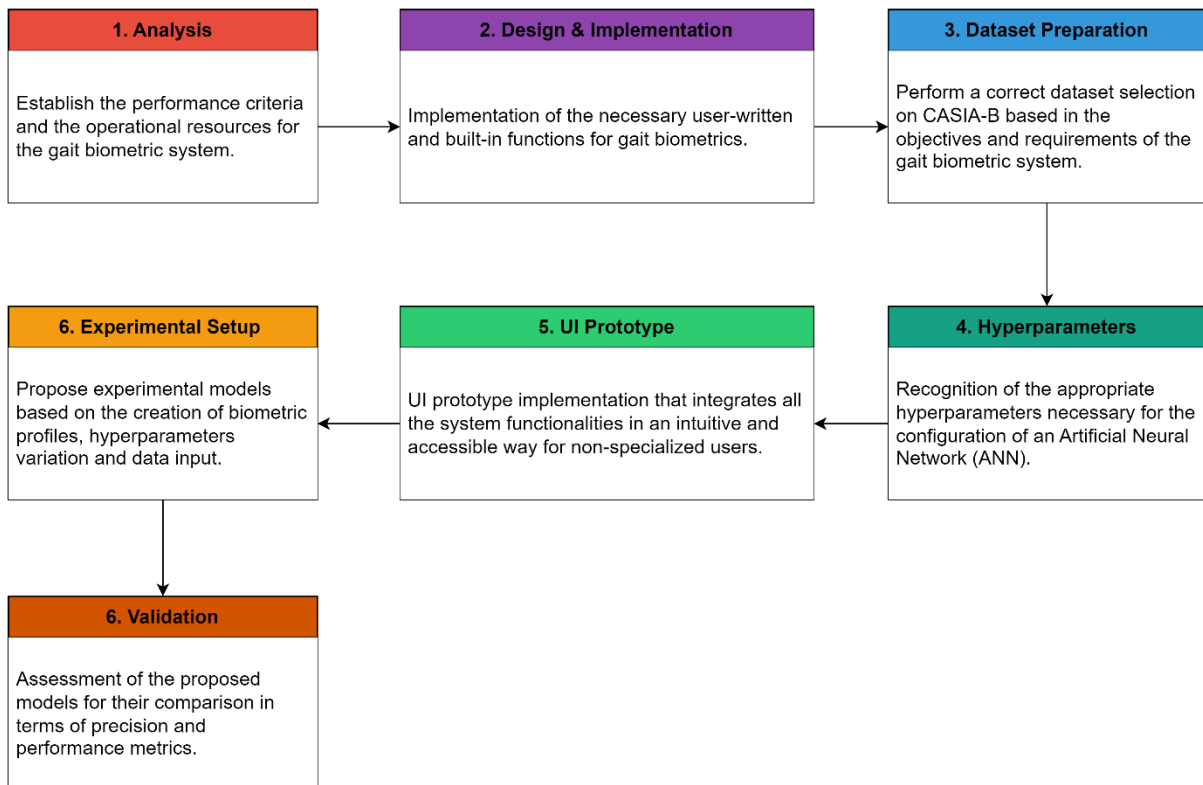


Figure 20. Key Components in the Material and Methods Framework.

3.1 Analysis

3.1.1 Performance criteria for the Gait Biometric System.

The primary objective of this research project was to develop a person recognition system based on gait analysis, necessitating the implementation of an effective silhouette classification model. The proposed model is reusable, enabling the creation and updating of

biometric profiles without necessitating a complete rewrite of the profiles. Furthermore, the system was designed to operate with low-to-medium computational resources. The key factors considered in the model design included dataset size, computational cost, and data management:

- *Dataset size:* The design of the silhouette recognition model for the gait-based person identification system prioritized small datasets. As the primary purpose of the gait biometric system was to work with low resources, it was crucial to minimize the number of classes. A reduced dataset size for limited computer resources enhances the accessibility of the system in low-to-medium computational resources and facilitates familiarization for new users in biometric identification tasks.
- *Low-to-medium computational cost:* The thesis project encountered the challenge of limited high-performance computational resources, necessitating the development of a silhouette recognition model and its associated system with low-to-medium computational cost, without dependence on a Graphical Processing Unit (GPU). Consequently, the model training process was executable on machines with average or even below average processing and memory resources, reflecting the average technology market. This approach ensured a broader accessibility of the model and its system, facilitating a more efficient and cost-effective implementation.
- *Data Handling Practicality:* For the proposed gait biometric system, user-written and built-in functions prioritized not only small identification tasks but also facilitating efficient data management throughout the feature extraction, classifier process, and biometric profiles. Consequently, efficient data handling enabled the integration of various functions into a user interface, resulting in a comprehensive

gait biometric system that enhanced utility and effectiveness for non-specialized users.

3.1.2 Operational Resources – Software

All data were processed in MATLAB (R2020a, The MathWorks, Natick, MA, USA) for user-written and built-in functions.

3.1.3 Operational Resources – Hardware Selection

Adhering to the goal of achieving low-to-medium computational cost in this thesis project, the training and validation of user-written and built-in functions were conducted solely using the available hardware resources of a laptop computer, without leveraging GPU capabilities. This approach ensures the functionalities of the model were accessible to a broader audience. The laptop computer utilized for this purpose had the following specifications:

- AMD Ryzen 5 4600H with Radeon Graphics (3.00 GHz)
- Windows 10 Home (21H2) Operative System
- 16 GB RAM

3.2 Design and Implementation

3.2.1 User-Written and Built-in Function for a Gait Biometrics System

At this stage, the primary factors considered in designing a model for geometric feature extraction and neural network architecture for the recognition system were established. Subsequently, the appropriate user-written and built-in functions were selected to implement the feature extraction technique and the ANN classifier.

In developing a gait biometrics system, it was essential to define the functionalities that constitute its operational options. The integration of functions that substantially

contribute to the operability of the system were prioritized, while desisting from adding quasi-significant extra features. Adhering to the principle of simplicity, the primary objective of this study - identifying individuals through gait analysis - was emphasized. In this sense the biometric system employs the spatial temporal-temporal parameter with an appearance-based approach. Subsequently, functionalities such as data reading, feature extraction, and storage of the acquired data in the form of biometric IDs were developed as separate code functions and later integrated into a single, more complex function that directly encompasses the three aforementioned processes. Likewise, functionalities such as artificial neural network classifier, training data partitioning, and confusion matrix generation were also developed as separate code functions and subsequently integrated into a single, more complex function that directly encompasses the three aforementioned processes. A final gait biometric function was created for new entries of gait info to identify potential ID biometric profiles. Notices that the functions were labeled in order to avoid a misunderstanding, given that the user-written occasionally are part of other user-functions function.

3.2.2 Data Reading

Ideally, the process for subject identification through a gait system commences with the loading of raw data. To achieve this, it is essential to consider that the input data consists solely of a sequence of gait silhouettes for each individual. Moreover, since the CASIA-B database is being utilized, data reading was structured to automate the loading of multiple sets of information. Thus, the folders contained in CASIA-B, with the xxx-mm-nn-ttt.PNG structure described previously in Section 2.3.2, facilitated faster and more efficient data reading. To load the data, the parent folder CASIA-B is first requested, followed by the number of subjects whose information is to be loaded, then the number of sequences to be loaded per individual, and finally the corresponding camera angle. This approach enables

multiple loading in terms of both the number of individuals and sequences for a single camera angle. The main structure is outlined below (see Figure 21):

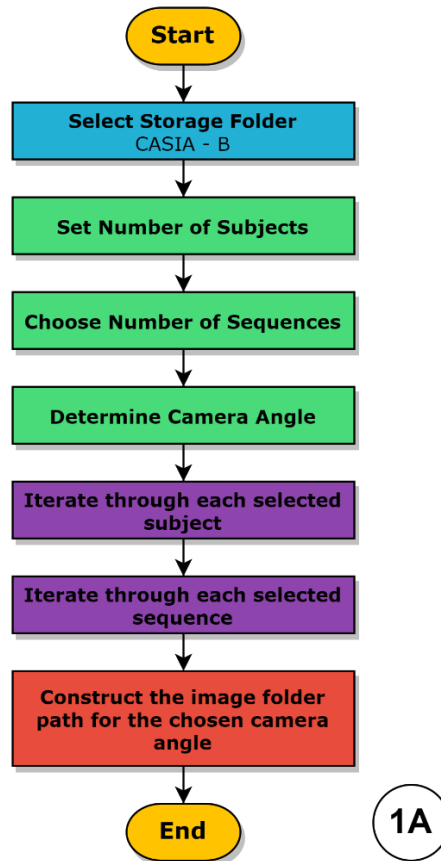


Figure 21. Flowchart for Multiple Raw Data Loading, 1A.

Additionally, a variant of this function was developed, designed for individual data loading, as multiple data loading or working with the CASIA-B database will not always be required. Consequently, this function only requests the final folder containing the gait sequence (See Figure 22).

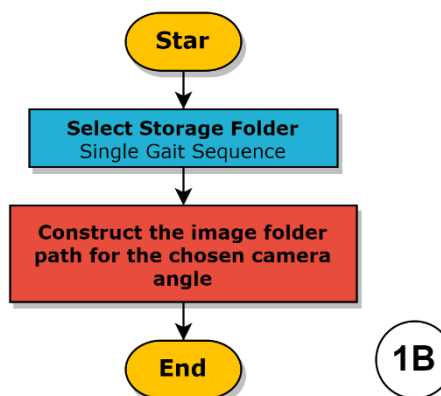


Figure 22. Flowchart for Solo Raw Data Loading, 1B.

3.2.3 Feature Extraction

Following the raw data reading, it is essential to perform a feature extraction for the gait silhouette sequences. Feature extraction involves generating a numerical vector containing relevant information about the gait pattern of the subject. At this point, it should be mentioned that the feature extraction algorithm encompasses three sections: image processing, feature extraction processing, and gait signature processing. Initially, for the image processing section, a folder with gait silhouette sequences is iterate using the directory generated previously in the data reading function. The code assesses whether the images are in RGB format and converts them to grayscale if necessary. Subsequently, a binarization threshold is applied to each image:

$$f(i,j) = B(i,j) = \begin{cases} 1 & \text{if value at pixel position} > \text{threshold} \\ 0 & \text{otherwise} \end{cases}, \quad (5)$$

Where,

$$f(i,j) = B(i,j)$$

Represents the adequate function to be replace at equation (1), (2), and (3) from section 2.4.2.

Subsequently, for the feature extraction processing section the Geometric Moments method is employed to calculate centroids for each gait image within the silhouettes sequence of the individual. The Euclidean distance method is then utilized to measure the distance from every pixel containing information to the computed centroids (See Figure 15). A histogram of the distances recorded in the Euclidean distances for the gait silhouette is generated. Ultimately, the relevant information pertaining to the distance histogram is saved as vectors, contributing to the creation of a unique gait signature for each individual. The primary structure is outlined below (See Figure 23):

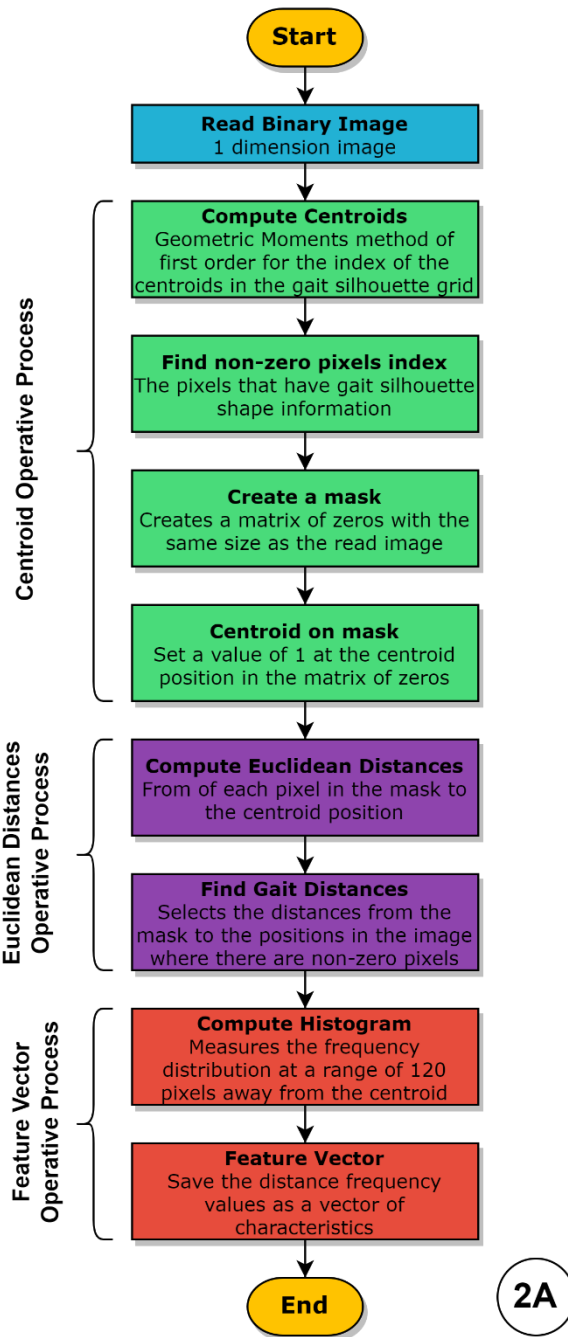


Figure 23. Flowchart for Feature Extraction Subprocess, 2A.

However, it is important to note that this is implemented as a separate function that receives the image and processes it to generate a vector. Note that the function for calculating geometric moments and measuring Euclidean distances becomes a subprocess of the final function.

Finally, for the gait signature processing section, the feature vector generated by the feature extraction is concatenated as each image within the gait sequence is read.

Additionally, the possibility of some images within a gait sequence containing significant noise or lacking uniform continuity for centroid calculation is considered. As a result, the algorithm is capable of disregarding the use of such images to prevent errors and proceeds to the next image. The main structure of the function for feature extraction is summarized in Figure 24 through its three operative sections.

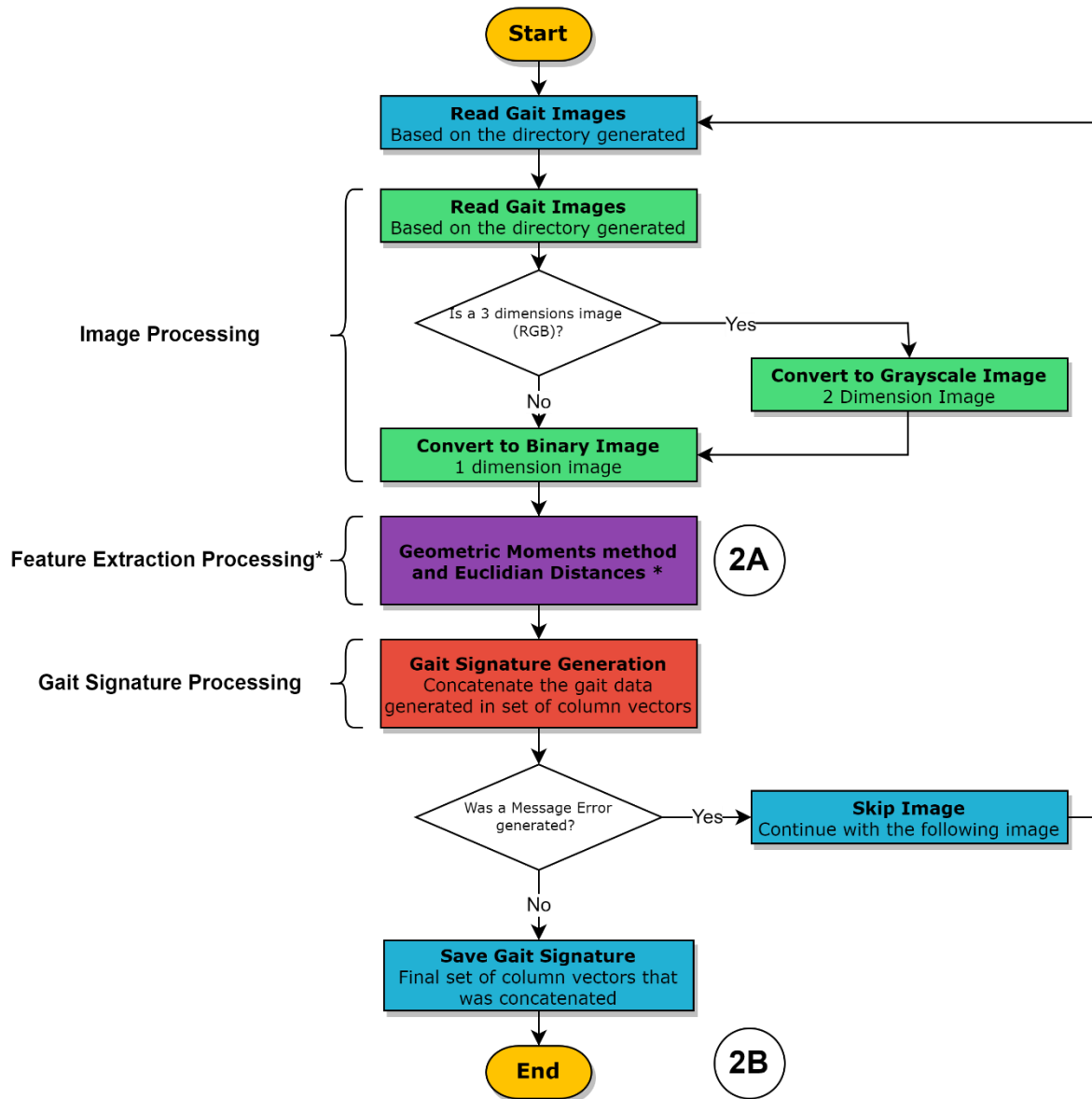


Figure 24. Flowchart for Feature Extraction Complete Process, 2B.

3.2.4 Storage of the Obtained Data

The information generated from the feature extraction was initially stored in variables. However, to enhance reusability of the gait biometric system, the variables containing

individual identification information were stored in a database in accordance with its implementation to a user interface. This approach facilitated better resource management and practical data handling. As a result, when information on a specific individual is required, the user only needs to access the assigned label to append new gait information for that individual. Furthermore, utilizing a database enables the assignment of different data types to distinct categories corresponding to the same individual allowing the managing as biometric profiles per subject. The main structure of the database includes the possibility to storage extracted features, subject IDs, maximum individual count, and features size (See Figure 25).

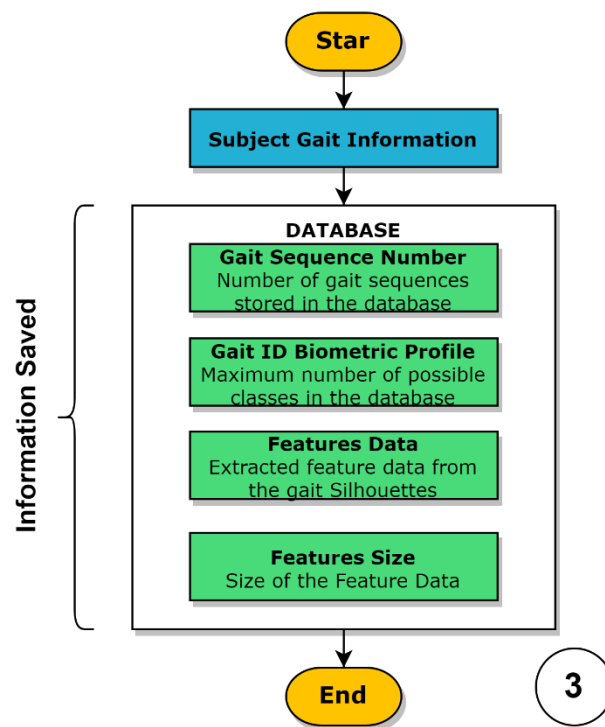


Figure 25. Main Database Storage Capacity, 3.

3.2.5 Integration of Functions for Gait Data

Upon developing the functions encompassing the three main processes for data reading, feature extraction, and storage of the obtained data, it is visualized that these functions collectively create a more complex and comprehensive algorithm. In this sense, the purpose of the algorithm is to convert gait silhouette images into gait information, labeled as

biometric IDs for each subject. Thus, the proposed system extracts features in an orderly and logical manner through single or multiple data inputs. It is worth mentioning that two variants of the final function, which combines the three main processes, were created due to the possibility of loading multiple data for a data structure like CASIA-B and individual data.

For the multiple loading variant, applicable solely to a data structure like CASIA-B, no verifications are needed for the assigned label number. This is because it is generated automatically as the data reading iterates through the parameters provided by the user. The final function for multiple data loading, feature extraction, and storage is detailed below (See Figure 26).

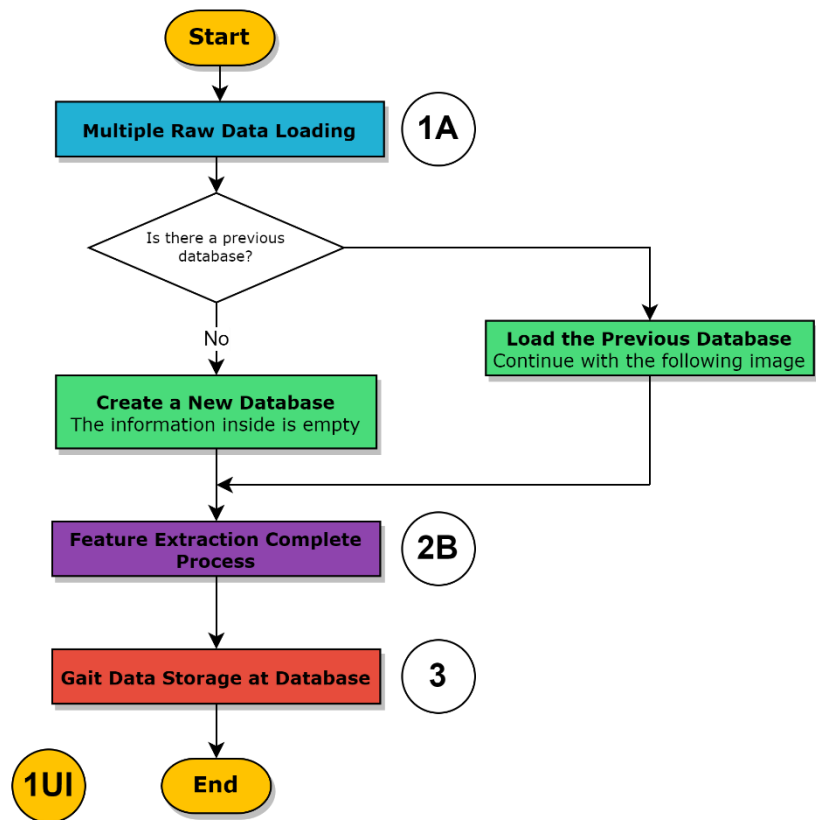


Figure 26. Integration of Functions for Multiple Gait Data, 1 UI.

For the single loading variant, applicable to any data structure since the folder containing the gait sequence is selected directly, verifications are required for the assigned label number. This is because, when providing the directory directly, it needs to be labeled by

the user. The final function for single data loading, feature extraction, and storage is detailed below (See Figure 27).

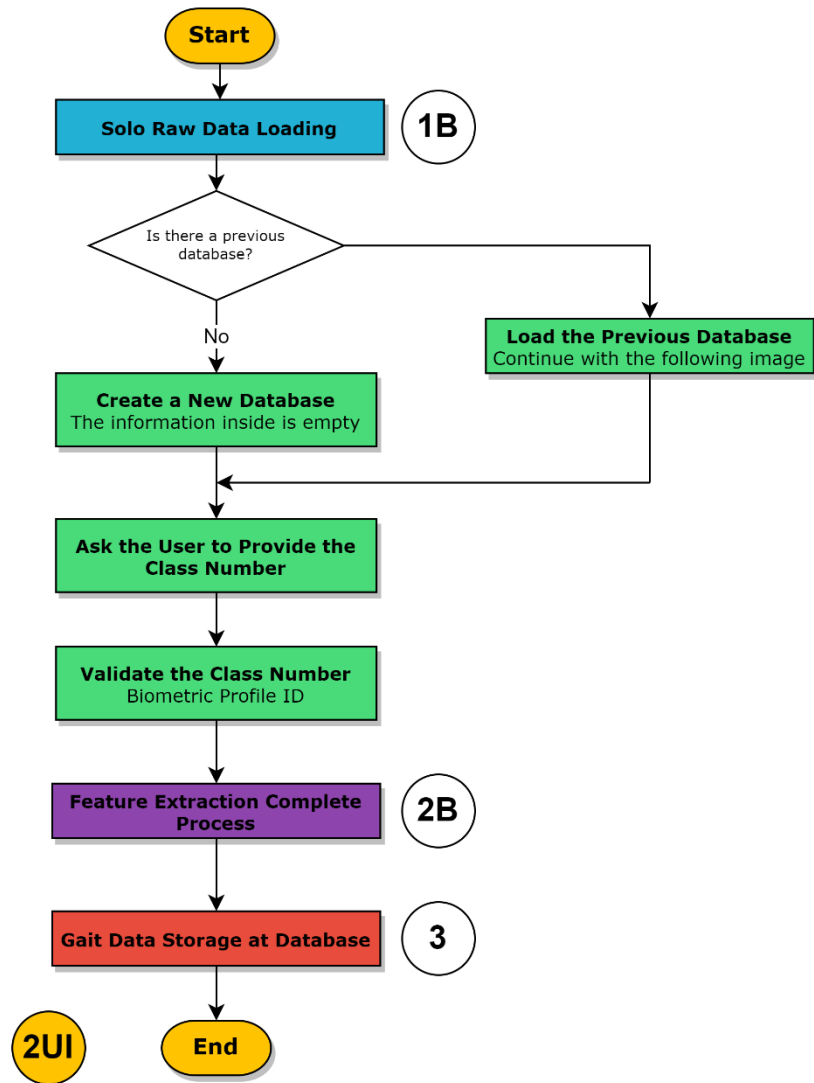


Figure 27. Integration of Functions for Solo Gait Data, 2 UI.

3.2.6 Artificial Neural Network Classifier Gait Biometrics

This functionality constitutes the central process of the current thesis project. To perform the identification task, it was essential to employ an Artificial Neural Network (ANN) as a classifier, enabling the assignment of extracted gait signatures to the corresponding subjects. The built-in MATLAB R2020a function *feedforwardnet* was utilized for this purpose.

During the ANN implementation, the input data is related to vectors of 120 values, as the feature extraction produces a gait signature with this gait data size. Subsequently, two hidden layers were employed. As a result, the neurons for the first hidden layer were calculated using the Nguyen-Widrow heuristic and the total number of existing classes at the time of training (total biometric profiles added). On the other hand, the neurons for the second hidden layer were determined only by the total number of existing classes at the time of training (total biometric profiles added). The Tansig activation function was applied to both hidden layers. The output layer is equal to the number of classes logically, and the Purelin activation function was employed. Figure 28 resumes the implementation of the ANN classifier for gait biometric recognition.

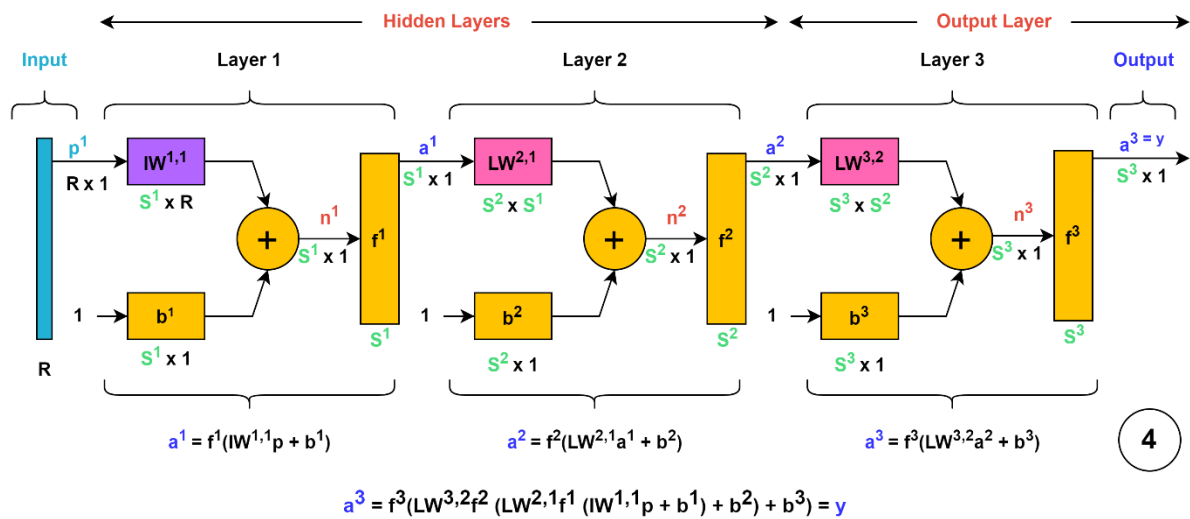


Figure 28. Artificial Neuronal Network (ANN) Designed for Gait Biometrics, 4.

Consequently, hyperparameter tuning serves as the primary strategy for identifying the most efficient configuration concerning the gait recognition model, with specific configuration detailed in Section 3.4 and Section 3.6. Once implemented the ANN architecture, the extracted gait features are trained within the ANN, generating a classification model for identification tasks. As a result, loading the trained model is the only requirement for classifying new data entries corresponding to respective subjects.

Additionally, a more comprehensive explanation concerning the neural network depicted in Figure 28 is provided below for users who are not specialized in artificial intelligence:

- R : The size of the data input, equal to 120 values given the size of the gait signature.
- S^1, S^2, S^3 : Number of neurons in Layer 1, Layer 2, Layer 3 respectively.
- S^1, S^2, S^3 : Number of neurons in Layer 1, Layer 2, Layer 3 respectively.
 - $S^1 = (120 + S^3) \div 2$ by the arithmetic mean heuristic.
 - $S^2 = \sqrt{120 \times S^3}$ by the geometric mean heuristic.
 - $S^3 =$ number of existing classes (biometric profiles).
- $IW^{1,1}$: Input Weight matrix for connection from Input (R) to Layer 1.
- $LW^{2,1}$: Layer Weight matrix for connection from Layer 1 to Layer 2.
- $LW^{3,1}$: Layer Weight matrix for connection from Layer 2 to Layer 3.
- f^1, f^2, f^3 : Activation functions.
 - f^1, f^2 corresponds to Tanh activation function.
 - f^3 corresponds to Purelin activation function.
- a^1, a^2, a^3 : Outputs.
- n^1, n^2, n^3 : Layers.

Thus, for data input to the model, it is necessary to divide the gait data into training, testing, and validation sets. A minor function was created to partition the gait data into 70% for training, 15% for testing, and 15% for validation. Subsequently, the model is trained with the divided data, the proposed architecture, and user-selected hyperparameters. Additionally, another minor function was developed to display a confusion matrix based on the artificial neural network classifier's performance on the validation set. Finally, once the network is

trained, the artificial neural network classifier model is stored. The following scheme outlines the structure of the function associated with the training and storage of the gait biometric model (See Figure 29).

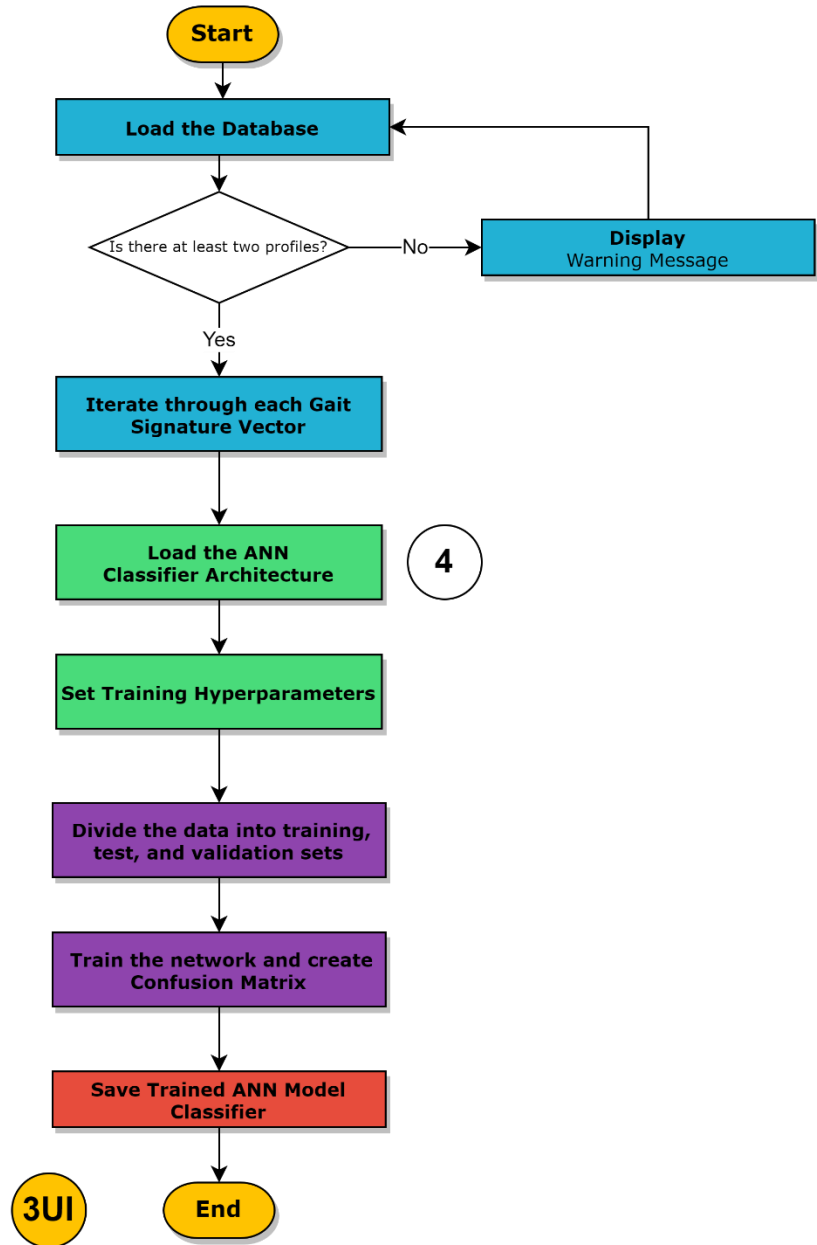


Figure 29. Complete Artificial Neuronal Network (ANN) Classifier Model, 3UI.

3.2.7 Gait Biometrics Identification

The identification of biometric profiles from gait silhouette sequences constitutes the final function of our gait system. This process involves inputting a folder containing a gait silhouette sequence, followed by loading the previously trained artificial neural network classifier model. The features are then extracted using the previously created feature extraction subprocess function and are utilized as input data for a classification simulation with the previously trained artificial neural network classifier model. Ultimately, the class, or biometric profile, with the highest probability is selected (See Figure 30).

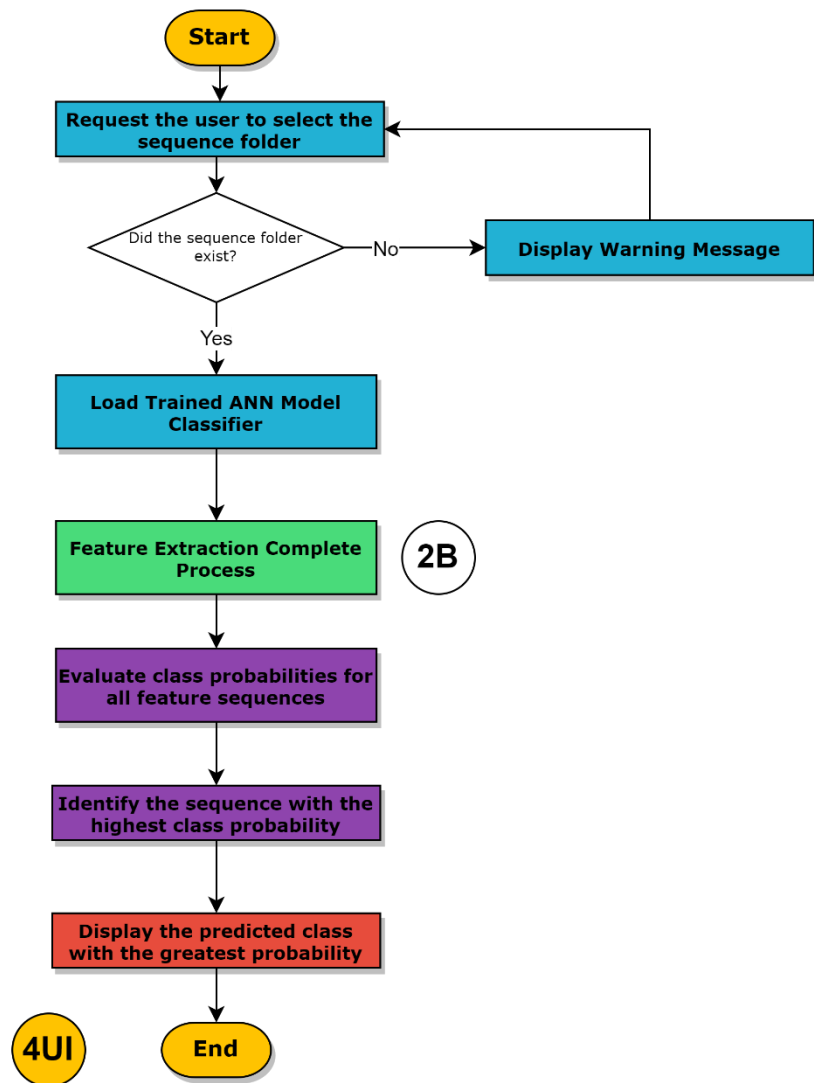


Figure 30. Gait Biometric Identification Schematic Function, 4UI.

3.3 Dataset Preparation

3.3.1 Dataset Selection

The database selected for this thesis project was CASIA-B. For the creation of our recognition system only normal gait (nm) status sequences were used. As a result, the gait status with a subject coat (cl) or a bag (bg) were omitted. Additionally, the walking sequences of subject 005 contain noise that can lead to system error and were not considered for a biometric profile creation. In consequence, the subject 101 was rename as 005 to replace the subject. Five of the normal gait (nm) status sequences were selected, out of the six existing sequences of this status. Additionally, the 11 existing camera angles will be used per walking record.

Thus, the sequence count per subject was $11 \times (6 - 1) = 55$. The remaining sequence was reserved for manual testing of the system or real-time demonstrations of its performance as desired. In order to gradually test the performance of the network with a low-computational cost approach, three dataset sizes were configured. These correspond to 5 subjects, 10 subjects and 25 subjects for the experimental setup. Additionally, the multiclass classification for 5 subjects is considered as the main model for the low-computational cost goal, given 25 subjects is usually presented in high-computational cost studies.

Finally, the prepared datasets sizes are calculated as (*subjects* \times *records* \times *camera angles* = *sequences*):

- *Dataset 1*: $5 \times (6 - 1)$ records \times 11 camera angles = 275 sequences
- *Dataset 2*: $10 \times (6 - 1)$ records \times 11 camera angles = 550 sequences
- *Dataset 3*: $25 \times (6 - 1)$ records \times 11 camera angles = 1375 sequences

3.4 Parameter Settings

3.4.1 Configurable Parameters

The following hyperparameters were utilized to configure the training process of the designed Artificial Neural Network (ANN) in MATLAB R2020a. A brief explanation of the purpose of each parameter is provided below:

- `trainFcn` = Training function name for optimisation algorithm to use.
- `net.trainParam.epochs` = The maximum number of epochs that will run during the training of the neural network.
- `net.trainParam.goal` = The error goal to be reached during training. Training stops when this goal is achieved.
- `net.trainParam.show` = The frequency at which information about the progress of the training will be displayed.
- `net.trainParam.mc` = The momentum term used in the training algorithm. This term helps to accelerate the convergence of the algorithm.
- `net.trainParam.min_grad` = The minimum value for the gradient. If the gradient falls below this value, training stops.
- `net.trainParam.mu` = The initial value for the update parameter μ used in the training algorithm. This parameter is better known as learning rate.
- `net.trainParam.mu_dec` = The rate at which the update parameter μ will be decreased during training.
- `net.trainParam.mu_inc` = The rate at which the update parameter μ will be increased during training

- `net.trainParam.max_fail` = the maximum number of consecutive epochs that the validation error can increase before training stops. This parameter helps to prevent overfitting as early stop.

Variations in the learning rate and optimization algorithm of the ANN were applied to the aforementioned hyperparameters, while keeping the others constant, with the aim of determining the optimal conditions for achieving the best performance and accuracy regarding the mean square error (MSE). A detailed description of the hyperparameters settings can be found in Section 3.4.1.

3.4.2 Hyperparameters Selection

The selection of hyperparameters involved establishing fixed and variable hyperparameters for the training processes of the proposed artificial neural network (ANN) in Section 3.2.5. The fixed parameters and their respective chosen values are detailed in Table 5.

Table 5. Fixed Hyperparameters for ANN Training.

<i>Hyperparameters</i>	<i>Set Configuration</i>
net.trainParam.epochs	2e+4
net.trainParam.goal	1e-9
net.trainParam.show	50
net.trainParam.mc	0.95
net.trainParam.min_grad	1e-10
net.trainParam.max_fail	2.5e+3

Similarly, the variable hyperparameters and their possible selected values correspond to those outlined in Table 6.

Table 6. Variable Hyperparameter for ANN Training.

<i>Hyperparameters</i>	<i>Set Configuration</i>	
trainFcn	traingd	trainrp

net.trainParam.mu	1e-3	
net.trainParam.mu_dec	0.1	
net.trainParam.mu_inc	10	
Configuration Tag	A	B

As a result of this configuration, the learning rate was adjusted in a procedural line using the parameter "net.trainParam.mu = 1e-3," making it more efficient than a single fixed setting for the entire training process of the ANN classifier. Consequently, as positive outcomes were achieved, the learning rate was automatically increased by an order of magnitude through the parameter "net.trainParam.mu_inc = 10" during training. Conversely, as negative outcomes were encountered, the learning rate was automatically decreased by an order of magnitude via the parameter "net.trainParam.mu_dec = 0.1" during training. Ultimately, two distinct optimization algorithms, suitable for the classification of large-scale data, were employed for two separate training sessions on the same dataset.

3.5 User Interface (UI) Prototype

3.5.1 User Interface Implementation – App Designer

The development of a user interface (UI) is an essential component for making this type of technology accessible to the general public. To achieve this, the App Designer tool from the MATLAB R2020a programming environment was utilized. This enabled the integration of person identification functionalities into a cohesive system. Additionally, the whole minor functionalities were incorporated to improve professionalism and user interaction with the system.

It is important to note that some functions were previously categorized (Figures 26, 27, 29, and 30) as 1UI, 2UI, 3UI, and 4UI, corresponding to User Interface (UI). These

functions were entirely transferred to App Designer, maintaining the same operational structure for the buttons containing these functions. In this way, our entire recognition system could be condensed into four convenient button options.

Additionally, a lamp was incorporated with a light that turns red while the selected button is in operation, changing to green once the function is completed, indicating to the user that they can proceed to use another function within the user interface. The decision was made to create the user interface in Spanish to make it accessible to a broader audience, thereby avoiding potential language barriers for new users. The following flowchart provides an overview of the person recognition system via gait biometrics (See Figure 31).



Figure 31. Final “BIOMETRIA DE LA MARCHA” User Interface.

3.6 Experimental Setup

3.6.1 Experiment 1: Dataset 1 – Configuration Tag A

For Experiment 1, the fixed hyperparameters described in Section 3.4.1 were considered, along with the variable hyperparameters in Configuration Tag A from Section 3.4.2. Additionally, Dataset 1, which consists of 5 subjects, was employed as described in Section 3.1.1. Table 7 summarizes the most significant variables to be considered for the training of the Artificial Neural Network (ANN) Classifier.

Table 7. Key Variables for ANN Classifier Training in Experiment 1 with Configuration Tag A and Dataset 1.

<i>CASIA-B Dataset</i>	<i>Configutarion Tag A</i>
5 Subjects	trainFcn = trainscg
	net.trainParam.mu = 1e-3
275 gait sequences	net.trainParam.mu_dec = 0.1
	net.trainParam.mu_inc = 10

3.6.2 Experiment 2: Dataset 1 – Configuration Tag B

For Experiment 2, the fixed hyperparameters described in Section 3.4.1 were considered, along with the variable hyperparameters in Configuration Tag B from Section 3.4.2. Additionally, Dataset 1, which consists of 5 subjects, was employed as described in Section 3.1.1. Table 8 summarizes the most significant variables to be considered for the training of the Artificial Neural Network (ANN) Classifier.

Table 8. Key Variables for ANN Classifier Training in Experiment 2 with Configuration Tag B and Dataset 1.

<i>CASIA-B Dataset</i>	<i>Configutarion Tag B</i>
5 Subjects	trainFcn = trainrp
	net.trainParam.mu = 1e-3
275 gait sequences	net.trainParam.mu_dec = 0.1
	net.trainParam.mu_inc = 10

3.6.3 Experiment 3: Dataset 2 – Configuration Tag A

For Experiment 3, the fixed hyperparameters described in Section 3.4.1 were considered, along with the variable hyperparameters in Configuration Tag A from Section 3.4.2. Additionally, Dataset 2, which consists of 10 subjects, was employed as described in Section 3.1.1. Table 9 summarizes the most significant variables to be considered for the training of the Artificial Neural Network (ANN) Classifier.

Table 9. Key Variables for ANN Classifier Training in Experiment 3 with Configuration Tag A and Dataset 2.

<i>CASIA-B Dataset</i>	<i>Configutarion Tag B</i>
10 Subjects	trainFcn = trainscg
	net.trainParam.mu = 1e-3
550 gait sequences	net.trainParam.mu_dec = 0.1
	net.trainParam.mu_inc = 10

3.6.4 Experiment 4: Dataset 2 – Configuration Tag B

For Experiment 4, the fixed hyperparameters described in Section 3.4.1 were considered, along with the variable hyperparameters in Configuration Tag B from Section 3.4.2. Additionally, Dataset 2, which consists of 10 subjects, was employed as described in Section 3.1.1. Table 10 summarizes the most significant variables to be considered for the training of the Artificial Neural Network (ANN) Classifier.

Table 10. Key Variables for ANN Classifier Training in Experiment 4 with Configuration Tag B and Dataset 2.

<i>CASIA-B Dataset</i>	<i>Configutarion Tag B</i>
10 Subjects	trainFcn = trainrp
	net.trainParam.mu = 1e-3
550 gait sequences	net.trainParam.mu_dec = 0.1
	net.trainParam.mu_inc = 10

3.6.5 Experiment 5: Dataset 3 – Configuration Tag A

For Experiment 5, the fixed hyperparameters described in Section 3.4.1 were considered, along with the variable hyperparameters in Configuration Tag A from Section

3.4.2. Additionally, Dataset 3, which consists of 25 subjects, was employed as described in Section 3.1.1. Table 11 summarizes the most significant variables to be considered for the training of the Artificial Neural Network (ANN) Classifier.

Table 11. Key Variables for ANN Classifier Training in Experiment 5 with Configuration Tag A and Dataset 3.

<i>CASIA-B Dataset</i>	<i>Configutarion Tag A</i>
25 Subjects	trainFcn = traincsg
	net.trainParam.mu = 1e-3
1375 gait sequences	net.trainParam.mu_dec = 0.1
	net.trainParam.mu_inc = 10

3.6.6 Experiment 6: Dataset 3 – Configuration Tag B

For Experiment 6, the fixed hyperparameters described in Section 3.4.1 were considered, along with the variable hyperparameters in Configuration Tag B from Section 3.4.2. Additionally, Dataset 3, which consists of 25 subjects, was employed as described in Section 3.1.1. Table 12 summarizes the most significant variables to be considered for the training of the Artificial Neural Network (ANN) Classifier.

Table 12. Key Variables for ANN Classifier Training in Experiment 6 with Configuration Tag B and Dataset 3.

<i>CASIA-B Dataset</i>	<i>Configutarion Tag B</i>
25 Subjects	trainFcn = trainrp
	net.trainParam.mu = 1e-3
1375 gait sequences	net.trainParam.mu_dec = 0.1
	net.trainParam.mu_inc = 10

3.7 Validation

3.7.1 Assessment Process

In general, the procedure for our gait biometric system involved input data in the form of gait silhouette sequences. To perform the feature extraction, the user-written function just

received the directory location, the number of sequences to load and the camera angle desired. These sequences underwent feature extraction, which generated a gait signature vector per image using geometric techniques described as the Geometric Moments Method and Euclidean Distance calculations. It is important to notice that a gait signature is generated per image present in a given sequence, as a result, the number of gait signatures is related to the number of images that were captured during the sequence recording originally.

The feature extracted gait signature vectors were stored in a database along with the assigned ID (biometric profile) for the corresponding subject. This allowed for the addition of various gait sequences to be assigned to the desired subject by simply indicating their ID.

Ultimately, the proposed Artificial Neural Network (ANN) architecture served as a low-computational resource classifier for small data sizes. Data division for all generated gait signatures vectors corresponding to 70% for training, 15% for test and 15% for validation. The ANN went under training according to the set hyperparameters and the generated model is saved for later use.

When loading a new gait sequence for identifying a potential user, the respective gait signature was extracted, the system loads the trained ANN classifier model with existing profiles, and the new gait signature was classified according to the most closely matching class. Furthermore, the integration of all these functionalities was achieved through a user interface for their respective execution as needed.

3.7.2 Metrics Calculation

In the context of performance evaluation for an Artificial Neural Networks (ANN), a fundamental approach is adopted by employing the Mean Squared Error (MSE) as a metric. The MSE serves as a prevalent measure for gauging the accuracy of an ANN when addressing regression-based problems. Essentially, the MSE quantifies the discrepancy

between the actual output variable value and the value predicted by the ANN. It is calculated as the average of squared errors for all predictions generated by the network on a given dataset. The squaring of errors is performed to impose a more stringent penalty on larger inaccuracies.

The formula for computing the MSE is expressed as follows:

$$MSE = \frac{1}{n} \times \sum (y - \hat{y})^2 \quad (6)$$

Where:

- n denotes the number of samples in the dataset.
- y represents the actual value of the output variable.
- \hat{y} corresponds to the value predicted by the ANN.

As a cost function, the MSE is employed during the training phase of the ANN, with the ultimate goal being its minimization. By reducing the MSE, the ANN enhances its ability to generate more accurate predictions, thereby improving its performance in tackling regression problems. Similarly, the R-value, also known as the correlation coefficient, ranges from -1 to 1. A value of 1 represents a perfect positive linear relationship, while -1 signifies a perfect negative linear relationship, and 0 indicates no linear relationship.

In a similar vein, confusion matrices were employed as they represent a more sophisticated approach in the generation of performance metrics. A confusion matrix is a commonly utilized tool in the field of machine learning, encompassing the use of Artificial Neural Networks (ANNs), for assessing the performance of classification models (See Figure 32).

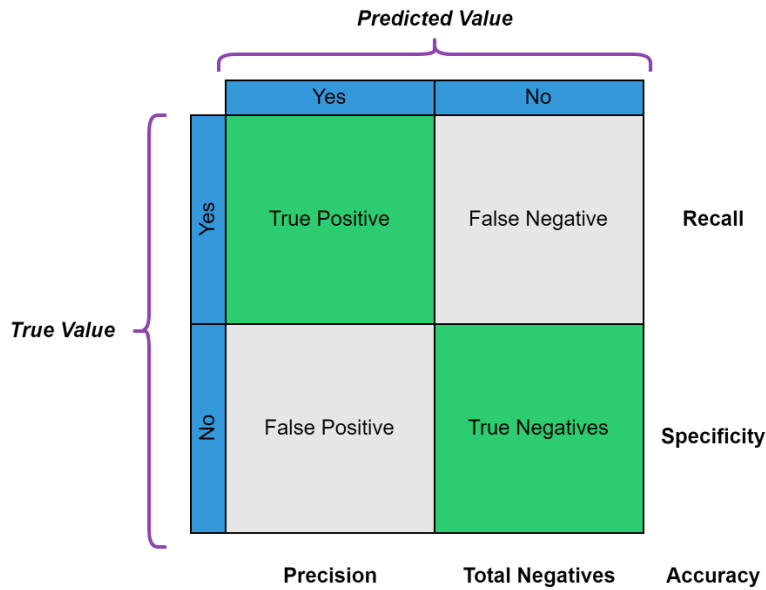


Figure 32. Schematic Representation for a Primary Confusion Matrix.

The confusion matrix entails the comparison of actual data labels with predictions made by the ANN. The matrix displays the prediction outcomes in tabular form, delineating classification results into four categories:

- *True Positives (TP)*: instances where the ANN accurately predicted a positive class.
- *False Positives (FP)*: instances where the ANN erroneously predicted a positive class.
- *True Negatives (TN)*: instances where the ANN accurately predicted a negative class.
- *False Negatives (FN)*: instances where the ANN erroneously predicted a negative class.

The confusion matrix facilitates the calculation of various metrics to evaluate the performance of the ANN, such as accuracy, sensitivity (also known as recall or true positive rate), specificity (true negative rate), and the F1 score. These metrics provide insights into the

performance of the ANN in classifying different classes, which can subsequently aid in refining and enhancing the model during the training process.

The metrics of precision, sensitivity, specificity, and F1-score are derived from the confusion matrix. The equations for each of these metrics are presented below:

- *Precision*: Measures the proportion of correct positive predictions among all positive predictions made by the ANN.

$$\mathbf{Precision} = \frac{\mathbf{TP}}{\mathbf{(TP + FP)}} \quad (7)$$

- *Sensitivity (Recall)*: Measures the proportion of true positives (TP) that were accurately identified by the ANN among all positive cases.

$$\mathbf{Sensitivity} = \frac{\mathbf{TP}}{\mathbf{(TP + FN)}} \quad (8)$$

- *Specificity*: measures the proportion of true negatives (TN) that were accurately identified by the ANN among all negative cases.

$$\mathbf{Specificity} = \frac{\mathbf{TN}}{\mathbf{(TN + FP)}} \quad (9)$$

- *F1-score*: a metric that combines the ANN's precision and sensitivity. It is particularly useful for evaluating the network's performance in cases involving imbalanced classes.

$$\mathbf{F1 - Score} = 2 \times \frac{\mathbf{Precision} \times \mathbf{Recall}}{\mathbf{Precision + Recall}} \quad (10)$$

- *Accuracy*: measures the total proportion of correct predictions, both positive and negative, made by the neural network among all predictions in the dataset.

$$\text{Accuracy} = \frac{(\text{TP} + \text{TN})}{(\text{TP} + \text{FP} + \text{TN} + \text{FN})} \quad (11)$$

In these equations, TP denotes the number of true positives, FP denotes the number of false positives, TN denotes the number of true negatives, and FN denotes the number of false negatives, all of which are obtained from the confusion matrix.

As a result, the literature preferred confusion matrices over MSE and the R-value of the regression coefficient for several reasons, especially when evaluating classification models. The main reason is that confusion matrices provide more comprehensive information about the performance of the model on different classes, while MSE and R-value are summary statistics that may not capture class-specific information. Some reasons for this preference include:

- **Interpretability:** Confusion matrices provide a clear, visual representation of the performance of the model across all classes, making it easy to interpret the results. It shows true positives, false positives, true negatives, and false negatives for each class, which enables a more detailed understanding of the strengths and weaknesses of the model.
- **Imbalanced datasets:** In cases where the dataset is imbalanced, with some classes having significantly more samples than others, the MSE and R-value may not provide a fair evaluation of the performance in the model. Confusion matrices can reveal how well the model performs on minority classes, which is crucial in many applications.
- **Multi-class problems:** For multi-class classification problems, confusion matrices can show the performance of a model for each class separately. In contrast, MSE and R-value give a single value summarizing the overall performance, which may not be informative enough for multi-class problems.

- Different error types: Confusion matrices allow users to differentiate between Type I (false positive) and Type II (false negative) errors, which may have different implications depending on the application. MSE and R-value do not provide this level of detail.
- Model comparison: Confusion matrices can be used to calculate various performance metrics, such as precision, recall, F1-score, and accuracy, which are helpful when comparing different models or tuning hyperparameters.

However, it is essential to note that using multiple evaluation metrics, including confusion matrices, MSE, and R-value, is able to provide a more comprehensive understanding of the performance in a model.

CHAPTER IV: Results

RESULTS

4.1 Results for Experimental Setups

4.1.1 Results – Experimental Setup 1

Experiment 1 involved training the artificial neural network classifier for a multiclass dataset 1 consisting of 5 individuals under the TAG A configuration. The recognition capabilities of the system were tested through its multiview evaluation, considering all 11 camera angles. Consequently, metrics related to the R-value for the correlation coefficient and mean squared error (MSE) were generated (Table 13). Then, confusion matrices were calculated for each camera angle and the metrics for precision, sensitivity, specificity, F1-score and accuracy and displayed in Appendix A, with the main accuracies per angle camera view summarized in Table 14. The main experimental results for the Experimental Setup 1 are presented below.

Table 13. Linear Regression (R-Value) and Mean Square Error Metrics (MSE) for All Camera View Angle, Dataset 1 – Configuration Tag A.

Camera Angle	Linear Regression (R-Value)				MSE
	Training	Test	Validation	All	Performance
0°	0.98278	0.94248	0.91903	0.96740	0.025019
18°	0.97322	0.86715	0.87080	0.94198	0.040402
36°	0.98438	0.83433	0.86822	0.94400	0.042631
54°	0.91560	0.79096	0.80501	0.88081	0.057774
72°	0.99735	0.89723	0.88599	0.96645	0.034948
90°	0.99953	0.94759	0.96549	0.98670	0.019070
108°	0.99799	0.90357	0.92468	0.97313	0.023683
126°	0.97366	0.86336	0.87818	0.94266	0.038307
144°	0.99123	0.81182	0.84446	0.94241	0.047809
162°	0.98238	0.89463	0.90428	0.95798	0.029624
180°	0.97765	0.90502	0.92080	0.95854	0.024629

Table 14. Total Accuracies Summarised for All Camera View Angle, Dataset 1 – Configuration Tag A.

Metrics (%)	Camera Angle										
	0°	18°	36°	54°	72°	90°	108°	126°	144°	162°	180°
Total Accuracy	97.18	92.11	87.81	87.40	93.36	97.84	94.98	91.72	91.32	94.48	97.20

4.1.2 Results – Experimental Setup 2

Experiment 2 involved training the artificial neural network classifier for a multiclass dataset 1 consisting of 5 individuals under the TAG B configuration. The recognition capabilities of the system were tested through its multiview evaluation, considering all 11 camera angles. Consequently, metrics related to the R-value for the correlation coefficient and mean squared error (MSE) were generated (Table 15). Then, confusion matrices were calculated for each camera angle and the metrics for precision, sensitivity, specificity, F1-score and accuracy and displayed in Appendix B, with the main accuracies per angle camera view summarized in Table 16. The main experimental results for the Experimental Setup 2 are presented below.

Table 15. Linear Regression (R-Value) and Mean Square Error Metrics (MSE) for All Camera View Angle, Dataset 1 – Configuration Tag B.

Camera Angle	Linear Regression (R-Value)			MSE	
	Training	Test	Validation	All	Performance
0°	0.97426	0.83439	0.88287	0.93879	0.037305
18°	0.96330	0.82488	0.79307	0.91666	0.064624
36°	0.94465	0.75281	0.75461	0.88625	0.076227
54°	0.95508	0.71967	0.73257	0.88702	0.081160
72°	0.97303	0.81897	0.81648	0.92554	0.058823
90°	0.99059	0.89809	0.92557	0.96716	0.023241
108°	0.96204	0.83480	0.86130	0.92756	0.043662
126°	0.93667	0.74981	0.77475	0.88443	0.067532
144°	0.89616	0.76093	0.79354	0.85953	0.062604
162°	0.98254	0.83523	0.82647	0.93635	0.055491
180°	0.97946	0.88602	0.88404	0.95140	0.036642

Table 16. Total Accuracy Summarised for All Camera View Angle, Dataset 1 – Configuration Tag B.

Metrics (%)	Camera Angle										
	0°	18°	36°	54°	72°	90°	108°	126°	144°	162°	180°
Total Accuracy	95.38	86.12	82.34	82.74	83.20	93.99	90.73	84.77	82.96	88.31	92.24

4.1.3 Results – Experimental Setup 3

Experiment 3 involved training the artificial neural network classifier for a multiclass dataset 2 consisting of 10 individuals under the TAG A configuration. The recognition capabilities of the system were tested through its multiview evaluation, considering all 11 camera angles. Consequently, metrics related to the R-value for the correlation coefficient and mean squared error (MSE) were generated (Table 17). Then, confusion matrices were calculated for each camera angle and the metrics for precision, sensitivity, specificity, F1-score and accuracy and displayed in Appendix C, with the main accuracies per angle camera view summarized in Table 18. The main experimental results for the Experimental Setup 3 are presented below.

Table 17. Linear Regression (R-Value) and Mean Square Error Metrics (MSE) for All Camera View Angle, Dataset 2 – Configuration Tag A.

Camera Angle	Linear Regression (R-Value)			MSE	
	Training	Test	Validation	All	Performance
0°	0.94883	0.81055	0.84430	0.91219	0.026447
18°	0.92364	0.76198	0.73816	0.87216	0.043779
36°	0.90072	0.65198	0.70123	0.83344	0.048695
54°	0.89469	0.69993	0.67725	0.83361	0.052714
72°	0.92951	0.76561	0.72785	0.87590	0.045132
90°	0.95506	0.82516	0.88625	0.92561	0.019658
108°	0.90931	0.78808	0.76348	0.87024	0.038495
126°	0.90794	0.72019	0.73188	0.85373	0.044347
144°	0.94012	0.74341	0.75885	0.88482	0.039717
162°	0.96897	0.76311	0.75653	0.90707	0.042133
180°	0.95947	0.83955	0.83439	0.92287	0.028711

Table 18. Total Accuracy Summarised for All Camera View Angle, Dataset 2 – Configuration Tag A.

Metrics (%)	Camera Angle										
	0°	18°	36°	54°	72°	90°	108°	126°	144°	162°	180°
Total Accuracy	90.26	77.84	71.36	71.14	79.11	90.52	82.74	75.64	76.30	82.00	90.08

4.1.4 Results – Experimental Setup 4

Experiment 4 involved training the artificial neural network classifier for a multiclass dataset 2 consisting of 10 individuals under the TAG B configuration. The recognition capabilities of the system were tested through its multiview evaluation, considering all 11 camera angles. Consequently, metrics related to the R-value for the correlation coefficient and mean squared error (MSE) were generated (Table 19). Then, confusion matrices were calculated for each camera angle and the metrics for precision, sensitivity, specificity, F1-score and accuracy and displayed in Appendix D, with the main accuracies per angle camera view summarized in Table 20. The main experimental results for the Experimental Setup 4 are presented below.

Table 19. Linear Regression (R-Value) and Mean Square Error Metrics (MSE) for All Camera View Angle, Dataset 2 – Configuration Tag B.

Camera Angle	Linear Regression (R-Value)			MSE	
	Training	Test	Validation	All	Performance
0°	0.88177	0.76312	0.72037	0.83798	0.047463
18°	0.75573	0.56435	0.56308	0.68191	0.064740
36°	0.69760	0.55179	0.52984	0.64816	0.069742
54°	0.72645	0.55888	0.53877	0.67144	0.067554
72°	0.87929	0.60555	0.64571	0.80237	0.057714
90°	0.84345	0.77188	0.74484	0.81832	0.040583
108°	0.91269	0.68260	0.70421	0.84670	0.049161
126°	0.80194	0.61283	0.60793	0.74376	0.060895
144°	0.77122	0.61663	0.60647	0.72245	0.058555
162°	0.81018	0.67288	0.63561	0.76242	0.057007
180°	0.91470	0.75289	0.75054	0.86387	0.043906

Table 20. Total Accuracy Summarised for All Camera View Angle, Dataset 2 – Configuration Tag B.

Metrics (%)	Camera Angle										
	0°	18°	36°	54°	72°	90°	108°	126°	144°	162°	180°
Total Accuracy	82.21	57.46	58.15	57.29	68.97	78.15	67.16	65.42	62.99	72.01	82.05

4.1.5 Results – Experimental Setup 5

Experiment 5 involved training the artificial neural network classifier for a multiclass dataset 3 consisting of 25 individuals under the TAG A configuration. The recognition capabilities of the system were tested through its multiview evaluation, considering all 11 camera angles. Consequently, metrics related to the R-value for the correlation coefficient and mean squared error (MSE) were generated (Table 21). Then, confusion matrices were calculated for each camera angle and the metrics for precision, sensitivity, specificity, F1-score and accuracy and displayed in Appendix E, with the main accuracies per angle camera view summarized in Table 22. The main experimental results for the Experimental Setup 5 are presented below.

Table 21. Linear Regression (R-Value) and Mean Square Error Metrics (MSE) for All Camera View Angle, Dataset 3 – Configuration Tag A.

Camera Angle	Linear Regression (R-Value)			MSE	
	Training	Test	Validation	All	Performance
0°	0.74166	0.62483	0.61395	0.70335	0.025057
18°	0.59563	0.47382	0.44969	0.55294	0.032088
36°	0.57787	0.38531	0.45408	0.52574	0.031327
54°	0.61992	0.46130	0.47746	0.57322	0.030624
72°	0.65822	0.54736	0.56941	0.62734	0.026447
90°	0.81688	0.70593	0.71199	0.78433	0.019204
108°	0.72557	0.57978	0.59799	0.68328	0.025775
126°	0.62667	0.48384	0.47784	0.58017	0.031314
144°	0.64771	0.48319	0.48182	0.59326	0.031919
162°	0.65519	0.53065	0.51254	0.61231	0.029540
180°	0.72533	0.61692	0.61968	0.68987	0.025033

Table 22. Total Accuracy Summarised for All Camera View Angle, Dataset 3 – Configuration Tag A.

Metrics (%)	Camera Angle										
	0°	18°	36°	54°	72°	90°	108°	126°	144°	162°	180°
Total Accuracy	64.01	43.35	39.67	45.69	52.99	71.85	56.59	50.30	49.27	51.33	64.90

4.1.6 Results – Experimental Setup 6

Experiment 6 involved training the artificial neural network classifier for a multiclass dataset 3 consisting of 25 individuals under the TAG B configuration. The recognition capabilities of the system were tested through its multiview evaluation, considering all 11 camera angles. Consequently, metrics related to the R-value for the correlation coefficient and mean squared error (MSE) were generated (Table 23). Then, confusion matrices were calculated for each camera angle and the metrics for precision, sensitivity, specificity, F1-score and accuracy and displayed in Appendix F, with the main accuracies per angle camera view summarized in Table 24. The main experimental results for the Experimental Setup 6 are presented below.

Table 23. Linear Regression (R-Value) and Mean Square Error Metrics (MSE) for All Camera View Angle, Dataset 3 – Configuration Tag B.

Camera Angle	Linear Regression (R-Value)			MSE	
	Training	Test	Validation	All	Performance
0°	0.52504	0.41695	0.43417	0.49229	0.032015
18°	0.43884	0.32578	0.34516	0.40536	0.034496
36°	0.42342	0.32188	0.32060	0.38927	0.035501
54°	0.49388	0.34824	0.36152	0.45004	0.034418
72°	0.59887	0.45270	0.48519	0.55730	0.030524
90°	0.74632	0.57145	0.61565	0.69736	0.024759
108°	0.61127	0.39803	0.46403	0.54800	0.031621
126°	0.56813	0.36214	0.41189	0.50803	0.033335
144°	0.46428	0.33024	0.31092	0.41753	0.036530
162°	0.58741	0.43741	0.44701	0.54258	0.031737
180°	0.50272	0.39495	0.39343	0.46786	0.033488

Table 24. Total Accuracy Summarised for All Camera View Angle, Dataset 3 – Configuration Tag B.

Metrics (%)	Camera Angle										
	0°	18°	36°	54°	72°	90°	108°	126°	144°	162°	180°
Total Accuracy	45.51	32.08	31.04	35.71	45.45	60.12	44.73	39.83	28.05	44.11	41.61

4.2 Results for User Interface (UI) Prototype

4.2.1 Inserting Individual Biometric Profile – Function

The individual data loading process, explained in Section 3.2.5, is designed for data structures different from CASIA-B, involving both the creation of new profiles and the addition of new information on an individual basis (See Figure 33).



Figure 33. User Interface Inserting Individual Biometric Profile – Function.

Upon executing the function, the user will be prompted to select the individual folder containing the image sequence to be added (See Figure 34).

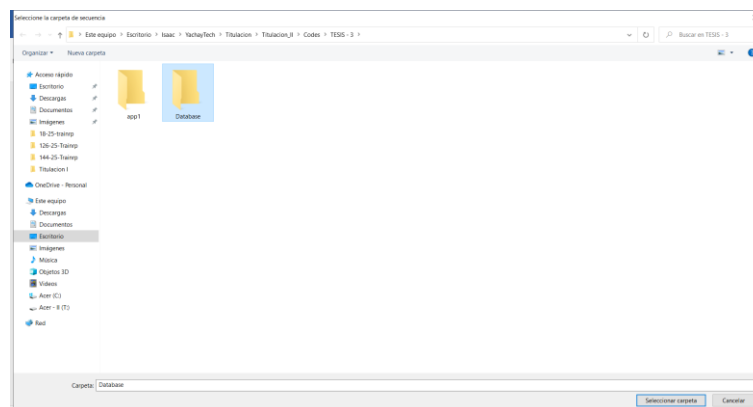


Figure 34. Selecting the Individual Folder for Image Sequence Addition.

Subsequently, it is necessary to provide the corresponding class number, ensuring it follows the proper numerical order. Thus, when entering a new biometric profile, the value can be the subsequent number to the highest existing class. Likewise, if the intention is to add new information to an existing biometric profile, simply assign the number of the profile to which the information will be added (See Figure 35).

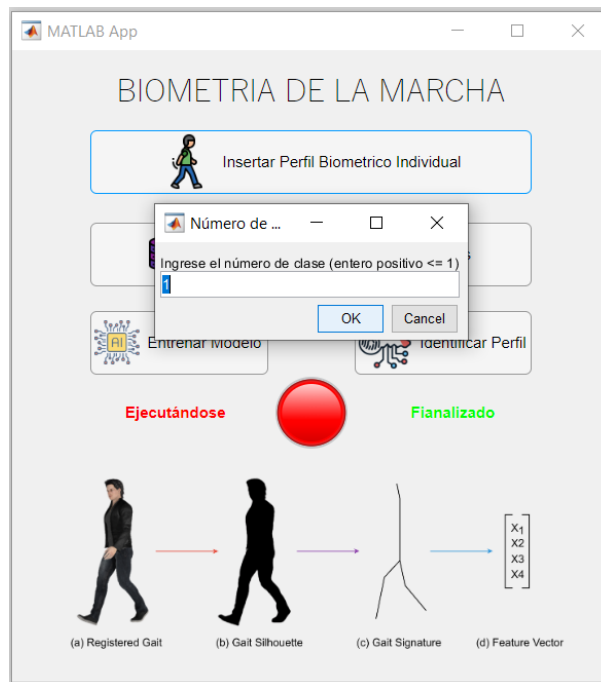


Figure 35. Providing Class Number for New and Existing Biometric Profiles.

Once this process is completed, the database will be created or updated with the newly added information. It is important to note that a lamp with a red LED will be lit while the function is in progress. Upon completion of the function execution, the lamp will change to a green LED, indicating that the user may now utilize the other available functions.

Additionally, the user can manually delete the database whenever required, either to load information from scratch or to test different configurations in data loading (See Figure 36).

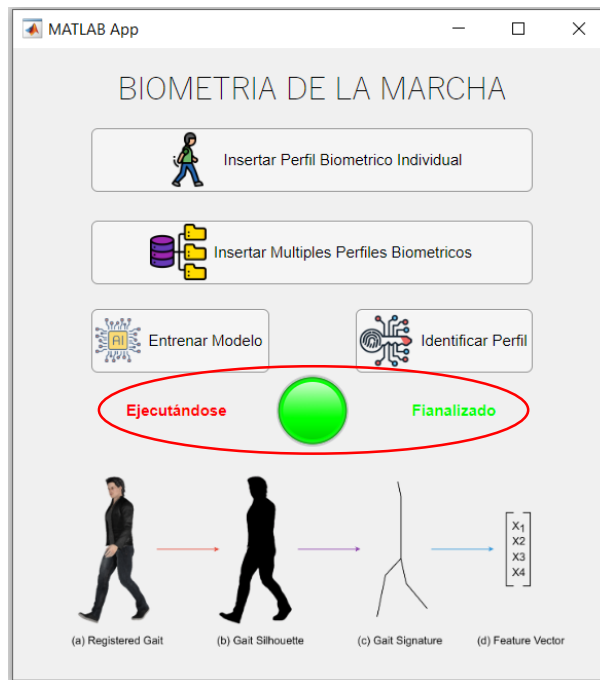


Figure 36. Final LED Indicators for Function Progress and Database Management.

4.2.2 Adding Multiple Biometric Profiles – Function

The multiple data loading method, as explained in Section 3.2.5, is designed for the CASIA-B data structure, as the data iteration requires a specific folder division and naming convention, similar to that presented in CASIA-B (See Figure 37).



Figure 37. User Interface Adding Multiple Biometric Profiles – Function.

Upon executing the function, the user will be prompted to select the CASIA-B folder, which will be stored as the parent folder for the process (See Figure 38).

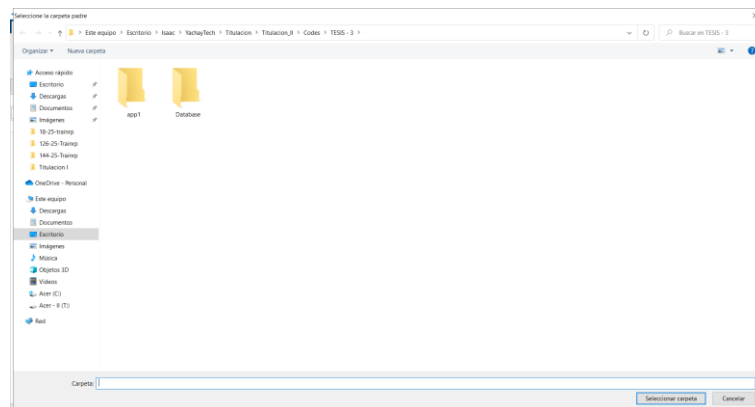


Figure 38. Selecting CASIA-B Folder Structure for Multiple Biometric Profiles.

Subsequently, the user must provide the number of subjects for which the information will be loaded, the number of sequences to load per subject, and the specific camera angle (See Figure 39).



Figure 39. Specifying Number of Subjects, Sequences, and Camera Angle.

After completing this process, the database will be created or updated with the new information added. Similarly, it is essential to consider that a lamp with a red LED will be lit while the function is in progress. Once the function execution is completed, the lamp will change to a green LED, allowing the user to utilize other available functions. Additionally, the user can manually delete the database whenever required, either to load information from scratch or to test different configurations in data loading.

4.2.3 Training Model – Function

The model training, as explained in Section 3.2.6, encompasses the neural network architecture and the necessary minor functions to load the existing data from the created database (See Figure 40).

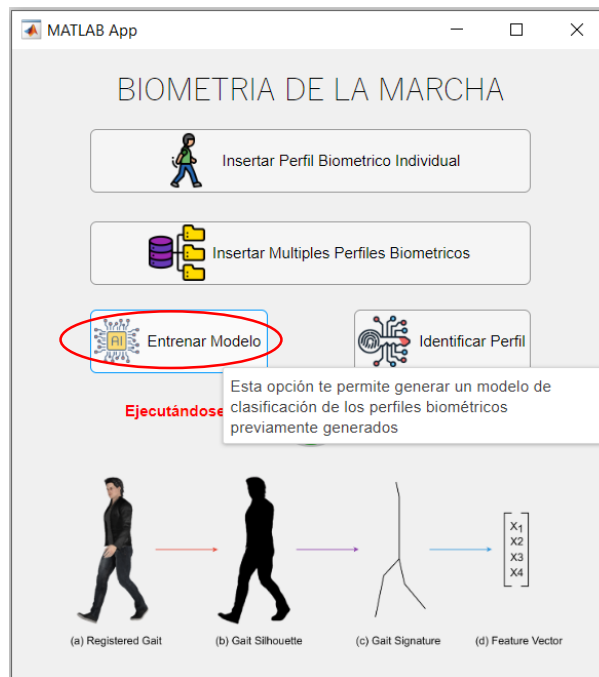


Figure 40. User Interface Training Model – Function.

Consequently, only an existing database is required for the function to be capable of training the model. This function generates a trained classifier model, metrics and confusion matrices to visualize the training results. Similar to the previous functions, it is essential to consider that a lamp with a red LED will be lit while the function is in progress. Once the function execution is completed, the lamp will change to a green LED, allowing the user to utilize other available functions.

4.2.4 Profile Identification – Function

Profile identification, as explained in Section 3.2.7, involves the process of biometric identification of a person through gait analysis (See Figure 41).



Figure 41. User Interface Profile Identification – Function.

Consequently, the data input corresponds to the selection of an individual folder containing the image sequence representing the gait of the person to be identified (See Figure 42).

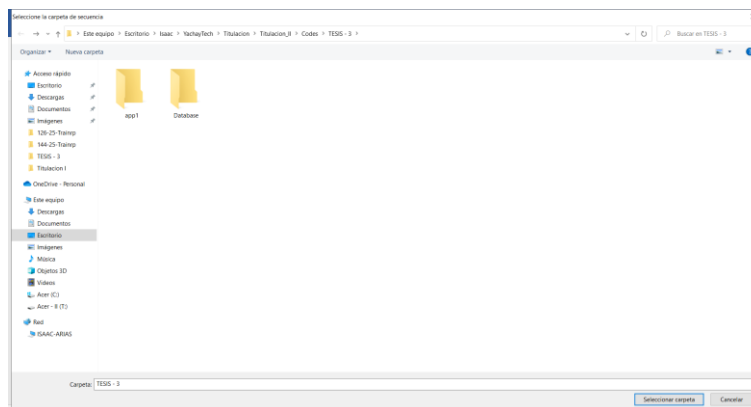


Figure 42. Selection of Individual Folder Containing the Image Sequence for Identification.

Upon completing this data input, the model displays the class with the highest prediction probability by simulating the data input in the previously trained model (See Figure 43).

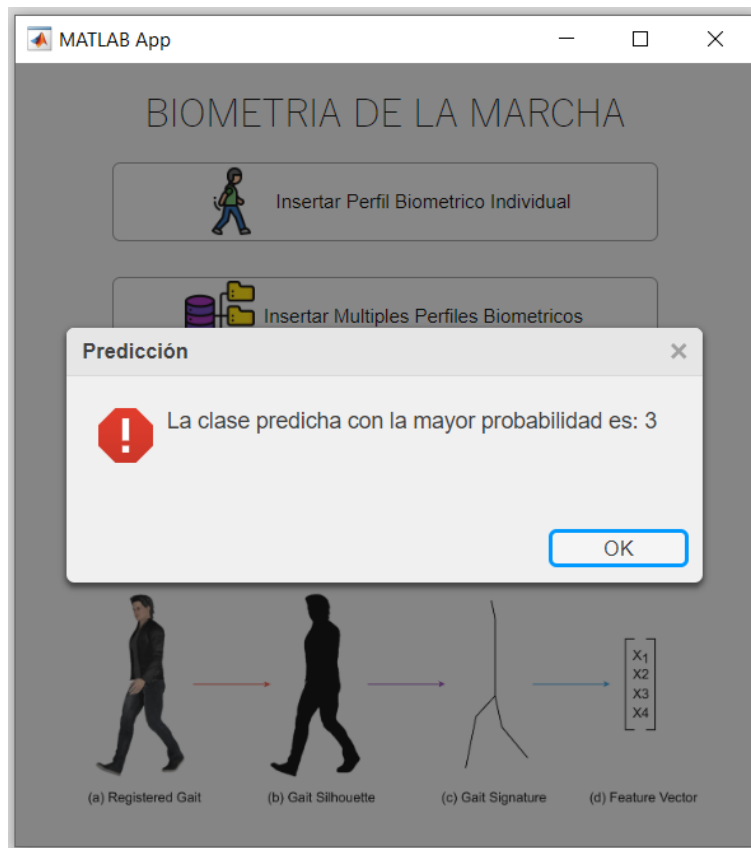


Figure 43. Selection of Individual Folder Containing the Image Sequence for Identification.

As with the previous functions, it is important to note that a lamp with a red LED will be lit while the function is in progress. Once the function execution is completed, the lamp will change to a green LED, allowing the user to utilize other available functions.

4.3 Biometric Software – Executable (.exe)

The user interface created in the App Designer environment enabled this research project to additionally generate an executable file (.exe) that encompasses all the features of the recognition system without requiring MATLAB to be installed. To accomplish this, the Application Compiler tool was first executed, which allowed for loading the parent file of our previously designed user interface (see Figure 44)

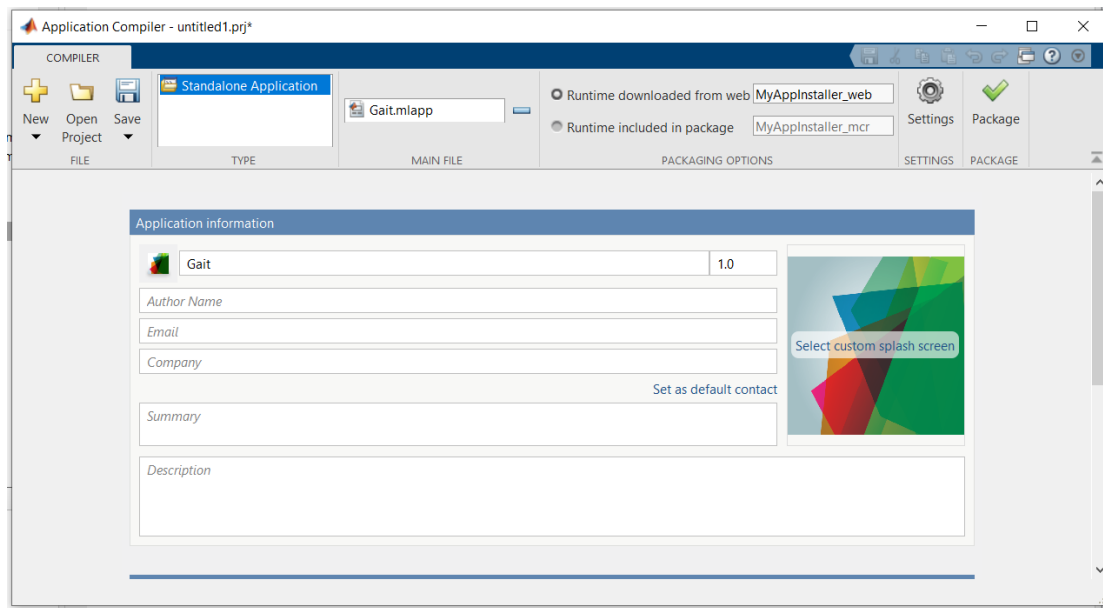


Figure 44. App Designer Interface and Application Compiler Tool.

Subsequently, the relevant information for redistributing our software upon executing the installer was provided. It is important to note that the information for the .exe installer was decided to be in Spanish to maintain the logical workflow initiated with the user interface, which also operates in Spanish (see Figure 45).

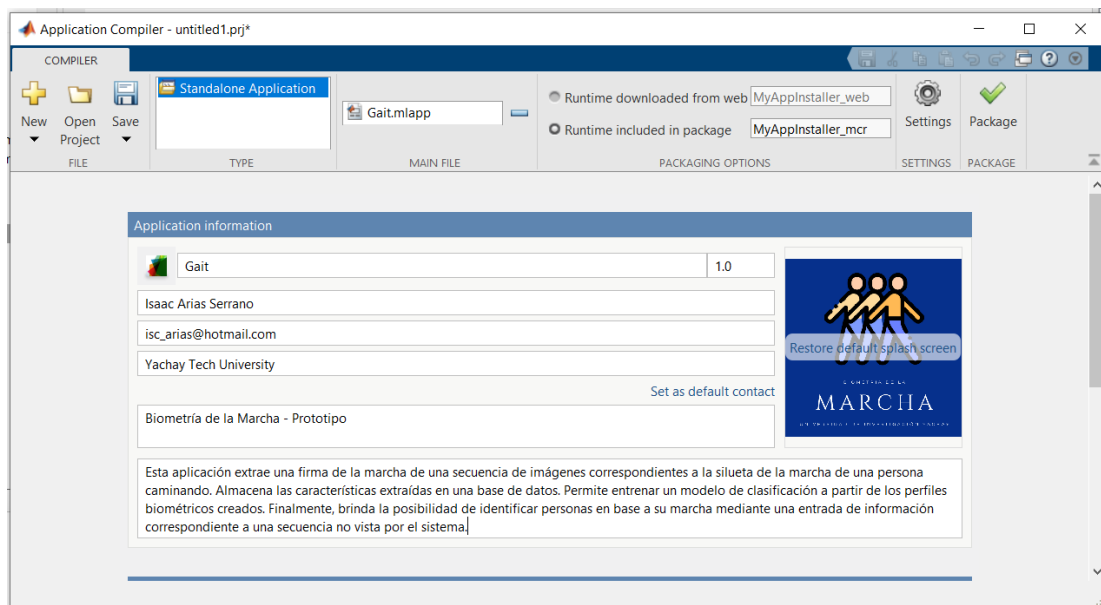


Figure 45. Application Installer Information.

After filling in the appropriate information, all the necessary functions for the user interface to operate were verified and loaded. This ensured that all functions described in Section 3.2 on Design and Implementation were entirely included and adequately

concatenated in the system compilation. Finally, an .exe file containing the complete gait biometrics software was compiled (see Figure 46).

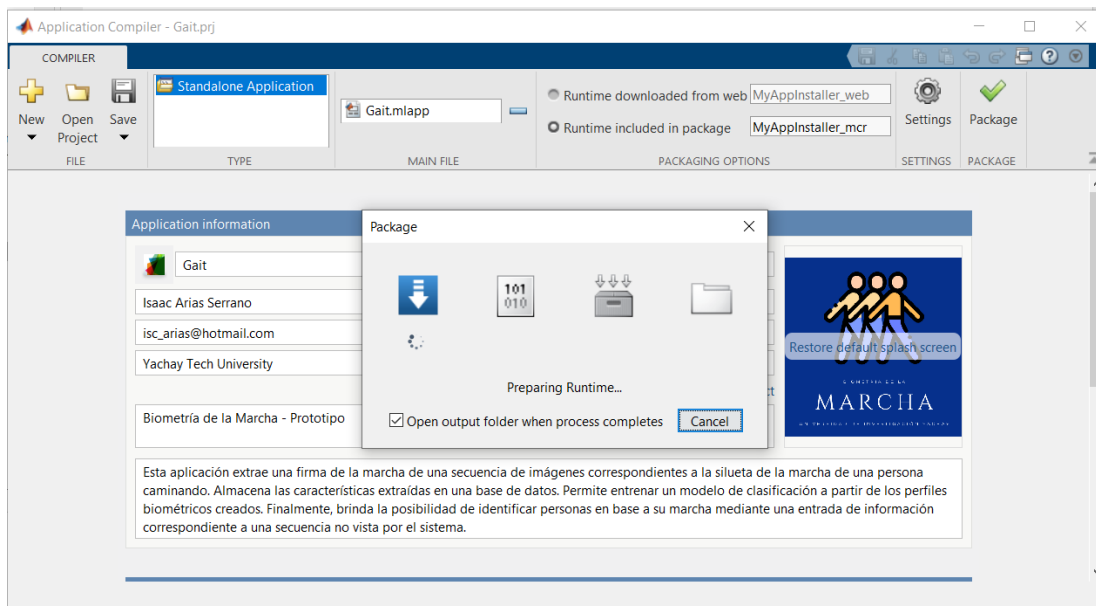


Figure 46. Application Installer Information.

CHAPTER V: Discussion

DISCUSSION

5.1 Discussion of Results

Upon completing the results report, it is essential to assess various aspects of the study. To this end, we must focus on the conducted experiments, where the evaluation of the proposed Artificial Neural Network (ANN) for gait biometrics was carried out across six distinct configurations. These configurations consisted of three separate dataset groups, each with two configurations labeled as TAG A and TAG B (Tables 5, 6).

In general, it is evident that the performance outcomes are considerably more favorable for the TAG A configuration (Tables 13, 14, 17, 18, 21, 22) compared to the TAG B configuration (Tables 15, 16, 19, 20, 23, 24). This observation holds true for both the metrics presented in Section 4.1 of Results and the advanced metrics featured in Appendices A, B, C, D, E, and F. A possible explanation for this performance difference lies in the hyperparameter settings associated with the two variants. Among the four configured hyperparameters, the "trainFcn" hyperparameter emerges as a potential factor contributing to the performance difference. As explained in Section 3.4.1 of Configurable Parameters, the "trainFcn" parameter determines the optimization algorithm employed for network learning.

The configurable hyperparameter "trainFcn" in MATLAB 2020a provides up to twelve possible optimization functions for designing an ANN. In this sense, according to (MathWorks, 2023b), there are no established rules regarding which hyperparameters perform best, nor are there optimal or default values. It is necessary to conduct experiments to identify the optimal hyperparameter configuration. In this sense, as mentioned in Section 3.4.2 of Hyperparameter Selection, the "trainscg" and "trainrp" functions are recommended for large data volumes (MathWorks, 2023b).

For the "trainscg" function, employed in the TAG A configuration, authors such as (Al-Kheraif et al., 2018) have reported their use for developing of a Charcot–Marie–Tooth disease recognition system using bacterial foraging optimization algorithm with ANN. Similarly, (Zhou et al., 2020) reported the use of the “trainscg” function for the electromyography (EMG) signal processing for hand motion pattern recognition using elemental machine learning algorithms. Also, (X. Zhang et al., 2018) employed the “trainscg” function for the determination of zinc oxide content of mineral medicine calamine using near-infrared spectroscopy based on ANN algorithms. According to (MathWorks, 2023b), the “trainscg” (Scaled Conjugate Gradient) function is a highly efficient optimization method requiring less memory since it does not need to store a second-order Hessian matrix. Instead, it utilizes first-order information (gradients) and scaled weight updates based on a line search approach.

Similarly, the performance demonstrated by the "trainrp" function, used in the TAG B configuration, should not be disregarded. Although it generated lower performance results, its application is also recommended for multiclass classification, as presented in this study. Authors such as (Ramkumar et al., 2021) reported the use for the electrocardiogram cardiac arrhythmias Classification using discrete wavelet transform, independent component analysis and multi-layer perceptron neural networks. Likewise, (Eshitha & Jose, 2018) used the “trainrp” function for hand and gesture recognition using ANNs. Equally, (Gandhi et al., 2022) described the usage of the “trainrp” function for a biosensor-assisted method for abdominal syndrome classification using a machine learning algorithm. According to (MathWorks, 2023b), the “trainrp” (Resilient Backpropagation) function is a variant of backpropagation that adjusts the weights and biases of the neural network using only the sign of the gradient, instead of its magnitude reporting efficacy and reduced memory usage at the computational level.

Linear regression (R-Value) and mean squared error (MSE) calculations, along with confusion matrices, are metrics that help evaluate the performance of an ANN. Nowadays, a reduced number of authors in gait biometrics literature has reported result in this format. For instance, (Sayed, 2018; Wang et al., 2018) compared the accuracy of Support Vector Machines, k-Nearest Neighbors, and ANNs classifiers for gait biometrics.

In the case of the proposed ANN classifier, higher performances can be observed in the six main experiments for the R-Values of the Training, Test, Validation, and All groups in the TAG A configuration (Tables 13, 17, 21) compared to those same groups in the TAG B configuration (Tables 15, 19, 23).

Similarly, it can be observed that the MSE calculation tends to be higher in the TAG B configuration, indicating that the classification conducted with this hyperparameter configuration is more prone to errors compared to the TAG A configuration. On the other hand, it is essential to consider the information mentioned in Section 3.7.2 of Metric Calculation, stating that although the R-Value and MSE are statistically significant metrics generated during the training of ANN models, they do not fully represent the behaviour of the model as confusion matrices do. However, they provide an initial general idea of the performance in a ANN.

Confusion matrices, like the R-Value and MSE, were calculated for each camera angle of each experiment. Given the extensive data generated by each experiment and camera angle, the metrics of Recall, Precision, Specificity, F1-Score, and Accuracy were comprehensively detailed in the Appendices of this thesis project. Nevertheless, to facilitate the display and analysis of the calculated metrics, it was decided to present only the Total Accuracy per camera angle in Section 4.1 of Results for Experimental Setups.

The schematic representation of total accuracy for the results report is based on the traditional format used by state-of-the-art gait biometrics authors such as (Battistone & Petrosino, 2019; Chao et al., 2019; Chen et al., 2018; Fan et al., 2020; Gupta, 2021; Y. He et al., 2019; Huang et al., 2021; Ibrahim et al., 2017; Liu et al., 2018; Luo et al., 2020; Ngo et al., 2014; Sokolova & Konushin, 2019; Song et al., 2019; Takemura et al., 2018; Wu et al., 2017; Yan et al., 2016; J. Zhang et al., 2020; Y. Zhang et al., 2020; Zou et al., 2018), who principally displayed the accuracies of their studies when making direct discussion comparisons to avoid excessive extension of results.

Upon analysing performance using the advanced metrics of Recall, Precision, Specificity, F1-Score, and Accuracy, detailed in the Appendices, the initial behaviour of the TAG A hyperparameter configuration outperforming the TAG B variant is reaffirmed. Furthermore, it is worth noting that the specificity of the ANN classification model remained globally above 90% for all experimental setups. On the other hand, recall, precision, and F1-score metrics tend to decline as the dataset size increases.

Likewise, some classes within the 25-subject groups exhibit performance rates of 0% in the confusion matrix metrics. However, the situation changes when examining the Accuracy of the model, as it represents the proportion of correct predictions relative to incorrect ones, providing a more global metric. Consequently, this is likely the primary reason why Total Accuracy is the preferred metric in gait biometrics research within the state of the art. By focusing on Total Accuracy, researchers avoid not only the need for extensive result metrics but also the display of low-performance metrics.

Although it is not within the objectives of this thesis project to propose a recognition model that surpasses the current state of the art in terms of gait biometrics performance metrics, the proposed gait biometrics model was also evaluated concerning a progressive data

volume to compare it with studies presented in the state of the art. In this regard, as observed in Section 3.3.1 of Data Selection, three different data volumes were proposed. A multiclass classification of five subjects was considered the primary approach, while classifications of 10 and 25 subjects were regarded as secondary classification approaches.

For the classification of 5 subjects, the model maintains an accuracy between 87.81% and 97.84% for the camera angles of the TAG A configuration (Table 14), with the 0° angle achieving 97.18%, the 90° angle reaching 97.84%, and the 180° angle attaining 97.20% as the best performing angles for individual identification. Conversely, the TAG B configuration (Table 16) exhibits lower performance, yielding metrics between 82.34% and 93.99%, with the 0° angle at 95.38%, the 90° angle at 93.99%, and the 180° angle at 92.24% continuing to demonstrate higher effectiveness in individual identification. For the Recall, Precision, Specificity, F1-Score, and Accuracy metrics, represented and calculated by camera angle in Appendix A and Appendix B, the TAG A configuration exhibits superiority over the TAG B configuration, making it the best configuration in this study for the identification of the 5-subject multiclass classification Dataset 1.

For the classification of 10 subjects, the model maintains a performance between 71.14% and 90.52% for the camera angles of the TAG A configuration (Table 18), with the 0° angle achieving 90.26%, the 90° angle reaching 90.52%, and the 180° angle attaining 90.08% as the best performing angles for individual identification, surpassing 90% in prediction performance compared to the other camera angles in the same experimental setup. On the other hand, the TAG B configuration (Table 20) exhibits lower performance, yielding metrics between 57.29% and 82.21%, with the 0° angle at 82.21%, the 90° angle at 78.15%, and the 180° angle at 82.05% continuing to demonstrate higher effectiveness in individual identification, albeit not as reliable as their TAG A counterpart. For the Recall, Precision, Specificity, F1-Score, and Accuracy metrics, represented and calculated by camera angle in

Appendix C and Appendix D, the TAG A configuration exhibits superiority over the TAG B configuration, making it the best configuration in this study for the identification of the 10-subject multiclass classification Dataset 2.

For the classification of 25 subjects, the model maintains a performance between 43.35% and 71.85% for the camera angles of the TAG A configuration (Table 22), with the 0° angle achieving 64.01%, the 90° angle reaching 71.85%, and the 180° angle attaining 64.90% as the best performing angles for individual identification. In contrast, the TAG B configuration (Table 24) exhibits lower performance, yielding metrics between 28.05% and 60.12%, with the 0° angle at 45.51%, the 90° angle at 60.12%, and the 180° angle at 41.61% continuing to demonstrate higher effectiveness in individual identification, albeit not as reliable as their TAG A counterpart. For the Recall, Precision, Specificity, F1-Score, and Accuracy metrics, represented and calculated by camera angle in Appendix E and Appendix F, the TAG A configuration exhibits superiority over the TAG B configuration, making it the best configuration in this study for the identification of the 25-subject multiclass classification Dataset 3.

Thus, although it is evident that both TAG A and TAG B configurations decline in performance as their datasets increase, it is at this point that the importance of selecting CASIA-B as the database for this study arises, as it allows for performance comparisons with other validated studies in the literature. In this regard, CASIA-B is the database employed by the majority of studies that have marked a turning point within the state-of-the-art in gait biometrics. Consequently, for generating multiclass classifications in CASIA-B, authors such as (Battistone & Petrosino, 2019; Chao et al., 2019; Fan et al., 2020; Y. He et al., 2019; Liu et al., 2018; Song et al., 2019; Wu et al., 2017; Yan et al., 2016; Y. Zhang et al., 2020) have proposed a high computational resource approach using Convolutional Neural Networks

(CNNs) and Graphics Processing Units (GPUs) that are fundamental for recognizing large data groups.

Utilizing CNNs and GPUs, these studies propose multiview identification models in which the models are generated by training on all possible views simultaneously. This approach contrasts with our low-resource, single-view model, where each classifier is trained exclusively with its respective camera angle. Consequently, multiview model evaluations omit identical-view assessments, whereas our single-view model employs the current view for evaluation. Comparing the results obtained in Table 24 for a 25-subject classification with the reported results in the literature for a 24-subject classification using the CASIA-B database with CNNs and GPUs, the following metrics have been obtained concerning the performance of the proposed models (Table 25).

Table 25. Total Accuracies for CASIA-B at 24-subjects Identification.

Accuracy (%)	Camera Angle										
	0°	18°	36°	54°	72°	90°	108°	126°	144°	162°	180°
VidDP (Hu et al., 2013)	–	–	–	59.1	–	50.2	–	57.5	–	–	–
CMCC (Kusakunniran et al., 2014)	46.3	–	–	52.4	–	48.3	–	56.9	–	–	–
CNN-LB (Wu et al., 2017)	54.8	–	–	77.8	–	64.9	–	76.1	–	–	–
GaitSet (Chao et al., 2022)	64.6	83.3	90.4	86.5	80.2	75.5	80.3	86.0	87.1	81.4	59.6
<i>Simple ANNs</i> (Ours)	64.01	43.35	39.67	45.69	52.99	71.85	56.59	50.30	49.27	51.33	64.90

As can be observed, our model, generated with low computational resources for the 25-subject dataset, is capable of competing with the reported literature in high computational resource classification tasks. It is on par with the 0°, 90°, and 180° views of a highly significant study nowadays, such as GaitSet reported by (Chao et al., 2022). However, our model can be considered only for single-view gait biometric identification since others evaluated all 11 possible camera angles.

It should be notice that the study presented by (Chao et al., 2022) marked a new standard in the state-of-the-art, as their classification capacity increases as the datasets grow, reaching accuracies of 90% in groups of 74-subjects in multiview classification, which is a remarkable achievement in the gait biometric literature. However, it is noticeable that the accuracies presented by (Chao et al., 2022) decline in performance as the dataset sizes decrease. In this regard, our classification model presented using ANN becomes reliable for small data groups and even competitive for 24-subject multiclass classification.

Additionally, (Chao et al., 2022) reported that it was necessary to employ eight GeForce GTX 1080 Ti GPUs to perform the classification tasks. Consequently, the required investment in computational resources to conduct research of this nature amounts to \$5,592, considering the retail price of each GeForce GTX 1080 Ti at \$699 according to (NVIDIA, 2017). In contrast, our study stands out significantly as the Artificial Neural Networks (ANNs) in our model are executed solely on a Central Processing Unit (CPU), entirely omitting the use of Convolutional Neural Networks (CNNs) and GPUs. This makes the investment cost for gait biometric research, such as those presented by (Chao et al., 2019) drop from \$5,592 to \$0.

From this perspective, it is important to notice that the low computational resource approach of this thesis project aimed to make gait biometrics a more accessible research area not to surpass the current literature, given high computational demand studies represent the main segment of state-of-the-art research. As a result, the fact that innovative literature currently reported in gait biometrics requires a substantial financial investment is an issue for average research. However, the proposed low computational resource model addresses the situation with an alternative low-cost model.

Furthermore, as described in the introduction of this thesis project, this study addresses the gap between recognition technologies and the prior knowledge required to employ them. Thus, a user-friendly, simple, and accessible user interface (UI) was developed, providing all the necessary functionalities to perform gait biometrics with low computational resources and allowing the management of biometric profiles by assigning a numeric ID to each subject (Figure 31). As outlined in Table 3 of the main authors in gait biometric systems reported in the literature, none of the reported systems by (Cao et al., 2018; Chao et al., 2019, 2022; Chen et al., 2018; Costilla-Reyes et al., 2021; Fan et al., 2020; Y. He et al., 2019; Liu et al., 2018; Luo et al., 2020; Martinho-Corbishley et al., 2019; Sokolova & Konushin, 2019; Song et al., 2019; Vandersmissen et al., 2018; Y. Zhang et al., 2020; Zou et al., 2018) offer a user interface.

The proposed user interface integrated the designed algorithms and functionalities into a single window with four main buttons, described in section 4.2 of Results for User Interface (UI) Prototype. In this sense, the UI was tested in their proposed function buttons to evaluate the interaction process, according to (Silistre et al., 2020) the user interface testing (UIT) is a validation process examining the state and behaviour of UI functions based on predetermined conditions established by the potential UI operator. From this point, it is debatable whether the number of integrated buttons and functionalities is sufficient since, according to (MathWorks, 2023a) in their App Building Manual, improvements in the integration of UI elements can always be applied.

For instance, while the Adding Multiple Biometric Profiles function allows for the generation of multiple profiles with a single command, it lacks the capability to perform multiple uploads for folders that deviate from the CASIA-B structure, making it an exclusive function for the CASIA-B repository. Consequently, the solution presented is the use of the

Inserting Individual Biometric Profile function, as the user provides the necessary labels, making it a viable function for adding other gait sequence repositories.

Similarly, the Training Model function, like Adding Multiple Biometric Profiles and Inserting Individual Biometric Profile, generates additional files for the user and the operation of the system. The user must independently explore the directory where the UI is located to obtain more information on the recognition aspects of the system. Although not strictly necessary, a possible option to avoid this is to create specific locations with buttons that allow users to view these files without manually opening them.

On the other hand, the integration of information loading through biometric profile labelling allows users to manage the gait features extracted at their discretion. This flexibility is highly restrictive in the current studies within the state of the art, as models presented by authors such as (Cao et al., 2018; Chao et al., 2019, 2022; Chen et al., 2018; Costilla-Reyes et al., 2021; Fan et al., 2020; Y. He et al., 2019; Liu et al., 2018; Luo et al., 2020; Martinho-Corbishley et al., 2019; Sokolova & Konushin, 2019; Song et al., 2019; Vandersmissen et al., 2018; Y. Zhang et al., 2020; Zou et al., 2018) focus solely on evaluating the performance of the model in a single-use context. This situation results in the gait information being non-editable and non-updatable, unlike our model, which allows the creation of biometric profiles as needed.

Moreover, this thesis project, with its UI developed in the App Designer environment, went beyond the research objectives and generated an executable file (.exe) to provide even greater accessibility to the gait biometric model. This is because the proposed model for person recognition through gait requires the user to have a version of MATLAB installed on their computer, as the process to execute the UI prototype still relies on the MATLAB programming environment. Based on the optimistic idea to provide an exceptional thesis

project, the gait biometric model was configured to be compiled, enabling to converted the proposed gait recognition model into inedited stand-alone software for installation on any computer. Consequently, the software was downloaded, installed (Figure 47 – 48), and successfully tested on a different computer with medium computational resources without GPU use, notice that the generated files by the biometric software containing metrics, biometric profiles and confusion matrices are circled in red (Figure 49 – 50).

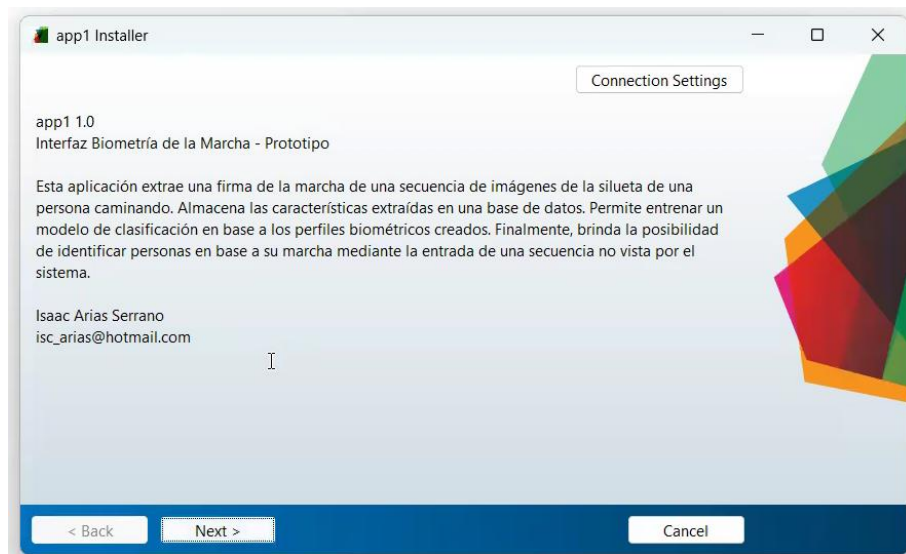


Figure 47. Final Software Installer .exe Information.

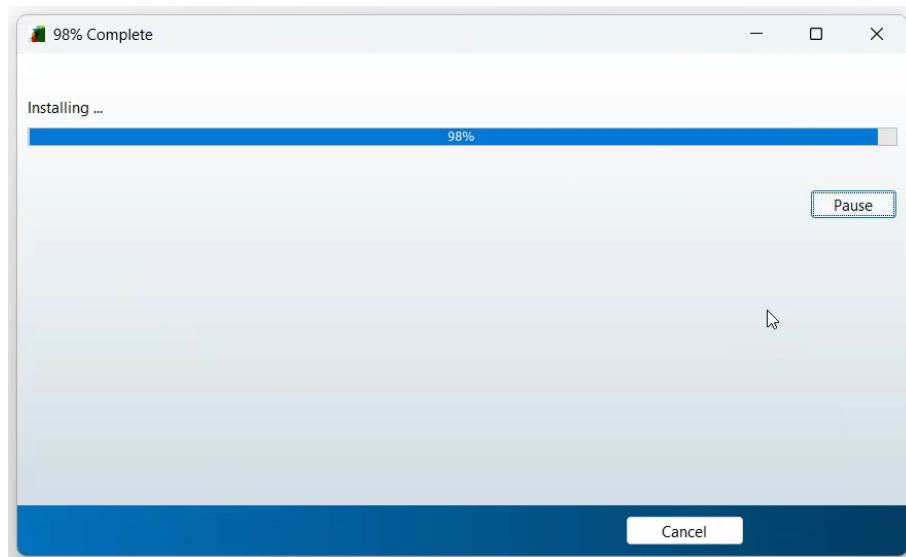


Figure 48. Installation of the Gait Biometric Software.

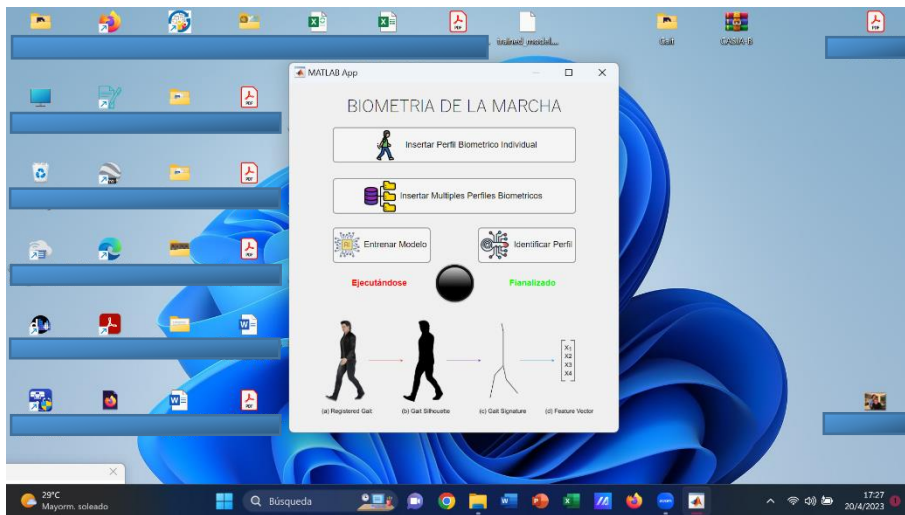


Figure 49. Main User Interface Window for the Gait Biometric Software.

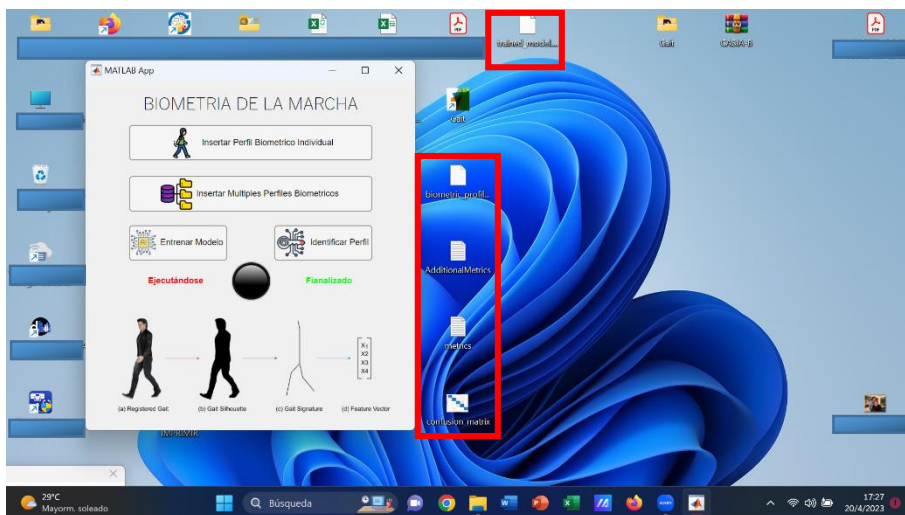


Figure 50. User Interface Testing Process for the Gait Biometric Software.

CHAPTER VI: Conclusions and Future Work

CONCLUSIONS AND FUTURE WORKS

6.1 Conclusions

This thesis project aimed to implement a neural network for the classification of gait features, maintaining low computational complexity for limited computational resources. Additionally, a user interface (UI) was created for non-specialist users to interact with the generated functionalities, enabling the management of data as biometric profiles. Consequently, the primary objective of the thesis project was achieved by maintaining a low-complexity computational approach through the use of elementary artificial intelligence techniques, as well as the presented UI prototype, which allowed for the effective, practical, and straightforward handling of the algorithms necessary for subject identification, while also managing the generated information as biometric IDs for labeled subjects.

Within the specific objectives, an elementary artificial neural network (ANN) for individual identification was developed. This ANN is described in terms of its functioning and architecture, providing a detailed understanding of the computational processing employed by the proposed model. Similarly, computer vision techniques were employed to analyze gait patterns of subjects for feature extraction, applying geometric moment methods and Euclidean distances.

Furthermore, not only was a UI proposed for non-specialist users, but the project went a step further beyond its specific objectives and generated an unprecedented software for gait biometrics. In addition to managing information as biometric profiles, the generated software can be installed on any computer without requiring MATLAB programming environment, thus making biometric technologies more accessible for researchers or average users.

Additionally, a database containing gait cycle images subject to clear protocols and accessible operability was acquired, ensuring a reliable data source and its validated use in the literature for other gait biometric research.

The proposed model was evaluated through various experimental sets encompassing a range of prediction models, differing in hyperparameter configurations and size. A total of sixty-six experiments were conducted due to the eleven camera angles and six proposed experimental sets, demonstrating the extensive evaluation and analysis efforts undertaken during the research.

While the current objective of the study is not to propose a gait biometrics model that competes with or surpasses the state-of-the-art, the supplementary comparison provides insight into the potential of the system. Although the model is limited compared to high computational resource studies, it effectively performs recognition tasks for small data groups.

6.2 Future Works

Future work could focus on surpassing performance metrics reported by other state-of-the-art studies. The currently proposed system provides a solid foundation for improvements focusing on more effective feature extraction, which has previously demonstrated its usefulness in person identification, considering that the implemented methods are accessible on low computational capacity computers.

Similarly, future work could develop research within the UI by complementing it with new functionalities that allow users better interaction between on-screen content and their actual requirements to fully exploit the capabilities of the software. Furthermore, new software versions could be generated that include continuous improvements to the biometric system, both in operability and the products generated from recognition tasks.

Finally, future work could implement the use of varied databases in their acquisition protocols, enabling the generation of gait biometric models with data inputs in uncontrolled scenarios. This would allow for simulating more realistic conditions in person identification tasks and enable a more comprehensive evaluation of the model compared to existing literature.

REFERENCES

- Adamović, S., Mišković, V., Maček, N., Milosavljević, M., Šarac, M., Saračević, M., & Gnjatović, M. (2020). An efficient novel approach for iris recognition based on stylometric features and machine learning techniques. *Future Generation Computer Systems*, *107*, 144–157. <https://doi.org/10.1016/j.future.2020.01.056>
- Al-Kheraif, A. A., Hashem, M., & Al Esawy, M. S. S. (2018). Developing Charcot–Marie–Tooth Disease Recognition System Using Bacterial Foraging Optimization Algorithm Based Spiking Neural Network. *Journal of Medical Systems*, *42*(10). <https://doi.org/10.1007/s10916-018-1049-8>
- Albeshar, R. A., Spittle, A. J., McGinley, J. L., & Dobson, F. L. (2019). Gait characteristics of children born preterm. *NeoReviews*, *20*(7), e397–e408. <https://doi.org/10.1542/neo.20-7-e397>
- Alharthi, A. S., Yunas, S. U., & Ozanyan, K. B. (2019). Deep Learning for Monitoring of Human Gait: A Review. *IEEE SENSORS JOURNAL*, *19*(21). <https://doi.org/10.1109/JSEN.2019.2928777>
- Amershi, S., Weld, D., Vorvoreanu, M., Fournery, A., Nushi, B., Collisson, P., Suh, J., Iqbal, S., Bennett, P. N., Inkpen, K., Teevan, J., Kikin-Gil, R., & Horvitz, E. (2019). Guidelines for human-AI interaction. *2020_ 스마트*, 1–13.
- B. Mazumdar, J. (2018). Retina Based Biometric Authentication System: a Review. *International Journal of Advanced Research in Computer Science*, *9*(1), 711–718. <https://doi.org/10.26483/ijarcs.v9i1.5322>
- Bach, M. M., Daffertshofer, A., & Dominici, N. (2021). The development of mature gait patterns in children during walking and running. *European Journal of Applied Physiology*, *121*(4), 1073–1085. <https://doi.org/10.1007/s00421-020-04592-2>
- Badihian, S., Adihian, N., & Yaghini, O. (2017). The Effect of Baby Walker on Child Development: A Systematic Review. *Iranian Journal of Child Neurology*, *11*(4), 1–6.
- Barbosa, I. B., Cristani, M., Del Bue, A., Bazzani, L., & Murino, V. (2012). Re-identification with RGB-D sensors. *Lecture Notes in Computer Science (Including Subseries Lecture Notes in Artificial Intelligence and Lecture Notes in Bioinformatics)*, *7583 LNCS(PART 1)*, 433–442. https://doi.org/10.1007/978-3-642-33863-2_43
- Battistone, F., & Petrosino, A. (2019). TGLSTM: A time based graph deep learning approach to gait recognition. *Pattern Recognition Letters*, *126*, 132–138. <https://doi.org/10.1016/j.patrec.2018.05.004>
- Bossard, L., Guillaumin, M., & Van, L. (2013). Event recognition in photo collections with a stopwatch HMM. *Proceedings of the IEEE International Conference on Computer Vision*, 1193–1200. <https://doi.org/10.1109/ICCV.2013.151>
- Bours, P., & Ellingsen, J. (2018). Cross Keyboard Keystroke Dynamics. *1st International Conference on Computer Applications and Information Security, ICCAIS 2018*. <https://doi.org/10.1109/CAIS.2018.8441945>
- Cao, P., Xia, W., Ye, M., Zhang, J., & Zhou, J. (2018). Radar-ID: Human identification based on radar micro-Doppler signatures using deep convolutional neural networks. *IET Radar, Sonar and Navigation*, *12*(7), 729–734. <https://doi.org/10.1049/iet-rsn.2017.0511>
- Chao, H., He, Y., Zhang, J., & Feng, J. (2019). GaitSet: Regarding gait as a set for cross-view gait recognition. *33rd AAAI Conference on Artificial Intelligence, AAAI 2019, 31st Innovative*

- Applications of Artificial Intelligence Conference, IAAI 2019 and the 9th AAI Symposium on Educational Advances in Artificial Intelligence, EAAI 2019, 16, 8126–8133.*
<https://doi.org/10.1609/aaai.v33i01.33018126>
- Chao, H., Wang, K., He, Y., Zhang, J., & Feng, J. (2022). GaitSet: Cross-View Gait Recognition Through Utilizing Gait As a Deep Set. *IEEE Transactions on Pattern Analysis and Machine Intelligence*, 44(7), 3467–3478. <https://doi.org/10.1109/TPAMI.2021.3057879>
- Chen, X., Weng, J., Lu, W., & Xu, J. (2018). Multi-Gait Recognition Based on Attribute Discovery. *IEEE Transactions on Pattern Analysis and Machine Intelligence*, 40(7), 1697–1710.
<https://doi.org/10.1109/TPAMI.2017.2726061>
- Cicirelli, G., Impedovo, D., Member, S., Dentamaro, V., Marani, R., Pirlo, G., & D, T. R. (2022). Human Gait Analysis in Neurodegenerative Diseases: A Review. *IEEE JOURNAL OF BIOMEDICAL AND HEALTH INFORMATICS*, 26(1), 229. <https://doi.org/10.1109/JBHI.2021.3092875>
- Code, P. W. (2023). CASIA-B. <https://paperswithcode.com/dataset/casia-b>
- Costilla-Reyes, O., Scully, P., Leroi, I., & Ozanyan, K. B. (2021). Age-Related Differences in Healthy Adults Walking Patterns under a Cognitive Task with Deep Neural Networks. *IEEE Sensors Journal*, 21(2), 2353–2363. <https://doi.org/10.1109/JSEN.2020.3021349>
- Eshitha, K. V., & Jose, S. (2018). Hand Gesture Recognition Using Artificial Neural Network. *2018 International Conference on Circuits and Systems in Digital Enterprise Technology, ICCSDET 2018*, 1–5. <https://doi.org/10.1109/ICCSDET.2018.8821076>
- Fan, C., Peng, Y., Cao, C., Liu, X., Hou, S., Chi, J., Huang, Y., Li, Q., & He, Z. (2020). GaitPart: Temporal part-based model for gait recognition. *Proceedings of the IEEE Computer Society Conference on Computer Vision and Pattern Recognition*, 14213–14221.
<https://doi.org/10.1109/CVPR42600.2020.01423>
- Filipi Gonçalves Dos Santos, C., Souza Oliveira, D. DE, Passos, L. A., Gonçalves Pires, R., Felipe Silva Santos, D., Pascotti Valem, L., Moreira, T. P., Cleison Santana, M. S., Roder, M., Paulo Papa, J., Paulo, S., Filipi Gonçalves dos Santos, C., de Souza Oliveira, D., Colombo, D., Luiz, W., & Carlos, S. (2021). Gait Recognition Based on Deep Learning: A Survey. *J. ACM*, 37(111), 35.
<https://doi.org/10.1145/3490235>
- Frank, J., Mannor, S., & Precup, D. (2011). Activity recognition with mobile phones. *Lecture Notes in Computer Science (Including Subseries Lecture Notes in Artificial Intelligence and Lecture Notes in Bioinformatics)*, 6913 LNAI(PART 3), 630–633. https://doi.org/10.1007/978-3-642-23808-6_44
- Frigon, A. (2017). The neural control of interlimb coordination during mammalian locomotion. *Journal of Neurophysiology*, 117(6), 2224–2241. <https://doi.org/10.1152/jn.00978.2016>
- Frigon, A., Akay, T., & Prilutsky, B. I. (2022). Control of Mammalian Locomotion by Somatosensory Feedback. *Comprehensive Physiology*, 12(1), 2877–2947.
<https://doi.org/10.1002/cphy.c210020>
- Gandhi, C., Ahmad, S. S., Mehbodniya, A., Webber, J. L., Hemalatha, S., Elwahsh, H., & Tiwari, B. (2022). Biosensor-Assisted Method for Abdominal Syndrome Classification Using Machine Learning Algorithm. *Computational Intelligence and Neuroscience*, 2022.
<https://doi.org/10.1155/2022/4454226>
- Gupta, S. K. (2021). Reduction of covariate factors from Silhouette image for robust gait recognition. *Multimedia Tools and Applications*, 80(28–29), 36033–36058. <https://doi.org/10.1007/s11042-021-10941-w>

- Hadjkacem, B., Ayedi, W., Ayed, M. Ben, Alshaya, S. A., & Abid, M. (2020). A novel Gait-Appearance-based Multi-Scale Video Covariance Approach for pedestrian (re)-identification. *Engineering Applications of Artificial Intelligence*, 91(February), 103566. <https://doi.org/10.1016/j.engappai.2020.103566>
- Harris, E. J., Khoo, I. H., & Demircan, E. (2022). A Survey of Human Gait-Based Artificial Intelligence Applications. *Frontiers in Robotics and AI*, 8(January), 1–28. <https://doi.org/10.3389/frobt.2021.749274>
- He, S., & Li, P. (2020). A MATLAB based graphical user interface (GUI) for quickly producing widely used hydrogeochemical diagrams. *Chemie Der Erde*, 80(4). <https://doi.org/10.1016/j.chemer.2019.125550>
- He, Y., Zhang, J., Shan, H., & Wang, L. (2019). Multi-Task GANs for view-specific feature learning in gait recognition. *IEEE Transactions on Information Forensics and Security*, 14(1), 102–113. <https://doi.org/10.1109/TIFS.2018.2844819>
- Hernandez-de-Menendez, M., Morales-Menendez, R., Escobar, C. A., & Arinez, J. (2021). Biometric applications in education. *International Journal on Interactive Design and Manufacturing*, 15(2–3), 365–380. <https://doi.org/10.1007/s12008-021-00760-6>
- Hofmann, M., Geiger, J., Bachmann, S., Schuller, B., & Rigoll, G. (2014). The TUM Gait from Audio, Image and Depth (GAID) database: Multimodal recognition of subjects and traits. *Journal of Visual Communication and Image Representation*, 25(1), 195–206. <https://doi.org/10.1016/j.jvcir.2013.02.006>
- Horst, F., Lapuschkin, S., Samek, W., Müller, K. R., & Schöllhorn, W. I. (2019). Explaining the unique nature of individual gait patterns with deep learning. *Scientific Reports*, 9(1), 1–13. <https://doi.org/10.1038/s41598-019-38748-8>
- Horst, F., Mildner, M., & Schöllhorn, W. I. (2017). One-year persistence of individual gait patterns identified in a follow-up study – A call for individualised diagnose and therapy. *Gait and Posture*, 58, 476–480. <https://doi.org/10.1016/j.gaitpost.2017.09.003>
- Hu, M., Wang, Y., Zhang, Z., Little, J. J., & Huang, D. (2013). View-Invariant discriminative projection for multi-View gait-Based human identification. *IEEE Transactions on Information Forensics and Security*, 8(12), 2034–2045. <https://doi.org/10.1109/TIFS.2013.2287605>
- Huang, B., Xiong, C., Chen, W., Liang, J., Sun, B.-Y., & Gong, X. (2021). *Common kinematic synergies of various human locomotor behaviours*. <https://doi.org/10.1098/rsos.210161>
- Ibrahim, D. R., Tamimi, A. A., Abdalla, A. M., & Modality, A. F. (2017). *Performance Analysis of Biometric Recognition Modalities*. 980–984.
- Israa, A. (2015). Physiological Biometric Authentication Systems, Advantages, Disadvantages And Future Development: A Review. *International Journal of Scientific & Technology Research.*, 1(1), 7.
- Isvoranu, G., Manole, E., & Neagu, M. (2021). Gait analysis using animal models of peripheral nerve and spinal cord injuries. *Biomedicines*, 9(8). <https://doi.org/10.3390/biomedicines9081050>
- Iwama, H., Okumura, M., Makihara, Y., & Yagi, Y. (2012). The OU-ISIR gait database comprising the large population dataset and performance evaluation of gait recognition. *IEEE Transactions on Information Forensics and Security*, 7(5), 1511–1521. <https://doi.org/10.1109/TIFS.2012.2204253>
- Jung, Y. J., & Yeop, J. (2016). *Gait Phase Detection Using Force Sensing Resistors*. 20(12), 210–211.

- Kabbaligere, R., & Layne, C. S. (2019). Adaptation in Gait to body-weight unloading. *Applied Sciences (Switzerland)*, *9*(21). <https://doi.org/10.3390/app9214494>
- Khan, S. A., & Naaz, S. (2020). Comparative Analysis of Finger Vein, Iris and Human Body Odor as Biometric Approach in Cyber Security System. *2nd International Conference on Innovative Mechanisms for Industry Applications, ICIMIA 2020 - Conference Proceedings, Icimia*, 525–530. <https://doi.org/10.1109/ICIMIA48430.2020.9074877>
- Khera, P., & Kumar, N. (2020). Role of machine learning in gait analysis: a review. *Journal of Medical Engineering and Technology*, *44*(8), 441–467. <https://doi.org/10.1080/03091902.2020.1822940>
- Klöpfer-Krämer, I., Brand, A., Wackerle, H., Müßig, J., Kröger, I., & Augat, P. (2020). Gait analysis – Available platforms for outcome assessment. *Injury*, *51*(xxxx), S90–S96. <https://doi.org/10.1016/j.injury.2019.11.011>
- Kuiper, M. J., Brandsma, R., Lunsing, R. J., Eggink, H., ter Horst, H. J., Bos, A. F., & Sival, D. A. (2019). The neurological phenotype of developmental motor patterns during early childhood. *Brain and Behavior*, *9*(1), 1–8. <https://doi.org/10.1002/brb3.1153>
- Kukreja, V., Kumar, D., & Kaur, A. (2021). Deep learning in Human Gait Recognition: An Overview. *2021 International Conference on Advance Computing and Innovative Technologies in Engineering, ICACITE 2021*, *7*, 9–13. <https://doi.org/10.1109/ICACITE51222.2021.9404611>
- Kusakunniran, W., Wu, Q., Zhang, J., Li, H., & Wang, L. (2014). Recognizing Gaits Across Views Through Correlated Motion Co-Clustering. *IEEE Transactions on Image Processing*, *23*(2), 696–709. <https://doi.org/10.1109/TIP.2013.2294552>
- Liu, W., Zhang, C., Ma, H., & Li, S. (2018). Learning Efficient Spatial-Temporal Gait Features with Deep Learning for Human Identification. *Neuroinformatics*, *16*(3–4), 457–471. <https://doi.org/10.1007/s12021-018-9362-4>
- Luo, C., Wu, J., Li, J., Wang, J., Xu, W., Ming, Z., Wei, B., Li, W., & Zomaya, A. Y. (2020). Gait Recognition as a Service for Unobtrusive User Identification in Smart Spaces. *ACM Transactions on Internet of Things*, *1*(1), 1–21. <https://doi.org/10.1145/3375799>
- Malloggi, C., Zago, M., Galli, M., Sforza, C., Scarano, S., & Tesio, L. (2021). Kinematic patterns during walking in children: Application of principal component analysis. *Human Movement Science*, *80*(November), 102892. <https://doi.org/10.1016/j.humov.2021.102892>
- Mani, H., Miyagishima, S., Kozuka, N., Inoue, T., Hasegawa, N., & Asaka, T. (2021). Development of the Relationships Among Dynamic Balance Control, Inter-limb Coordination, and Torso Coordination During Gait in Children Aged 3–10 Years. *Frontiers in Human Neuroscience*, *15*(October), 1–11. <https://doi.org/10.3389/fnhum.2021.740509>
- Mansouri, N., Issa, M. A., & Jemaa, Y. Ben. (2018). Gait features fusion for efficient automatic age classification. *IET Computer Vision*, *12*(1), 69–75. <https://doi.org/10.1049/iet-cvi.2017.0055>
- Marín, J., Blanco, T., de la Torre, J., & Marín, J. J. (2020). Gait analysis in a box: A system based on magnetometer-free IMUs or clusters of optical markers with automatic event detection. *Sensors (Switzerland)*, *20*(12), 1–27. <https://doi.org/10.3390/s20123338>
- Marín, J., Blanco, T., Marín, J. J., Moreno, A., Martitegui, E., & Aragüés, J. C. (2019). Integrating a gait analysis test in hospital rehabilitation: A service design approach. *PLoS ONE*, *14*(10), 1–23. <https://doi.org/10.1371/journal.pone.0224409>
- Marin, J., Marin, J. J., Blanco, T., de la Torre, J., Salcedo, I., & Martitegui, E. (2020). Is my patient improving? Individualized gait analysis in rehabilitation. *Applied Sciences (Switzerland)*, *10*(23),

1–18. <https://doi.org/10.3390/app10238558>

- Martinho-Corbishley, D., Nixon, M. S., & Carter, J. N. (2019). Super-Fine Attributes with Crowd Prototyping. *IEEE Transactions on Pattern Analysis and Machine Intelligence*, 41(6), 1486–1500. <https://doi.org/10.1109/TPAMI.2018.2836900>
- MathWorks. (2015). Creating Graphical User Interfaces R2015a. In *The MathWorks, Inc.*
- MathWorks. (2023a). App Building R2023a. *The MathWorks, Inc.*
- MathWorks. (2023b). Programming Fundamentals R2023a. In *The MathWorks, Inc.*
- Mitchell, C., & Shing, C. C. (2018). Discussing alternative login methods and their advantages and disadvantages. *ICNC-FSKD 2018 - 14th International Conference on Natural Computation, Fuzzy Systems and Knowledge Discovery*, 1353–1356. <https://doi.org/10.1109/FSKD.2018.8687163>
- More, S. A., & Deore, P. J. (2018). Gait Recognition by Cross Wavelet Transform and Graph Model. *IEEE/CAA Journal of Automatica Sinica*, 5(3), 718–726. <https://doi.org/10.1109/JAS.2018.7511081>
- Ngo, T. T., Makihara, Y., Nagahara, H., Mukaigawa, Y., & Yagi, Y. (2014). The largest inertial sensor-based gait database and performance evaluation of gait-based personal authentication. *Pattern Recognition*, 47(1), 228–237. <https://doi.org/10.1016/j.patcog.2013.06.028>
- NVIDIA. (2017). *GeForce GTX 1080 Ti*. <https://www.nvidia.com/en-us/geforce/news/gfecnt/nvidia-geforce-gtx-1080-ti/#:~:text=Featuring the most powerful and,the %241200 NVIDIA TITAN X.>
- Parashar, A., Parashar, A., Ding, W., Shekhawat, R. S., & Rida, I. (2023). Deep learning pipelines for recognition of gait biometrics with covariates: a comprehensive review. *Artificial Intelligence Review*, 1–65. <https://doi.org/10.1007/S10462-022-10365-4/TABLES/6>
- Prakash, C., Kumar, R., & Mittal, N. (2018). Recent developments in human gait research: parameters, approaches, applications, machine learning techniques, datasets and challenges. *Artificial Intelligence Review*, 49(1), 1–40. <https://doi.org/10.1007/s10462-016-9514-6>
- Ramkumar, M., Ganesh Babu, C., Vinoth Kumar, K., Hepsiba, D., Manjunathan, A., & Sarath Kumar, R. (2021). ECG Cardiac arrhythmias Classification using DWT, ICA and MLP Neural Networks. *Journal of Physics: Conference Series*, 1831(1). <https://doi.org/10.1088/1742-6596/1831/1/012015>
- Ratcliffe, L., & Puthusserypady, S. (2020). Importance of Graphical User Interface in the design of P300 based Brain–Computer Interface systems. *Computers in Biology and Medicine*, 117(December 2019), 103599. <https://doi.org/10.1016/j.compbiomed.2019.103599>
- Rathor, R., Kumar Singh, A., Choudhary, H., Goswami, C., & Fekete, G. (2020). A systematic review on gait analysis methods and assistive devices in lower limb prosthetics. *Materials Today: Proceedings*, 44(xxxx), 4251–4255. <https://doi.org/10.1016/j.matpr.2020.10.541>
- Rayner, M. L. D., Brown, H. L., Wilcox, M., Phillips, J. B., & Quick, T. J. (2020). Quantifying regeneration in patients following peripheral nerve injury. *Journal of Plastic, Reconstructive and Aesthetic Surgery*, 73(2), 201–208. <https://doi.org/10.1016/j.bjps.2019.10.007>
- Rose, V. L., & Arellano, C. J. (2021). Simple models highlight differences in the walking biomechanics of young children and adults. *Journal of Experimental Biology*, 224(22). <https://doi.org/10.1242/jeb.243040>
- Russo, A. Di, Stanev, D., Armand, S., & Ijspeert, A. (2021). Sensory modulation of gait characteristics in human locomotion: A neuromusculoskeletal modeling study. In *PLoS Computational Biology*

(Vol. 17, Issue 5). <https://doi.org/10.1371/journal.pcbi.1008594>

- Sarkar, S., Phillips, P. J., Liu, Z., Vega, I. R., Grother, P., & Bowyer, K. W. (2005). The humanID gait challenge problem: Data sets, performance, and analysis. *IEEE Transactions on Pattern Analysis and Machine Intelligence*, 27(2), 162–177. <https://doi.org/10.1109/TPAMI.2005.39>
- Sayed, M. (2018). Biometric gait recognition based on machine learning algorithms. *Journal of Computer Science*, 14(7), 1064–1073. <https://doi.org/10.3844/jcssp.2018.1064.1073>
- Senut, B., Pickford, M., Gommery, D., & Ségalen, L. (2018). Palaeoenvironments and the origin of hominid bipedalism. *Historical Biology*, 30(1–2), 284–296. <https://doi.org/10.1080/08912963.2017.1286337>
- Silistre, A., Kilincceker, O., Belli, F., Challenger, M., & Kardas, G. (2020). Models in Graphical User Interface Testing: Study Design. *2020 Turkish National Software Engineering Symposium, UYMS 2020 - Proceedings*. <https://doi.org/10.1109/UYMS50627.2020.9247072>
- Sokolova, A., & Konushin, A. (2019). Pose-based deep gait recognition. *IET Biometrics*, 8(2), 134–143. <https://doi.org/10.1049/iet-bmt.2018.5046>
- Song, C., Huang, Y., Huang, Y., Jia, N., & Wang, L. (2019). GaitNet: An end-to-end network for gait based human identification. *Pattern Recognition*, 96, 106988. <https://doi.org/10.1016/j.patcog.2019.106988>
- Stenum, J., Cherry-Allen, K. M., Pyles, C. O., Reetzke, R. D., Vignos, M. F., & Roemmich, R. T. (2021). Applications of pose estimation in human health and performance across the lifespan. *Sensors*, 21(21). <https://doi.org/10.3390/s21217315>
- Takemura, N., Makihara, Y., Muramatsu, D., Echigo, T., & Yagi, Y. (2018). Multi-view large population gait dataset and its performance evaluation for cross-view gait recognition. *IPSI Transactions on Computer Vision and Applications*, 10(1). <https://doi.org/10.1186/s41074-018-0039-6>
- Thiele, M., Hepach, R., Michel, C., & Haun, D. (2021). Infants' Preference for Social Interactions Increases from 7 to 13 Months of Age. *Child Development*, 92(6), 2577–2594. <https://doi.org/10.1111/cdev.13636>
- Vandersmissen, B., Knudde, N., Jalalvand, A., Couckuyt, I., Bourdoux, A., De Neve, W., & Dhaene, T. (2018). Indoor Person Identification Using a Low-Power FMCW Radar. *IEEE Transactions on Geoscience and Remote Sensing*, 56(7), 3941–3952. <https://doi.org/10.1109/TGRS.2018.2816812>
- Vera-Rodriguez, R., Mason, J. S. D., Fierrez, J., & Ortega-Garcia, J. (2013). Comparative analysis and fusion of spatiotemporal information for footstep recognition. *IEEE Transactions on Pattern Analysis and Machine Intelligence*, 35(4), 823–834. <https://doi.org/10.1109/TPAMI.2012.164>
- Wang, H., Fan, Y., Fang, B., & Dai, S. (2018). Generalized linear discriminant analysis based on euclidean norm for gait recognition. *International Journal of Machine Learning and Cybernetics*, 9(4), 569–576. <https://doi.org/10.1007/s13042-016-0540-0>
- Wu, Z., Huang, Y., Wang, L., Wang, X., & Tan, T. (2017). A Comprehensive Study on Cross-View Gait Based Human Identification with Deep CNNs. *IEEE Transactions on Pattern Analysis and Machine Intelligence*, 39(2), 209–226. <https://doi.org/10.1109/TPAMI.2016.2545669>
- Xu, C., Makihara, Y., Yagi, Y., & Lu, J. (2019). Gait-based age progression/regression: a baseline and performance evaluation by age group classification and cross-age gait identification. *Machine Vision and Applications*, 30(4), 629–644. <https://doi.org/10.1007/s00138-019-01015-x>
- Xu, S., & Mok, K. (2022). *The Study of Complex Human Locomotion Behaviors: From Crawling to*

Walking. <http://arxiv.org/abs/2211.06766>

- Yan, C., Zhang, B., & Coenen, F. (2016). Multi-attributes gait identification by convolutional neural networks. *Proceedings - 2015 8th International Congress on Image and Signal Processing, CISP 2015, Cisp*, 642–647. <https://doi.org/10.1109/CISP.2015.7407957>
- Yu, S., Tan, D., & Tan, T. (2006). A framework for evaluating the effect of view angle, clothing and carrying condition on gait recognition. *Proceedings - International Conference on Pattern Recognition*, 4, 441–444. <https://doi.org/10.1109/ICPR.2006.67>
- Zhang, J., Wei, B., & Cheng, J. (2020). HARaaS: HAR as a service using wifi signal in IoT-enabled edge computing: Poster abstract. *SenSys 2020 - Proceedings of the 2020 18th ACM Conference on Embedded Networked Sensor Systems*, 681–682. <https://doi.org/10.1145/3384419.3430469>
- Zhang, X., Chen, L., Sun, Y., Bai, Y., Huang, B., & Chen, K. (2018). Determination of zinc oxide content of mineral medicine calamine using near-infrared spectroscopy based on MIV and BP-ANN algorithm. *Spectrochimica Acta - Part A: Molecular and Biomolecular Spectroscopy*, 193, 133–140. <https://doi.org/10.1016/j.saa.2017.12.019>
- Zhang, Y., Huang, Y., Wang, L., & Yu, S. (2019). A comprehensive study on gait biometrics using a joint CNN-based method. *Pattern Recognition*, 93, 228–236. <https://doi.org/10.1016/j.patcog.2019.04.023>
- Zhang, Y., Huang, Y., Yu, S., & Wang, L. (2020). Cross-view gait recognition by discriminative feature learning. *IEEE Transactions on Image Processing*, 29(c), 1001–1015. <https://doi.org/10.1109/TIP.2019.2926208>
- Zhou, Y., Chen, C., Ni, J., Ni, G., Li, M., Xu, G., Cheng, M., & Lemos, S. (2020). EMG Signal Processing for Hand Motion Pattern Recognition Using Machine Learning Algorithms. *Archives of Orthopaedics*, 1(1), 17–26. <https://doi.org/10.33696/orthopaedics.1.005>
- Zou, H., Zhou, Y., Yang, J., Gu, W., Xie, L., & Spanos, C. J. (2018). WiFi-based human identification via convex tensor shapelet learning. *32nd AAAI Conference on Artificial Intelligence, AAAI 2018*, 1711–1718. <https://doi.org/10.1609/aaai.v32i1.11497>

Appendix A

Experimental Setup 1 – Confusion Matrices & Metrics Tables

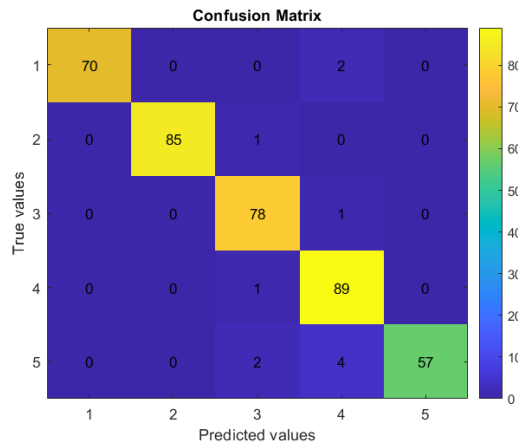


Figure 1A. Confusion Matrix for 0° Camera View Angle, Dataset 1 – Configuration Tag A.

Table 1A. Performance Metrics for 0° Camera View Angle, Dataset 1 – Configuration Tag A.

Metrics (%)	Class Number (Biometric ID Profile)				
	1	2	3	4	5
Recall	97.22	98.84	98.73	98.89	90.48
Precision	100.00	100.00	95.12	92.71	100.00
Specificity	100.00	100.00	98.71	97.67	100.00
F1-Score	98.59	99.42	96.89	95.70	95.00
Accuracy	97.18				

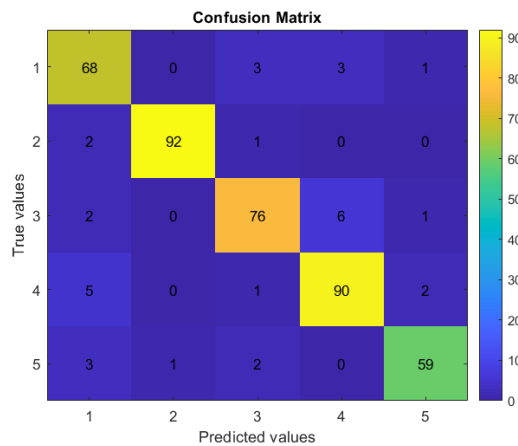


Figure 2A. Confusion Matrix for 18° Camera View Angle, Dataset 1 – Configuration Tag A.

Table 2A. Performance Metrics for 18° Camera View Angle, Dataset 1 – Configuration Tag A.

Metrics (%)	Class Number (Biometric ID Profile)				
	1	2	3	4	5
Recall	90.67	96.84	89.41	91.84	90.77
Precision	85.00	98.92	91.57	90.91	93.65
Specificity	96.50	99.69	97.90	97.19	98.87
F1-Score	87.74	97.87	90.48	91.37	92.19
Accuracy	92.11				

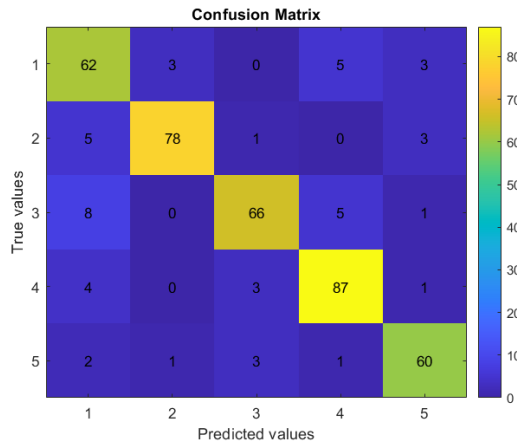


Figure 3A. Confusion Matrix for 36° Camera View Angle, Dataset 1 – Configuration Tag A.

Table 3A. Performance Metrics for 36° Camera View Angle, Dataset 1 – Configuration Tag A.

Metrics (%)	Class Number (Biometric ID Profile)				
	1	2	3	4	5
Recall	84.93	89.66	82.50	91.58	89.55
Precision	76.54	95.12	90.41	88.78	88.24
Specificity	94.22	98.73	97.83	96.42	97.61
F1-Score	80.52	92.31	86.27	90.16	88.89
Accuracy	87.81				

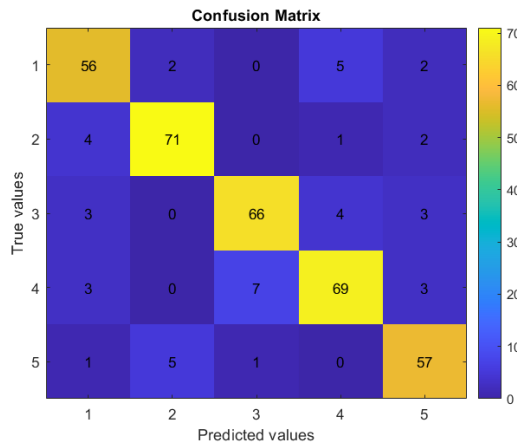


Figure 4A. Confusion Matrix for 54° Camera View Angle, Dataset 1 – Configuration Tag A.

Table 4A. Performance Metrics for 54° Camera View Angle, Dataset 1 – Configuration Tag A.

Metrics (%)	Class Number (Biometric ID Profile)				
	1	2	3	4	5
Recall	86.15	91.03	86.84	84.15	89.06
Precision	83.58	91.03	89.19	87.34	85.07
Specificity	96.33	97.56	97.23	96.47	96.68
F1-Score	84.85	91.03	88.00	85.71	87.02
Accuracy	87.40				

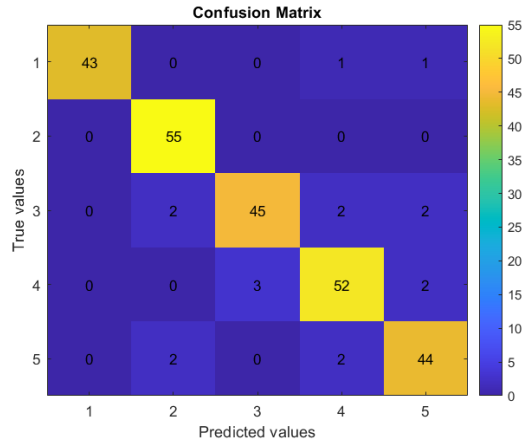


Figure 5A. Confusion Matrix for 72° Camera View Angle, Dataset 1 – Configuration Tag A.

Table 5A. Performance Metrics for 72° Camera View Angle, Dataset 1 – Configuration Tag A.

Metrics (%)	Class Number (Biometric ID Profile)				
	1	2	3	4	5
Recall	95.56	100.00	88.24	91.23	91.67
Precision	100.00	93.22	93.75	91.23	89.80
Specificity	100.00	98.01	98.54	97.49	97.60
F1-Score	97.73	96.49	90.91	91.23	90.72
Accuracy	93.36				

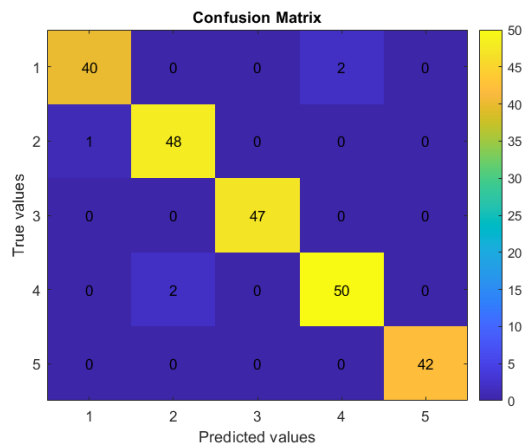


Figure 6A. Confusion Matrix for 90° Camera View Angle, Dataset 1 – Configuration Tag A.

Table 6A. Performance Metrics for 90° Camera View Angle, Dataset 1 – Configuration Tag A.

Metrics (%)	Class Number (Biometric ID Profile)				
	1	2	3	4	5
Recall	95.24	97.96	100.00	96.15	100.00
Precision	97.56	96.00	100.00	96.15	100.00
Specificity	99.47	98.91	100.00	98.89	100.00
F1-Score	96.39	96.97	100.00	96.15	100.00
Accuracy	97.84				

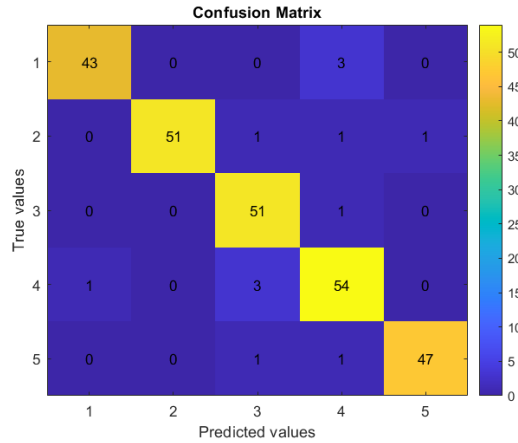


Figure 7A. Confusion Matrix for 108° Camera View Angle, Dataset 1 – Configuration Tag A.

Table 7A. Performance Metrics for 108° Camera View Angle, Dataset 1 – Configuration Tag A.

Metrics (%)	Class Number (Biometric ID Profile)				
	1	2	3	4	5
Recall	93.48	94.44	98.08	93.10	95.92
Precision	97.73	100.00	91.07	90.00	97.92
Specificity	99.53	100.00	97.58	97.01	99.52
F1-Score	95.56	97.14	94.44	91.53	96.91
Accuracy	94.98				

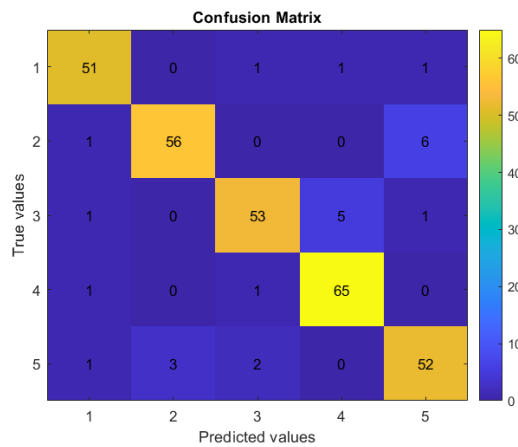


Figure 8A. Confusion Matrix for 126° Camera View Angle, Dataset 1 – Configuration Tag A.

Table 8A. Performance Metrics for 126° Camera View Angle, Dataset 1 – Configuration Tag A.

Metrics (%)	Class Number (Biometric ID Profile)				
	1	2	3	4	5
Recall	94.44	88.89	88.33	97.01	89.66
Precision	92.73	94.92	92.98	91.55	86.67
Specificity	98.39	98.74	98.35	97.45	96.72
F1-Score	93.58	91.80	90.60	94.20	88.14
Accuracy	91.72				

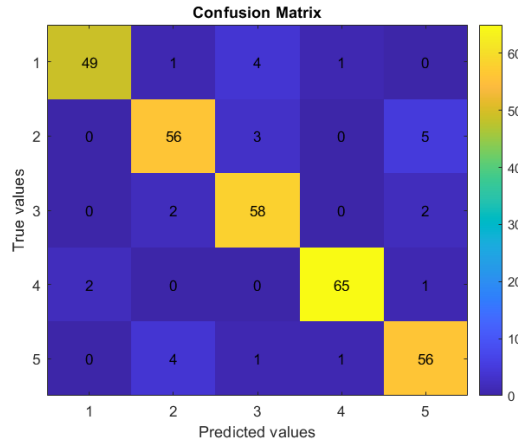


Figure 9A. Confusion Matrix for 144° Camera View Angle, Dataset 1 – Configuration Tag A.

Table 9A. Performance Metrics for 144° Camera View Angle, Dataset 1 – Configuration Tag A.

Metrics (%)	Class Number (Biometric ID Profile)				
	1	2	3	4	5
Recall	89.09	87.50	93.55	95.59	90.32
Precision	96.08	88.89	87.88	97.01	87.50
Specificity	99.22	97.17	96.79	99.18	96.79
F1-Score	92.45	88.19	90.63	96.30	88.89
Accuracy	91.32				

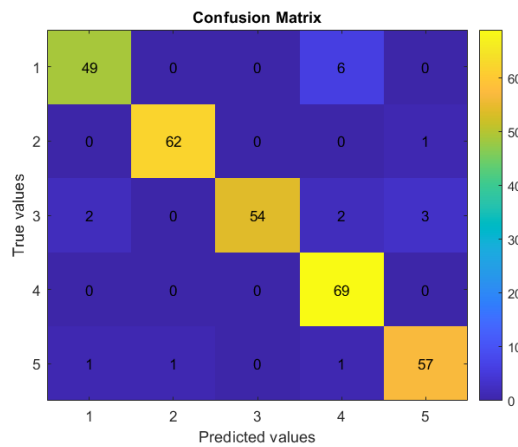


Figure 10A. Confusion Matrix for 162° Camera View Angle, Dataset 1 – Configuration Tag A.

Table 10A. Performance Metrics for 162° Camera View Angle, Dataset 1 – Configuration Tag A.

Metrics (%)	Class Number (Biometric ID Profile)				
	1	2	3	4	5
Recall	89.09	98.41	88.52	100.00	95.00
Precision	94.23	98.41	100.00	88.46	93.44
Specificity	98.81	99.59	100.00	96.23	98.39
F1-Score	91.59	98.41	93.91	93.88	94.21
Accuracy	94.48				

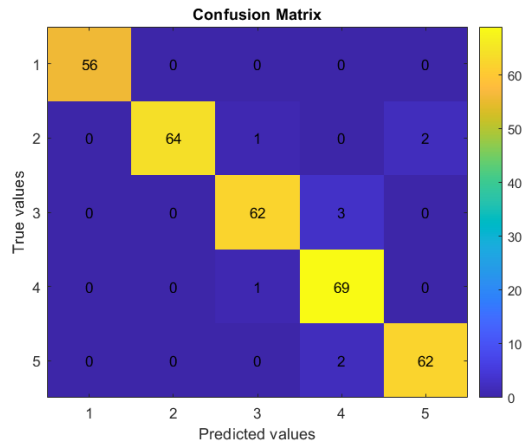


Figure 11A. Confusion Matrix for 180° Camera View Angle, Dataset 1 – Configuration Tag A.

Table 11A. Performance Metrics for 180° Camera View Angle, Dataset 1 – Configuration Tag A.

<i>Metrics (%)</i>	<i>Class Number (Biometric ID Profile)</i>				
	<i>1</i>	<i>2</i>	<i>3</i>	<i>4</i>	<i>5</i>
Recall	100.00	95.52	95.38	98.57	96.88
Precision	100.00	100.00	96.88	93.24	96.88
Specificity	100.00	100.00	99.22	98.02	99.22
F1-Score	100.00	97.71	96.12	95.83	96.88
Accuracy	97.20				

Appendix B

Experimental Setup 2 – Confusion Matrices & Metrics Tables

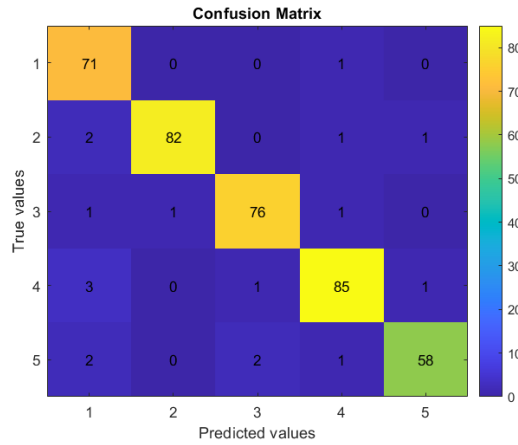


Figure 1B. Confusion Matrix for 0° Camera View Angle, Dataset 1 – Configuration Tag B.

Table 1B. Performance Metrics for 0° Camera View Angle, Dataset 1 – Configuration Tag B.

Metrics (%)	Class Number (Biometric ID Profile)				
	1	2	3	4	5
Recall	98.61	95.35	96.20	94.44	92.06
Precision	89.87	98.80	96.20	95.51	96.67
Specificity	97.48	99.67	99.04	98.67	99.39
F1-Score	94.04	97.04	96.20	94.97	94.31
Accuracy	95.38				

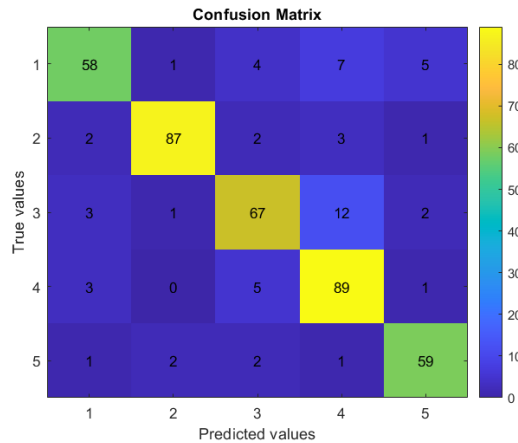


Figure 2B. Confusion Matrix for 18° Camera View Angle, Dataset 1 – Configuration Tag B.

Table 2B. Performance Metrics for 18° Camera View Angle, Dataset 1 – Configuration Tag B.

Metrics (%)	Class Number (Biometric ID Profile)				
	1	2	3	4	5
Recall	77.33	91.58	78.82	90.82	90.77
Precision	86.57	95.60	83.75	79.46	86.76
Specificity	97.38	98.76	96.10	92.81	97.45
F1-Score	81.69	93.55	81.21	84.76	88.72
Accuracy	86.12				

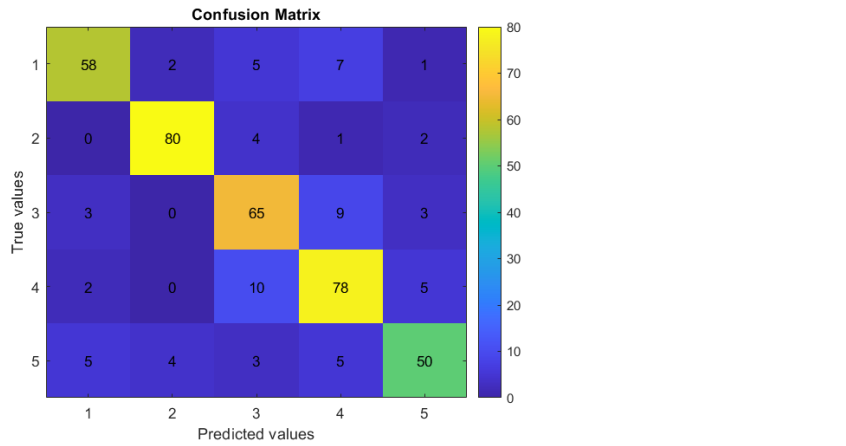


Figure 3B Confusion Matrix for 36° Camera View Angle, Dataset 1 – Configuration Tag B.

Table 3B. Performance Metrics for 36° Camera View Angle, Dataset 1 – Configuration Tag B.

Metrics (%)	Class Number (Biometric ID Profile)				
	1	2	3	4	5
Recall	79.45	91.95	81.25	82.11	74.63
Precision	85.29	93.02	74.71	78.00	81.97
Specificity	96.96	98.10	93.17	92.83	96.72
F1-Score	82.27	92.49	77.84	80.00	78.13
Accuracy	82.34				

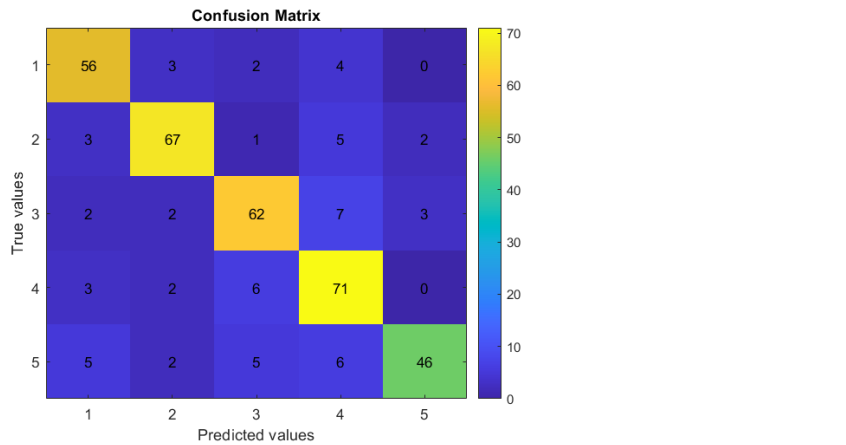


Figure 4B. Confusion Matrix for 54° Camera View Angle, Dataset 1 – Configuration Tag B.

Table 4B. Performance Metrics for 54° Camera View Angle, Dataset 1 – Configuration Tag B.

Metrics (%)	Class Number (Biometric ID Profile)				
	1	2	3	4	5
Recall	86.15	85.90	81.58	86.59	71.88
Precision	81.16	88.16	81.58	76.34	90.20
Specificity	95.67	96.86	95.16	92.23	98.34
F1-Score	83.58	87.01	81.58	81.14	80.00
Accuracy	82.74				

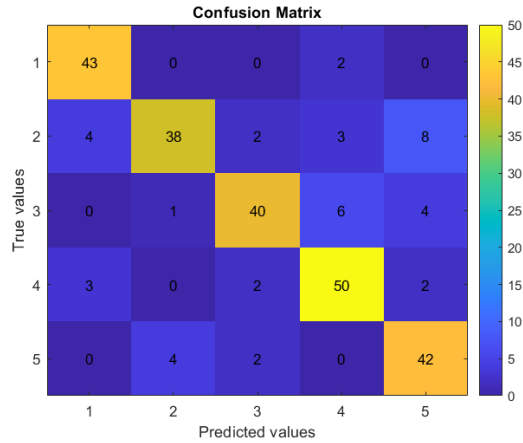


Figure 5B. Confusion Matrix for 72° Camera View Angle, Dataset 1 – Configuration Tag B.

Table 5B. Performance Metrics for 72° Camera View Angle, Dataset 1 – Configuration Tag B.

Metrics (%)	Class Number (Biometric ID Profile)				
	1	2	3	4	5
Recall	95.56	69.09	78.43	87.72	87.50
Precision	86.00	88.37	86.96	81.97	75.00
Specificity	96.68	97.51	97.07	94.47	93.27
F1-Score	90.53	77.55	82.47	84.75	80.77
Accuracy	83.20				

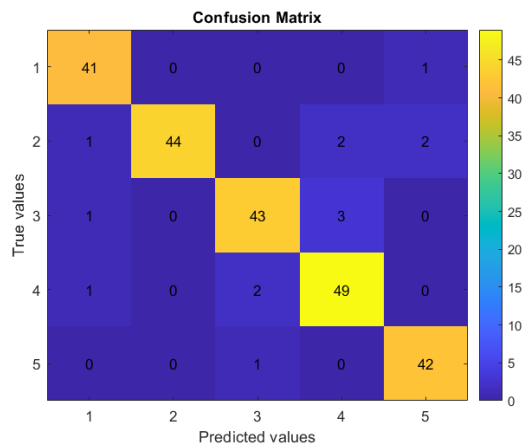


Figure 6B. Confusion Matrix for 90° Camera View Angle, Dataset 1 – Configuration Tag B.

Table 6B. Performance Metrics for 90° Camera View Angle, Dataset 1 – Configuration Tag B.

Metrics (%)	Class Number (Biometric ID Profile)				
	1	2	3	4	5
Recall	97.62	89.80	91.49	94.23	97.67
Precision	93.18	100.00	93.48	90.74	93.33
Specificity	98.43	100.00	98.39	97.24	98.42
F1-Score	95.35	94.62	92.47	92.45	95.45
Accuracy	93.99				

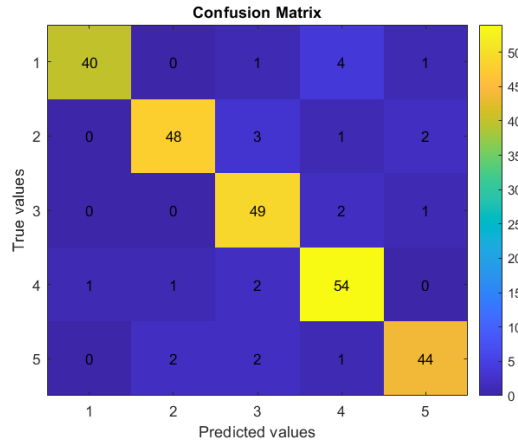


Figure 7B. Confusion Matrix for 108° Camera View Angle, Dataset 1 – Configuration Tag B.

Table 7B. Performance Metrics for 108° Camera View Angle, Dataset 1 – Configuration Tag B.

Metrics (%)	Class Number (Biometric ID Profile)				
	1	2	3	4	5
Recall	86.96	88.89	94.23	93.10	89.80
Precision	97.56	94.12	85.96	87.10	91.67
Specificity	99.53	98.54	96.14	96.02	98.10
F1-Score	91.95	91.43	89.91	90.00	90.72
Accuracy	90.73				

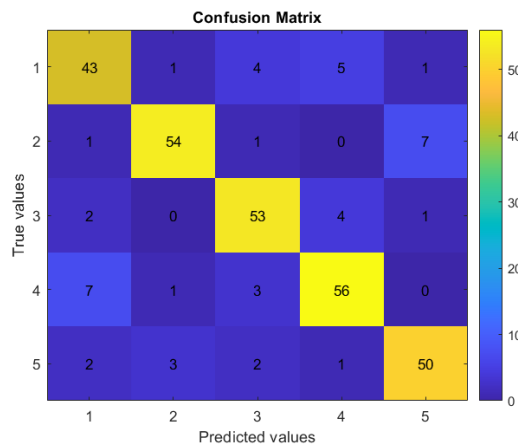


Figure 8B. Confusion Matrix for 126° Camera View Angle, Dataset 1 – Configuration Tag B.

Table 8B. Performance Metrics for 126° Camera View Angle, Dataset 1 – Configuration Tag B.

Metrics (%)	Class Number (Biometric ID Profile)				
	1	2	3	4	5
Recall	79.63	85.71	88.33	83.58	86.21
Precision	78.18	91.53	84.13	84.85	84.75
Specificity	95.16	97.91	95.87	95.74	96.31
F1-Score	78.90	88.52	86.18	84.21	85.47
Accuracy	84.77				

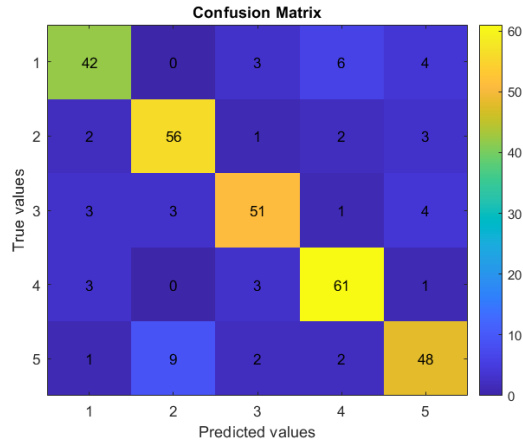


Figure 9B. Confusion Matrix for 144° Camera View Angle, Dataset 1 – Configuration Tag B.

Table 9B. Performance Metrics for 144° Camera View Angle, Dataset 1 – Configuration Tag B.

Metrics (%)	Class Number (Biometric ID Profile)				
	1	2	3	4	5
Recall	76.36	87.50	82.26	89.71	77.42
Precision	82.35	82.35	85.00	84.72	80.00
Specificity	96.48	95.14	96.39	95.47	95.18
F1-Score	79.25	84.85	83.61	87.14	78.69
Accuracy	82.96				

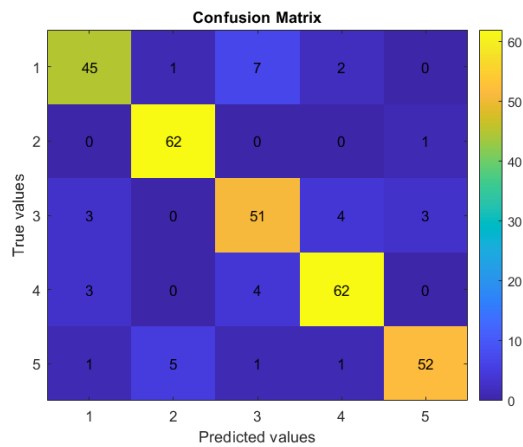


Figure 10B. Confusion Matrix for 162° Camera View Angle, Dataset 1 – Configuration Tag B.

Table 10B. Performance Metrics for 162° Camera View Angle, Dataset 1 – Configuration Tag B.

Metrics (%)	Class Number (Biometric ID Profile)				
	1	2	3	4	5
Recall	81.82	98.41	83.61	89.86	86.67
Precision	86.54	91.18	80.95	89.86	92.86
Specificity	97.23	97.55	95.14	97.07	98.39
F1-Score	84.11	94.66	82.26	89.86	89.66
Accuracy	88.31				

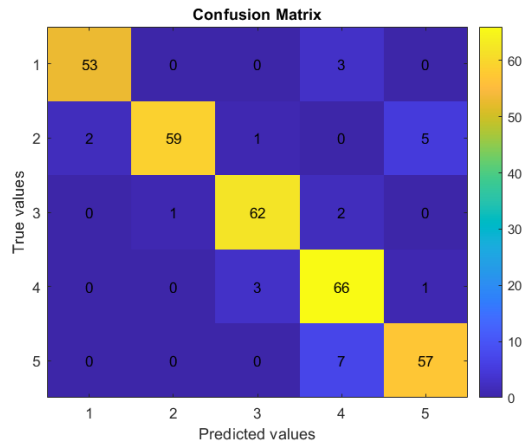


Figure 11B. Confusion Matrix for 180° Camera View Angle, Dataset 1 – Configuration Tag B.

Table 11B. Performance Metrics for 180° Camera View Angle, Dataset 1 – Configuration Tag B.

<i>Metrics (%)</i>	<i>Class Number (Biometric ID Profile)</i>				
	<i>1</i>	<i>2</i>	<i>3</i>	<i>4</i>	<i>5</i>
Recall	94.64	88.06	95.38	94.29	89.06
Precision	96.36	98.33	93.94	84.62	90.48
Specificity	99.25	99.61	98.44	95.24	97.67
F1-Score	95.50	92.91	94.66	89.19	89.76
Accuracy	92.24				

Appendix C

Experimental Setup 3 – Confusion Matrices & Metrics Tables

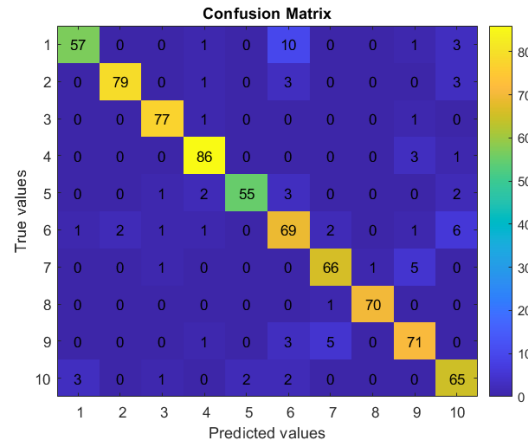


Figure 1C. Confusion Matrix for 0° Camera View Angle, Dataset 2 – Configuration Tag A.

Table 1C. Performance Metrics for 0° Camera View Angle, Dataset 2 – Configuration Tag A.

Metrics (%)	Class Number (Biometric ID Profile)									
	1	2	3	4	5	6	7	8	9	10
Recall	79.17	91.86	97.47	95.56	87.30	83.13	90.41	98.59	88.75	89.04
Precision	93.44	97.53	95.06	92.47	96.49	76.67	89.19	98.59	86.59	81.25
Specificity	99.43	99.71	99.42	98.97	99.72	96.94	98.85	99.86	98.41	97.85
F1-Score	85.71	94.61	96.25	93.99	91.67	79.77	89.80	98.59	87.65	84.97
Accuracy	90.26									

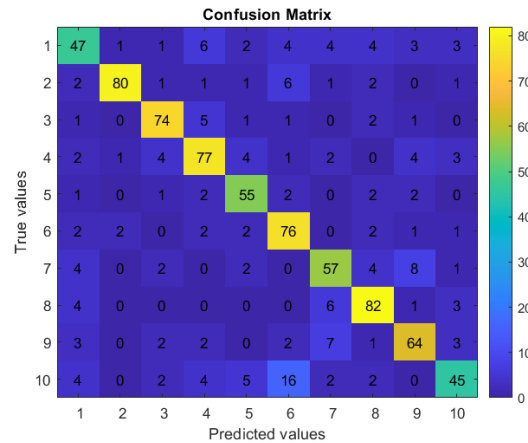


Figure 2C. Confusion Matrix for 18° Camera View Angle, Dataset 2 – Configuration Tag A.

Table 2C. Performance Metrics for 18° Camera View Angle, Dataset 2 – Configuration Tag A.

Metrics (%)	Class Number (Biometric ID Profile)									
	1	2	3	4	5	6	7	8	9	10
Recall	62.67	84.21	87.06	78.57	84.62	86.36	73.08	85.42	76.19	56.25
Precision	67.14	95.24	85.06	77.78	76.39	70.37	72.15	81.19	76.19	75.00
Specificity	97.01	99.47	98.29	97.05	97.82	95.77	97.13	97.46	97.37	98.04
F1-Score	64.83	89.39	86.05	78.17	80.29	77.55	72.61	83.25	76.19	64.29
Accuracy	77.84									

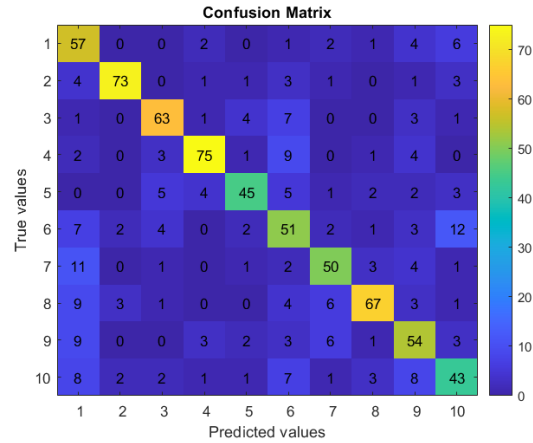


Figure 3C. Confusion Matrix for 36° Camera View Angle, Dataset 2 – Configuration Tag A.

Table 3C. Performance Metrics for 36° Camera View Angle, Dataset 2 – Configuration Tag A.

Metrics (%)	Class Number (Biometric ID Profile)									
	1	2	3	4	5	6	7	8	9	10
Recall	78.08	83.91	78.75	78.95	67.16	60.71	68.49	71.28	66.67	56.58
Precision	52.78	91.25	79.75	86.21	78.95	55.43	72.46	84.81	62.79	58.90
Specificity	93.08	99.03	97.81	98.32	98.38	94.35	97.42	98.32	95.61	95.91
F1-Score	62.98	87.43	79.25	82.42	72.58	57.95	70.42	77.46	64.67	57.72
Accuracy	71.36									

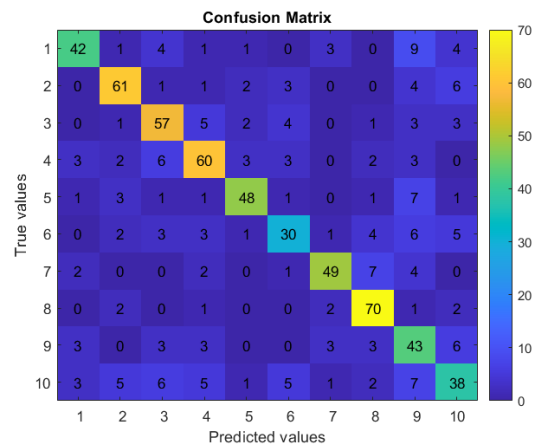


Figure 4C. Confusion Matrix for 54° Camera View Angle, Dataset 2 – Configuration Tag A.

Table 4C. Performance Metrics for 54° Camera View Angle, Dataset 2 – Configuration Tag A.

Metrics (%)	Class Number (Biometric ID Profile)									
	1	2	3	4	5	6	7	8	9	10
Recall	64.62	78.21	75.00	73.17	75.00	54.55	75.38	89.74	67.19	52.05
Precision	77.78	79.22	70.37	73.17	82.76	63.83	83.05	77.78	49.43	58.46
Specificity	98.11	97.43	96.15	96.44	98.43	97.36	98.43	96.78	93.08	95.69
F1-Score	70.59	78.71	72.61	73.17	78.69	58.82	79.03	83.33	56.95	55.07
Accuracy	71.14									

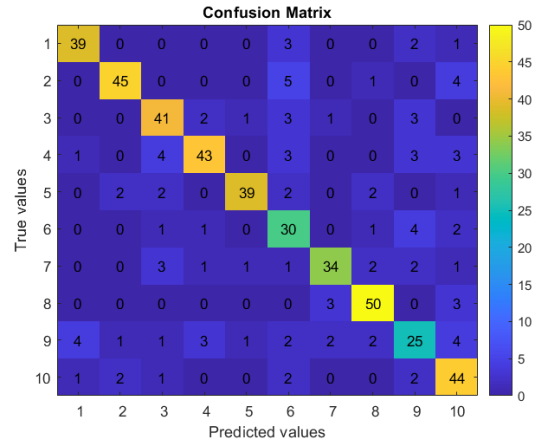


Figure 5C. Confusion Matrix for 72° Camera View Angle, Dataset 2 – Configuration Tag A.

Table 5C. Performance Metrics for 72° Camera View Angle, Dataset 2 – Configuration Tag A.

Metrics (%)	Class Number (Biometric ID Profile)									
	1	2	3	4	5	6	7	8	9	10
Recall	86.67	81.82	80.39	75.44	81.25	76.92	75.56	89.29	55.56	84.62
Precision	86.67	90.00	77.36	86.00	92.86	58.82	85.00	86.21	60.98	69.84
Specificity	98.66	98.86	97.29	98.39	99.33	95.37	98.66	98.17	96.43	95.69
F1-Score	86.67	85.71	78.85	80.37	86.67	66.67	80.00	87.72	58.14	76.52
Accuracy	79.11									

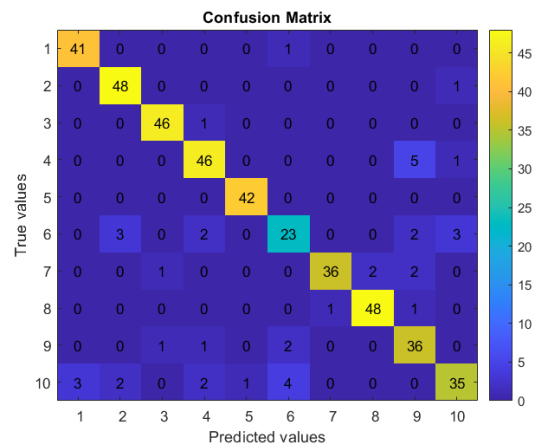


Figure 6C. Confusion Matrix for 90° Camera View Angle, Dataset 2 – Configuration Tag A.

Table 6C. Performance Metrics for 90° Camera View Angle, Dataset 2 – Configuration Tag A.

Metrics (%)	Class Number (Biometric ID Profile)									
	1	2	3	4	5	6	7	8	9	10
Recall	97.62	97.96	97.87	88.46	100.00	69.70	87.80	96.00	90.00	74.47
Precision	93.18	90.57	95.83	88.46	97.67	76.67	97.30	96.00	78.26	87.50
Specificity	99.25	98.73	99.49	98.47	99.75	98.29	99.75	99.49	97.52	98.74
F1-Score	95.35	94.12	96.84	88.46	98.82	73.02	92.31	96.00	83.72	80.46
Accuracy	90.52									

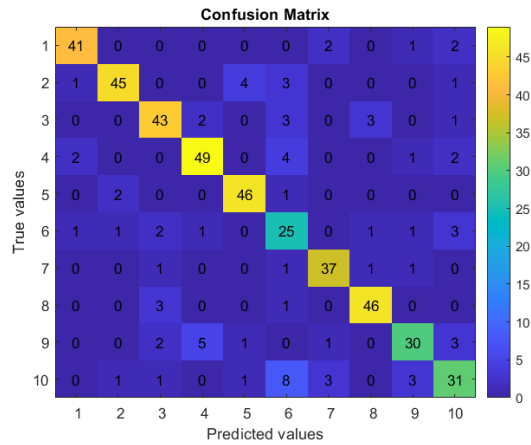


Figure 7C. Confusion Matrix for 108° Camera View Angle, Dataset 2 – Configuration Tag A.

Table 7C. Performance Metrics for 108° Camera View Angle, Dataset 2 – Configuration Tag A.

Metrics (%)	Class Number (Biometric ID Profile)									
	1	2	3	4	5	6	7	8	9	10
Recall	89.13	83.33	82.69	84.48	93.88	71.43	90.24	92.00	71.43	64.58
Precision	91.11	91.84	82.69	85.96	88.46	54.35	86.05	90.20	81.08	72.09
Specificity	91.11	91.84	82.69	85.96	88.46	54.35	86.05	90.20	81.08	72.09
F1-Score	90.11	87.38	82.69	85.22	91.09	61.73	88.10	91.09	75.95	68.13
Accuracy	82.74									

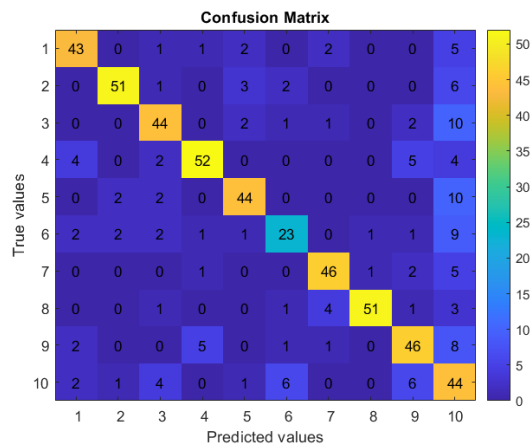


Figure 8C. Confusion Matrix for 126° Camera View Angle, Dataset 2 – Configuration Tag A.

Table 8C. Performance Metrics for 126° Camera View Angle, Dataset 2 – Configuration Tag A.

Metrics (%)	Class Number (Biometric ID Profile)									
	1	2	3	4	5	6	7	8	9	10
Recall	79.63	80.95	73.33	77.61	75.86	54.76	83.64	83.61	73.02	68.75
Precision	81.13	91.07	77.19	86.67	83.02	67.65	85.19	96.23	73.02	42.31
Specificity	98.12	99.05	97.53	98.46	98.30	97.98	98.50	99.62	96.76	88.53
F1-Score	80.37	85.71	75.21	81.89	79.28	60.53	84.40	89.47	73.02	52.38
Accuracy	75.64									

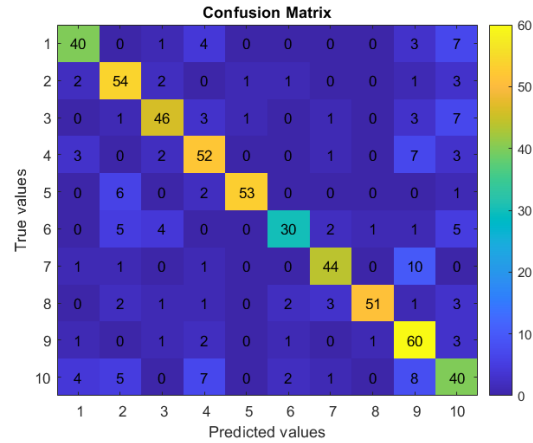


Figure 9C. Confusion Matrix for 144° Camera View Angle, Dataset 2 – Configuration Tag A.

Table 9C. Performance Metrics for 144° Camera View Angle, Dataset 2 – Configuration Tag A.

Metrics (%)	Class Number (Biometric ID Profile)									
	1	2	3	4	5	6	7	8	9	10
Recall	72.73	84.38	74.19	76.47	85.48	62.50	77.19	79.69	86.96	59.70
Precision	78.43	72.97	80.70	72.22	96.36	83.33	84.62	96.23	63.83	55.56
Specificity	98.04	96.38	98.01	96.35	99.64	98.94	98.57	99.64	93.78	94.17
F1-Score	75.47	78.26	77.31	74.29	90.60	71.43	80.73	87.18	73.62	57.55
Accuracy	76.30									

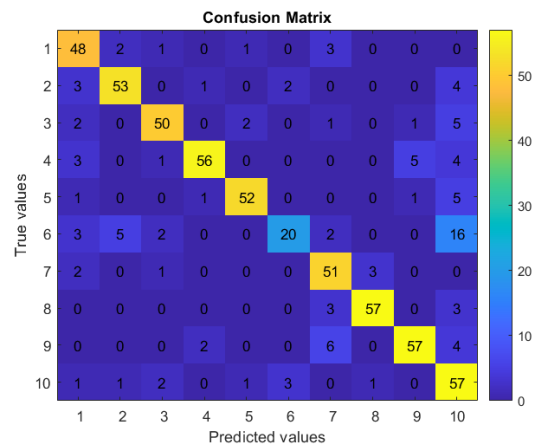


Figure 10C. Confusion Matrix for 162° Camera View Angle, Dataset 2 – Configuration Tag A.

Table 10C. Performance Metrics for 162° Camera View Angle, Dataset 2 – Configuration Tag A.

Metrics (%)	Class Number (Biometric ID Profile)									
	1	2	3	4	5	6	7	8	9	10
Recall	87.27	84.13	81.97	81.16	86.67	41.67	89.47	90.48	82.61	86.36
Precision	76.19	86.89	87.72	93.33	92.86	80.00	77.27	93.44	89.06	58.16
Specificity	97.30	98.54	98.73	99.26	99.27	99.11	97.29	99.27	98.71	92.48
F1-Score	81.36	85.48	84.75	86.82	89.66	54.79	82.93	91.94	85.71	69.51
Accuracy	82.00									

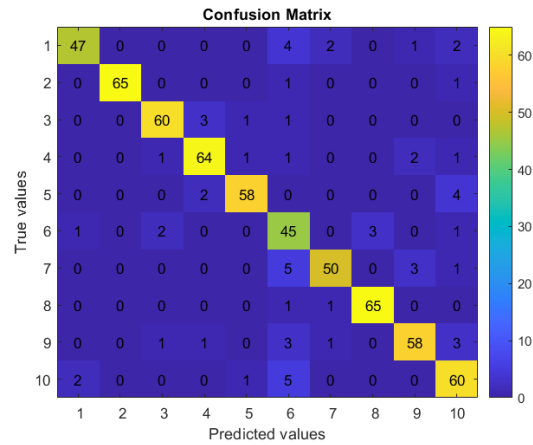


Figure 11B. Confusion Matrix for 180° Camera View Angle, Dataset 2 – Configuration Tag A.

Table 11B. Performance Metrics for 180° Camera View Angle, Dataset 2 – Configuration Tag A.

Metrics (%)	Class Number (Biometric ID Profile)									
	1	2	3	4	5	6	7	8	9	10
Recall	83.93	97.01	92.31	91.43	90.63	86.54	84.75	97.01	86.57	88.24
Precision	94.00	100.00	93.75	91.43	95.08	68.18	92.59	95.59	90.63	82.19
Specificity	99.48	100.00	99.30	98.94	99.47	96.40	99.31	99.47	98.94	97.71
F1-Score	88.68	98.48	93.02	91.43	92.80	76.27	88.50	96.30	88.55	85.11
Accuracy	90.08									

Appendix D

Experimental Setup 4 – Confusion Matrices & Metrics Tables

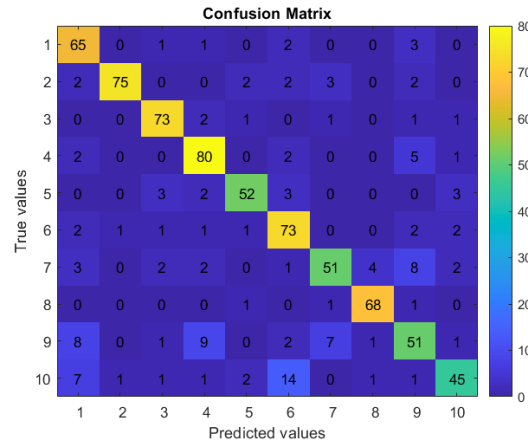


Figure 1D. Confusion Matrix for 0° Camera View Angle, Dataset 2 – Configuration Tag B.

Table 1D. Performance Metrics for 0° Camera View Angle, Dataset 2 – Configuration Tag B.

Metrics (%)	Class Number (Biometric ID Profile)									
	1	2	3	4	5	6	7	8	9	10
Recall	90.28	87.21	92.41	88.89	82.54	87.95	69.86	95.77	63.75	61.64
Precision	73.03	97.40	89.02	81.63	88.14	73.74	80.95	91.89	68.92	81.82
Specificity	96.56	99.71	98.70	97.35	99.01	96.22	98.28	99.14	96.67	98.57
F1-Score	80.75	92.02	90.68	85.11	85.25	80.22	75.00	93.79	66.23	70.31
Accuracy	82.21									

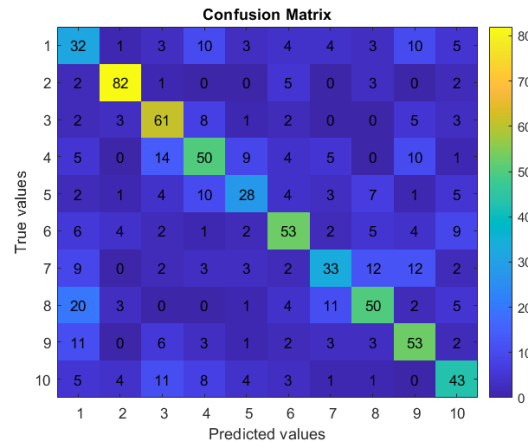


Figure 2D. Confusion Matrix for 18° Camera View Angle, Dataset 2 – Configuration Tag B.

Table 2D. Performance Metrics for 18° Camera View Angle, Dataset 2 – Configuration Tag B.

Metrics (%)	Class Number (Biometric ID Profile)									
	1	2	3	4	5	6	7	8	9	10
Recall	42.67	86.32	71.76	51.02	43.08	60.23	42.31	52.08	63.10	53.75
Precision	34.04	83.67	58.65	53.76	53.85	63.86	53.23	59.52	54.64	55.84
Specificity	91.94	97.86	94.33	94.24	96.92	96.03	96.21	95.45	94.21	95.55
F1-Score	37.87	84.97	64.55	52.36	47.86	61.99	47.14	55.56	58.56	54.78
Accuracy	57.46									

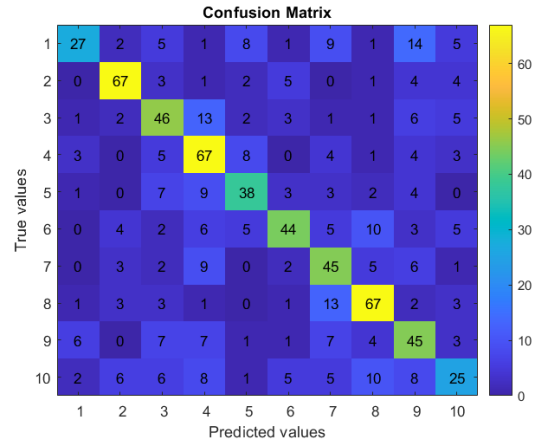


Figure 3D. Confusion Matrix for 36° Camera View Angle, Dataset 2 – Configuration Tag B.

Table 3D. Performance Metrics for 36° Camera View Angle, Dataset 2 – Configuration Tag B.

Metrics (%)	Class Number (Biometric ID Profile)									
	1	2	3	4	5	6	7	8	9	10
Recall	36.99	77.01	57.50	70.53	56.72	52.38	61.64	71.28	55.56	32.89
Precision	65.85	77.01	53.49	54.92	58.46	67.69	48.91	65.69	46.88	46.30
Specificity	98.10	97.23	94.52	92.31	96.37	97.11	93.62	95.11	93.00	96.05
F1-Score	47.37	77.01	55.42	61.75	57.58	59.06	54.55	68.37	50.85	38.46
Accuracy	58.15									

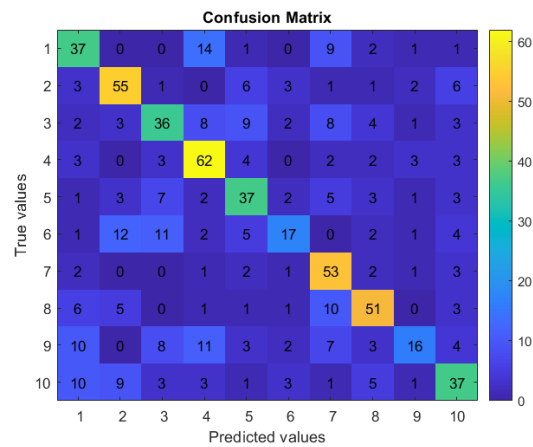


Figure 4D. Confusion Matrix for 54° Camera View Angle, Dataset 2 – Configuration Tag B.

Table 4D. Performance Metrics for 54° Camera View Angle, Dataset 2 – Configuration Tag B.

Metrics (%)	Class Number (Biometric ID Profile)									
	1	2	3	4	5	6	7	8	9	10
Recall	56.92	70.51	47.37	75.61	57.81	30.91	81.54	65.38	25.00	50.68
Precision	49.33	63.22	52.17	59.62	53.62	54.84	55.21	68.00	59.26	55.22
Specificity	94.02	94.86	94.71	93.20	94.97	97.83	93.23	96.14	98.27	95.22
F1-Score	52.86	66.67	49.66	66.67	55.64	39.53	65.84	66.67	35.16	52.86
Accuracy	57.29									

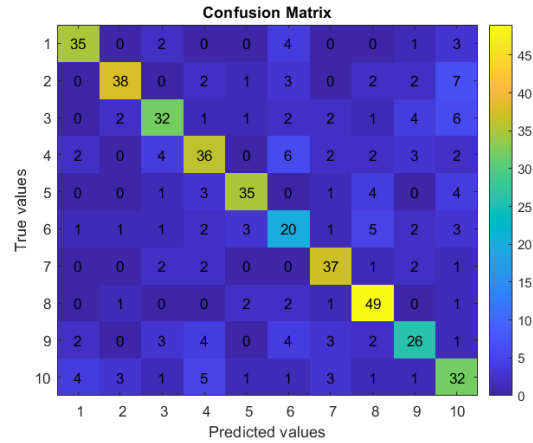


Figure 5D. Confusion Matrix for 72° Camera View Angle, Dataset 2 – Configuration Tag B.

Table 5D. Performance Metrics for 72° Camera View Angle, Dataset 2 – Configuration Tag B.

Metrics (%)	Class Number (Biometric ID Profile)									
	1	2	3	4	5	6	7	8	9	10
Recall	77.78	69.09	62.75	63.16	72.92	51.28	82.22	87.50	57.78	61.54
Precision	79.55	84.44	69.57	65.45	81.40	47.62	74.00	73.13	63.41	53.33
Specificity	97.99	98.40	96.83	95.64	98.20	95.15	97.10	95.88	96.65	93.65
F1-Score	78.65	76.00	65.98	64.29	76.92	49.38	77.89	79.67	60.47	57.14
Accuracy	68.97									

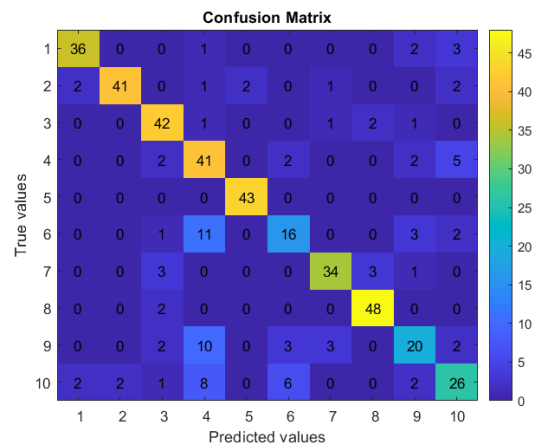


Figure 6D. Confusion Matrix for 90° Camera View Angle, Dataset 2 – Configuration Tag B.

Table 6D. Performance Metrics for 90° Camera View Angle, Dataset 2 – Configuration Tag B.

Metrics (%)	Class Number (Biometric ID Profile)									
	1	2	3	4	5	6	7	8	9	10
Recall	85.71	83.67	89.36	78.85	100.00	48.48	82.93	96.00	50.00	55.32
Precision	90.00	95.35	79.25	56.16	95.56	59.26	87.18	90.57	64.52	65.00
Specificity	99.00	99.49	97.23	91.84	99.50	97.32	98.76	98.73	97.28	96.47
F1-Score	87.80	89.13	84.00	65.60	97.73	53.33	85.00	93.20	56.34	59.77
Accuracy	78.15									

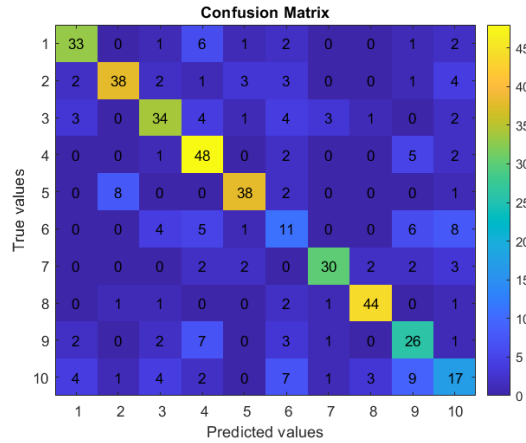


Figure 7D. Confusion Matrix for 108° Camera View Angle, Dataset 2 – Configuration Tag B.

Table 7D. Performance Metrics for 108° Camera View Angle, Dataset 2 – Configuration Tag B.

Metrics (%)	Class Number (Biometric ID Profile)									
	1	2	3	4	5	6	7	8	9	10
Recall	71.74	70.37	65.38	82.76	77.55	31.43	73.17	88.00	61.90	35.42
Precision	75.00	79.17	69.39	64.00	82.61	30.56	83.33	88.00	52.00	41.46
Specificity	97.44	97.62	96.45	93.53	98.12	94.32	98.62	98.59	94.46	94.38
F1-Score	73.33	74.51	67.33	72.18	80.00	30.99	77.92	88.00	56.52	38.20
Accuracy	67.16									

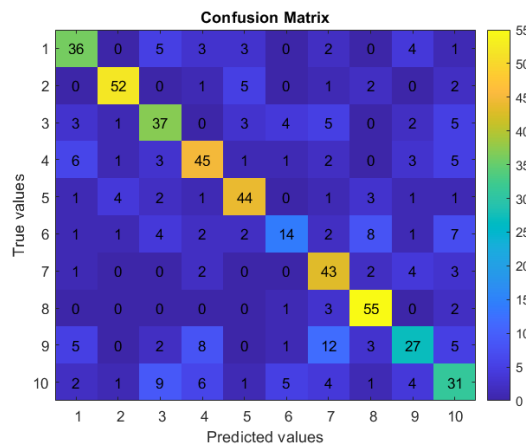


Figure 8D. Confusion Matrix for 126° Camera View Angle, Dataset 2 – Configuration Tag B.

Table 8D. Performance Metrics for 126° Camera View Angle, Dataset 2 – Configuration Tag B.

Metrics (%)	Class Number (Biometric ID Profile)									
	1	2	3	4	5	6	7	8	9	10
Recall	66.67	82.54	61.67	67.16	75.86	33.33	78.18	90.16	42.86	48.44
Precision	65.45	86.67	59.68	66.18	74.58	53.85	57.33	74.32	58.70	50.00
Specificity	96.44	98.47	95.26	95.58	97.16	97.80	93.98	96.39	96.37	94.07
F1-Score	66.06	84.55	60.66	66.67	75.21	41.18	66.15	81.48	49.54	49.21
Accuracy	65.42									

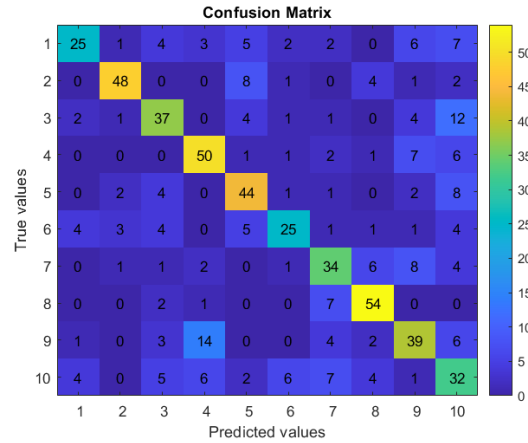


Figure 9D. Confusion Matrix for 144° Camera View Angle, Dataset 2 – Configuration Tag B.

Table 9D. Performance Metrics for 144° Camera View Angle, Dataset 2 – Configuration Tag B.

Metrics (%)	Class Number (Biometric ID Profile)									
	1	2	3	4	5	6	7	8	9	10
Recall	45.45	75.00	59.68	73.53	70.97	52.08	59.65	84.38	56.52	47.76
Precision	69.44	85.71	61.67	65.79	63.77	65.79	57.63	75.00	56.52	39.51
Specificity	98.04	98.55	95.85	95.26	95.49	97.71	95.53	96.74	94.52	91.07
F1-Score	54.95	80.00	60.66	69.44	67.18	58.14	58.62	79.41	56.52	43.24
Accuracy	62.99									

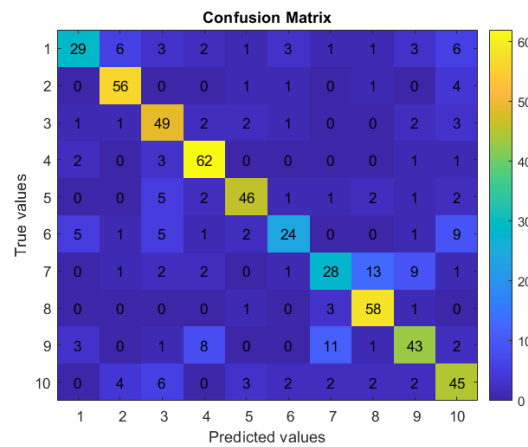


Figure 10D. Confusion Matrix for 162° Camera View Angle, Dataset 2 – Configuration Tag B.

Table 10D. Performance Metrics for 162° Camera View Angle, Dataset 2 – Configuration Tag B.

Metrics (%)	Class Number (Biometric ID Profile)									
	1	2	3	4	5	6	7	8	9	10
Recall	52.73	88.89	80.33	89.86	76.67	50.00	49.12	92.06	62.32	68.18
Precision	72.50	81.16	66.22	78.48	82.14	72.73	60.87	74.36	68.25	61.64
Specificity	98.02	97.63	95.45	96.86	98.19	98.40	96.75	96.35	96.31	94.86
F1-Score	61.05	84.85	72.59	83.78	79.31	59.26	54.37	82.27	65.15	64.75
Accuracy	72.01									

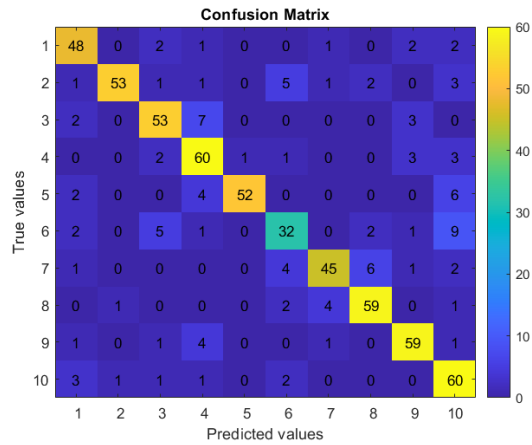


Figure 11D. Confusion Matrix for 180° Camera View Angle, Dataset 2 – Configuration Tag B.

Table 11D. Performance Metrics for 180° Camera View Angle, Dataset 2 – Configuration Tag B.

Metrics (%)	Class Number (Biometric ID Profile)									
	1	2	3	4	5	6	7	8	9	10
Recall	85.71	79.10	81.54	85.71	81.25	61.54	76.27	88.06	88.06	88.24
Precision	80.00	96.36	81.54	75.95	98.11	69.57	86.54	85.51	85.51	68.97
Specificity	97.93	99.65	97.89	96.64	99.82	97.60	98.78	98.24	98.24	95.24
F1-Score	82.76	86.89	81.54	80.54	88.89	65.31	81.08	86.76	86.76	77.42
Accuracy	82.05									

Appendix E

Experimental Setup 5 – Confusion Matrices & Metrics Tables

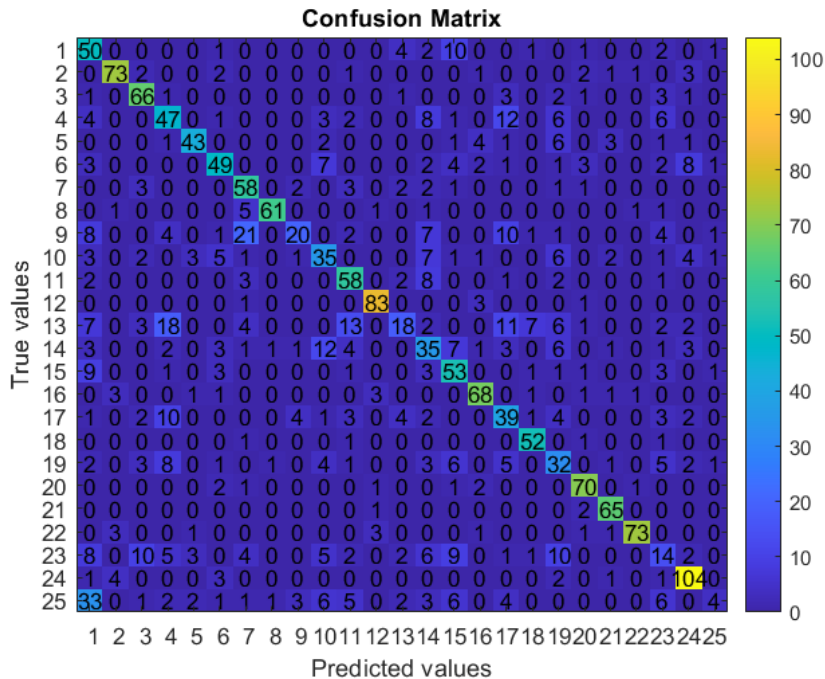


Figure 1E. Confusion Matrix for 0° Camera View Angle, Dataset 3 – Configuration Tag A.

Table 1E. Performance Metrics for 0° Camera View Angle, Dataset 3 – Configuration Tag A.

Class Number (Biometric ID Profile)	Metrics (%)				
	Recall	Precision	Specificity	F1-Score	Accuracy
1	69.44	37.04	95.55	48.31	64.01
2	84.88	86.90	99.42	85.88	
3	83.54	71.74	98.64	77.19	
4	52.22	47.47	97.25	49.74	
5	68.25	81.13	99.48	74.14	
6	59.04	67.12	98.74	62.82	
7	79.45	57.43	97.75	66.67	
8	85.92	95.31	99.84	90.37	
9	25.00	64.52	99.42	36.04	
10	47.95	46.67	97.91	47.30	
11	75.32	60.42	98.01	67.05	
12	94.32	90.22	99.53	92.22	
13	19.15	51.43	99.10	27.91	
14	41.67	38.46	97.05	40.00	
15	68.83	53.00	97.54	59.89	
16	85.00	81.93	99.21	83.44	
17	51.32	42.86	97.27	46.71	
18	92.86	80.00	99.33	85.95	
19	42.67	37.21	97.17	39.75	
20	89.74	81.4	99.16	85.37	
21	95.59	85.53	99.43	90.28	
22	87.95	94.81	99.79	91.25	
23	17.07	24.56	97.74	20.14	
24	89.66	78.79	98.50	83.87	
25	5.00	40.00	99.68	8.89	

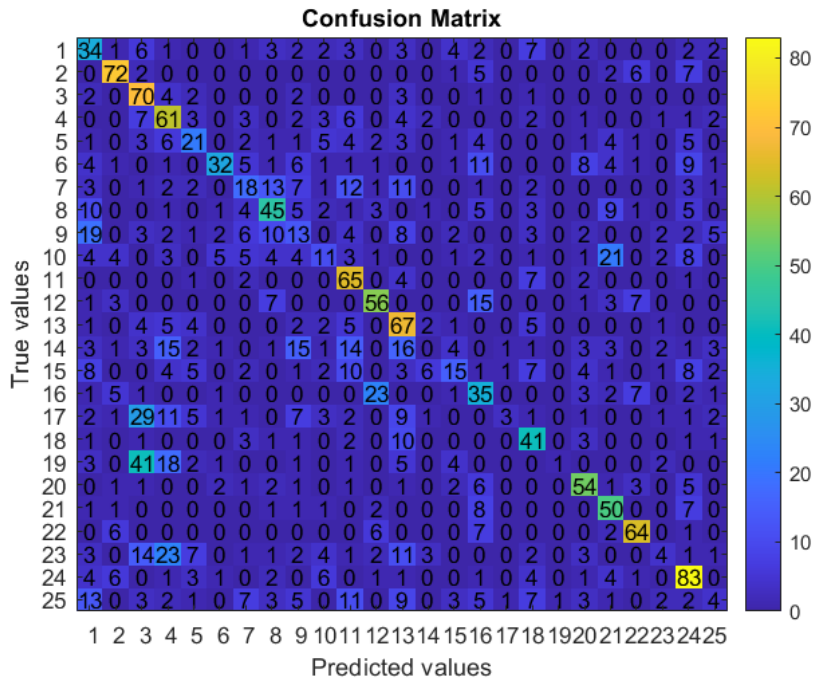


Figure 2E. Confusion Matrix for 18° Camera View Angle, Dataset 3 – Configuration Tag A.

Table 2E. Performance Metrics for 18° Camera View Angle, Dataset 3 – Configuration Tag A.

Class Number (Biometric ID Profile)	Metrics (%)				
	Recall	Precision	Specificity	F1-Score	Accuracy
1	45.33	28.81	95.89	35.23	43.35
2	75.79	70.59	98.52	73.10	
3	82.35	37.04	94.15	51.09	
4	62.24	38.13	95.10	47.29	
5	32.31	35.59	98.15	33.87	
6	36.36	68.09	99.26	47.41	
7	23.08	29.51	97.89	25.90	
8	46.88	47.37	97.53	47.12	
9	15.48	16.67	96.81	16.05	
10	13.75	25.00	98.38	17.74	
11	79.27	44.52	96.03	57.02	
12	60.22	57.14	97.93	58.64	
13	67.68	39.88	95.00	50.19	
14	0.00	0.00	99.26	0.00	
15	18.52	37.50	98.77	24.79	
16	42.68	32.11	96.37	36.65	
17	3.70	50.00	99.85	6.90	
18	63.08	43.62	97.42	51.57	
19	1.27	50.00	99.95	2.47	
20	66.67	58.06	98.09	62.07	
21	69.44	46.73	97.22	55.87	
22	74.42	70.33	98.67	72.32	
23	4.82	22.22	99.31	7.92	
24	69.75	53.55	96.40	60.58	
25	4.82	16.00	98.97	7.41	

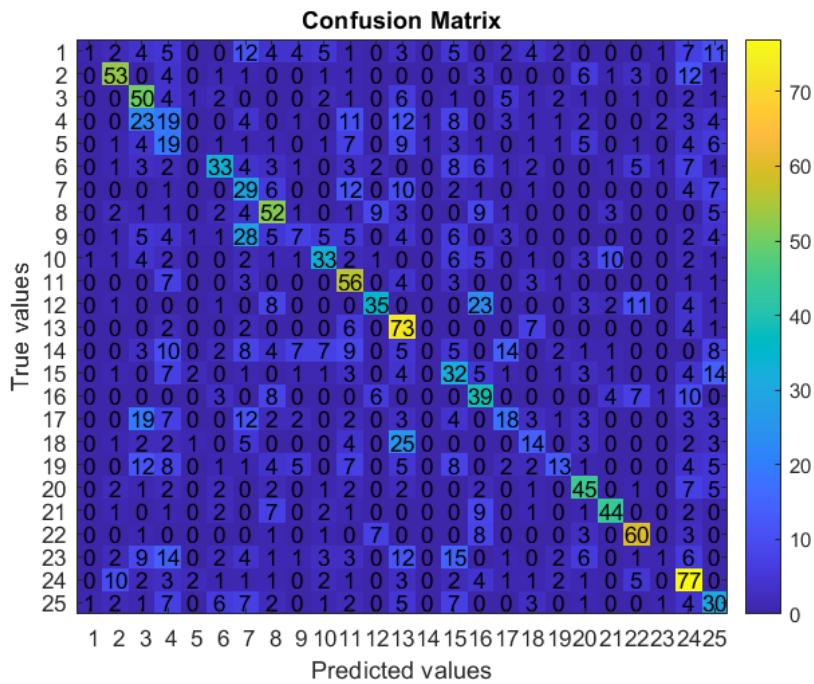


Figure 3E. Confusion Matrix for 36° Camera View Angle, Dataset 3 – Configuration Tag A.

Table 3E. Performance Metrics for 36° Camera View Angle, Dataset 3 – Configuration Tag A.

Class Number (Biometric ID Profile)	Metrics (%)				
	Recall	Precision	Specificity	F1-Score	Accuracy
1	1.37	33.33	99.90	2.63	
2	60.92	65.43	98.58	63.10	
3	62.50	34.72	95.23	44.64	
4	20.00	14.50	94.28	16.81	
5	0.00	0.00	99.65	0.00	
6	39.29	55.00	98.63	45.83	
7	39.73	22.48	94.95	28.71	
8	55.32	46.43	96.94	50.49	
9	8.64	22.58	98.78	12.50	
10	43.42	50.77	98.38	46.81	
11	70.89	40.00	95.74	51.14	
12	39.33	58.33	98.73	46.98	
13	76.84	38.83	94.12	51.59	39.67
14	0.00	0.00	99.90	0.00	
15	39.51	27.83	95.79	32.65	
16	50.00	33.91	96.15	40.41	
17	21.95	34.62	98.27	26.87	
18	22.58	30.43	98.39	25.93	
19	16.67	46.43	99.24	24.53	
20	60.00	51.14	97.82	55.21	
21	61.97	65.67	98.84	63.77	
22	71.43	63.16	98.22	67.04	
23	1.20	14.29	99.70	2.22	
24	64.71	44.25	94.98	52.56	
25	37.50	26.79	95.84	31.25	

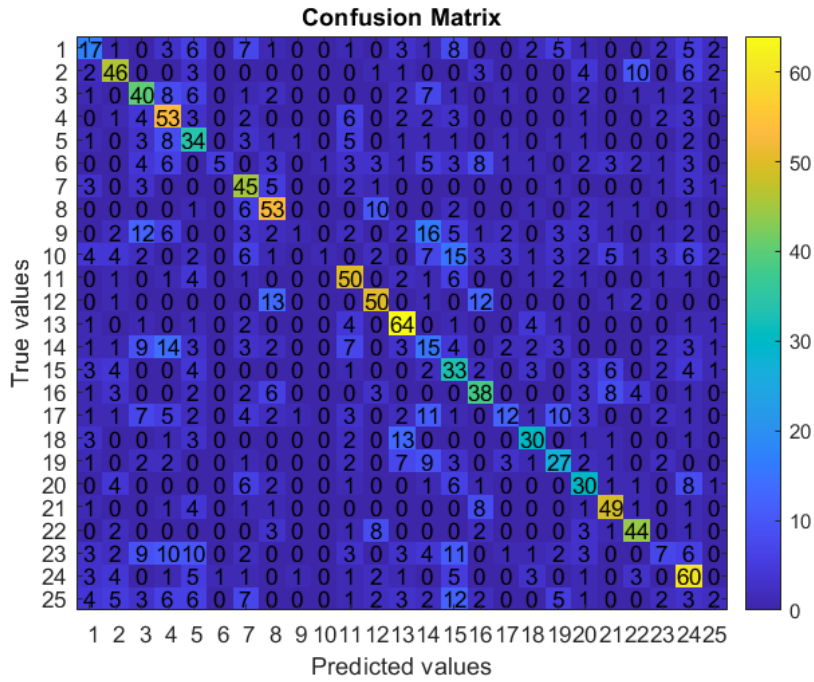


Figure 4E. Confusion Matrix for 54° Camera View Angle, Dataset 3 – Configuration Tag A.

Table 4E. Performance Metrics for 54° Camera View Angle, Dataset 3 – Configuration Tag A.

Class Number (Biometric ID Profile)	Metrics (%)				
	Recall	Precision	Specificity	F1-Score	Accuracy
1	26.15	34.00	98.06	29.57	45.69
2	58.97	56.10	97.86	57.50	
3	52.63	40.40	96.50	45.71	
4	64.63	42.40	95.72	51.21	
5	53.13	34.34	96.18	41.72	
6	9.09	83.33	99.94	16.39	
7	69.23	43.69	96.59	53.57	
8	67.95	54.64	97.39	60.57	
9	1.56	25.00	99.82	2.94	
10	1.37	50.00	99.94	2.67	
11	69.44	52.63	97.34	59.88	
12	62.50	60.98	98.10	61.73	
13	79.01	58.18	97.27	67.02	
14	20.00	17.65	95.86	18.75	
15	48.53	27.50	94.87	35.11	
16	53.52	47.50	97.52	50.33	
17	17.39	46.15	99.17	25.26	
18	54.55	58.82	98.77	56.60	
19	42.86	42.86	97.88	42.86	
20	48.39	42.86	97.65	45.45	
21	72.06	62.82	98.29	67.12	
22	67.69	62.86	98.47	65.19	
23	9.09	24.14	98.70	13.21	
24	65.22	48.39	96.17	55.56	
25	3.03	14.29	99.29	5.00	

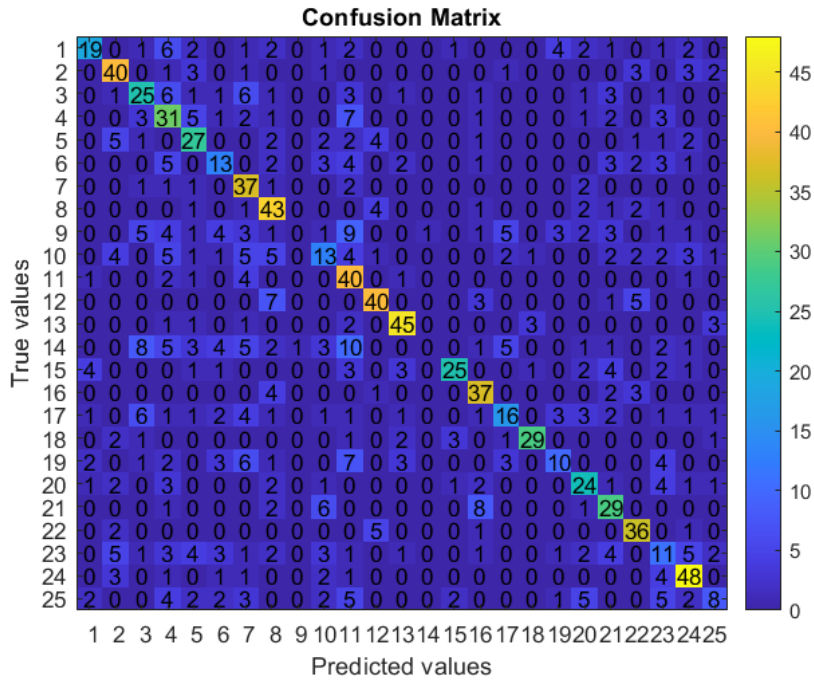


Figure 5E. Confusion Matrix for 72° Camera View Angle, Dataset 3 – Configuration Tag A.

Table 5E. Performance Metrics for 72° Camera View Angle, Dataset 3 – Configuration Tag A.

Class Number (Biometric ID Profile)	Metrics (%)				
	Recall	Precision	Specificity	F1-Score	Accuracy
1	42.22	63.33	99.06	50.67	52.99
2	72.73	62.50	97.94	67.23	
3	49.02	47.17	97.60	48.08	
4	54.39	37.80	95.61	44.60	
5	56.25	49.09	97.61	52.43	
6	33.33	36.11	98.05	34.67	
7	82.22	45.68	96.25	58.73	
8	76.79	54.43	96.90	63.70	
9	0.00	0.00	99.91	0.00	
10	25.00	33.33	97.77	28.57	
11	80.00	38.46	94.53	51.95	
12	71.43	72.73	98.71	72.07	
13	80.36	76.27	98.80	78.26	
14	0.00	0.00	99.91	0.00	
15	53.19	78.13	99.40	63.29	
16	78.72	61.67	98.04	69.16	
17	34.04	48.48	98.55	40.00	
18	72.50	85.29	99.58	78.38	
19	23.81	45.45	98.98	31.25	
20	55.81	50.00	97.96	52.75	
21	61.70	49.15	97.44	54.72	
22	80.00	66.67	98.47	72.73	
23	22.00	23.91	97.01	22.92	
24	78.69	65.75	97.84	71.64	
25	18.60	42.11	99.06	25.81	

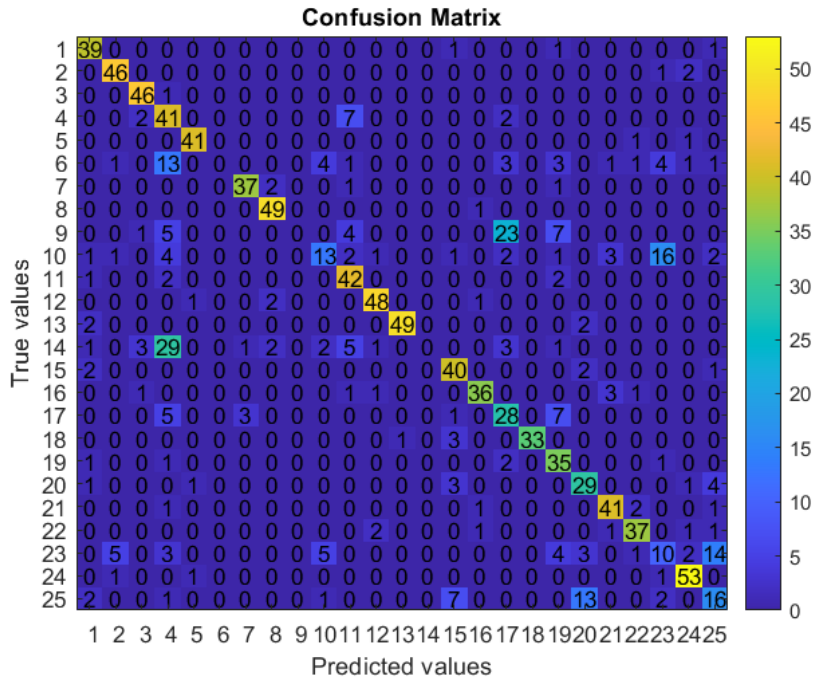


Figure 6E. Confusion Matrix for 90° Camera View Angle, Dataset 3 – Configuration Tag A.

Table 6E. Performance Metrics for 90° Camera View Angle, Dataset 3 – Configuration Tag A.

Class Number (Biometric ID Profile)	Metrics (%)				
	Recall	Precision	Specificity	F1-Score	Accuracy
1	92.86	78.00	98.99	84.78	71.85
2	93.88	85.19	99.26	89.32	
3	97.87	86.79	99.35	92.00	
4	78.85	38.68	93.95	51.90	
5	95.35	93.18	99.72	94.25	
6	0.00	0.00	100.00	0.00	
7	90.24	90.24	99.63	90.24	
8	98.00	89.09	99.44	93.33	
9	0.00	0.00	100.00	0.00	
10	27.66	52.00	98.89	36.11	
11	89.36	66.67	98.05	76.36	
12	92.31	90.57	99.53	91.43	
13	92.45	98.00	99.91	95.15	
14	0.00	0.00	100.00	0.00	
15	88.89	71.43	98.52	79.21	
16	83.72	90.00	99.63	86.75	
17	63.64	44.44	96.77	52.34	
18	89.19	100.00	100.00	94.29	
19	87.50	56.45	97.51	68.63	
20	74.36	59.18	98.16	65.91	
21	89.13	83.67	99.26	86.32	
22	86.05	86.05	99.45	86.05	
23	21.28	28.57	97.68	24.39	
24	94.64	86.89	99.25	90.60	
25	38.10	39.02	97.69	38.55	

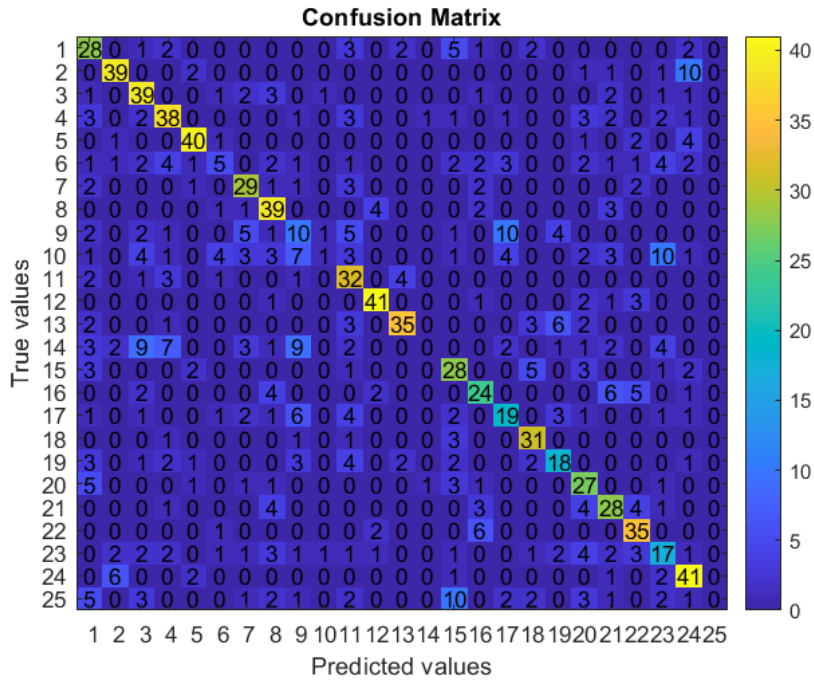


Figure 7E. Confusion Matrix for 108° Camera View Angle, Dataset 3 – Configuration Tag A.

Table 7E. Performance Metrics for 108° Camera View Angle, Dataset 3 – Configuration Tag A.

Class Number (Biometric ID Profile)	Metrics (%)				
	Recall	Precision	Specificity	F1-Score	Accuracy
1	60.87	45.16	96.89	51.85	56.59
2	72.22	76.47	98.89	74.29	
3	75.00	56.52	97.24	64.46	
4	65.52	60.32	97.69	62.81	
5	81.63	80.00	99.08	80.81	
6	14.29	31.25	99.00	19.61	
7	70.73	60.42	98.27	65.17	
8	78.00	59.09	97.52	67.24	
9	23.81	23.81	97.08	23.81	
10	2.08	25.00	99.72	3.85	
11	72.73	47.06	96.71	57.14	
12	83.67	82.00	99.17	82.83	
13	67.31	81.40	99.26	73.68	
14	0.00	0.00	99.82	0.00	
15	62.22	46.67	97.07	53.33	
16	54.55	55.81	98.26	55.17	
17	44.19	46.34	97.99	45.24	
18	83.78	67.39	98.64	74.70	
19	46.15	52.94	98.54	49.32	
20	65.85	48.21	97.36	55.67	
21	62.22	52.83	97.71	57.14	
22	79.55	63.64	98.17	70.71	
23	36.96	36.17	97.25	36.56	
24	77.36	59.42	97.42	67.21	
25	0.00	0.00	100.00	0.00	

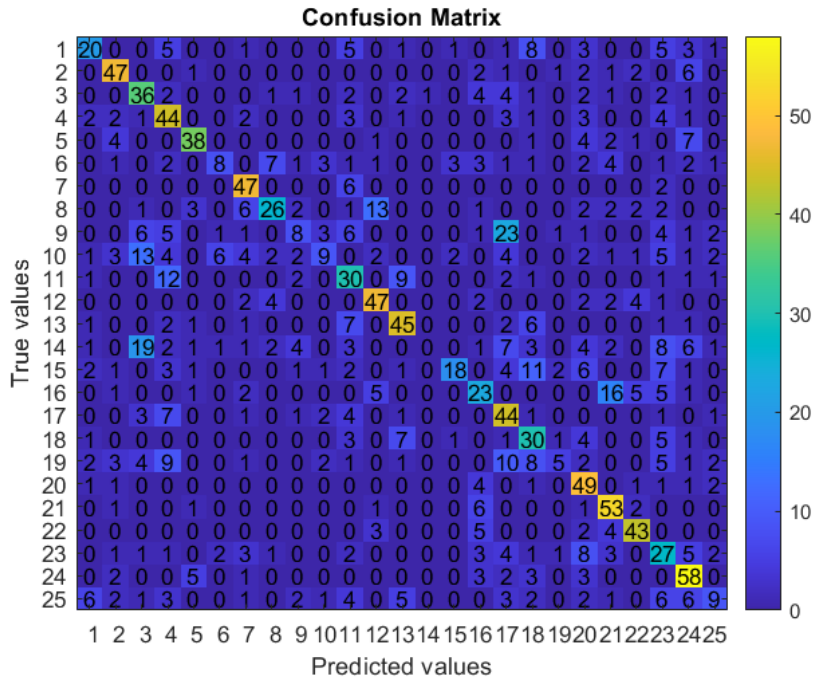


Figure 8E. Confusion Matrix for 126° Camera View Angle, Dataset 3 – Configuration Tag A.

Table 8E. Performance Metrics for 126° Camera View Angle, Dataset 3 – Configuration Tag A.

Class Number (Biometric ID Profile)	Metrics (%)				
	Recall	Precision	Specificity	F1-Score	Accuracy
1	37.04	52.63	98.77	43.48	50.30
2	74.60	68.12	98.49	71.21	
3	60.00	42.35	96.64	49.66	
4	65.67	43.56	96.07	52.38	
5	65.52	73.08	99.04	69.09	
6	19.05	44.44	99.32	26.67	
7	85.45	63.51	98.16	72.87	
8	42.62	60.47	98.83	50.00	
9	12.70	33.33	98.90	18.39	
10	14.06	42.86	99.18	21.18	
11	50.00	37.50	96.57	42.86	
12	73.44	64.38	98.21	68.61	
13	67.16	61.64	98.07	64.29	
14	0.00	0.00	99.93	0.00	
15	29.51	72.00	99.52	41.86	
16	38.98	39.66	97.60	39.32	
17	66.67	37.93	95.04	48.35	
18	55.56	37.97	96.66	45.11	
19	8.93	45.45	99.59	14.93	
20	80.33	47.12	96.23	59.39	
21	81.54	57.61	97.32	67.52	
22	75.44	70.49	98.77	72.88	
23	41.54	29.03	95.46	34.18	
24	75.32	55.77	96.81	64.09	
25	16.67	37.50	98.98	23.08	

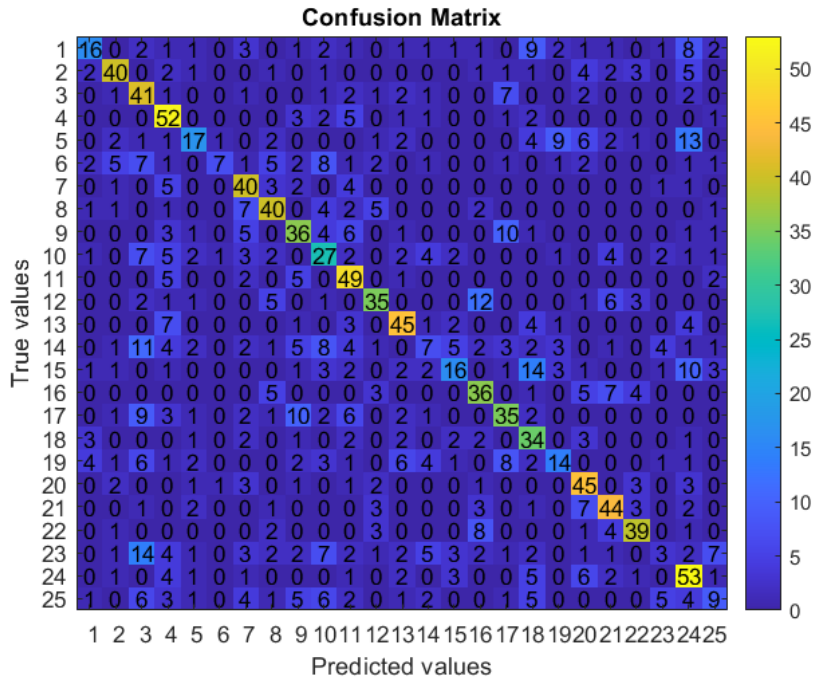


Figure 9E. Confusion Matrix for 144° Camera View Angle, Dataset 3 – Configuration Tag A.

Table 9E. Performance Metrics for 144° Camera View Angle, Dataset 3 – Configuration Tag A.

Class Number (Biometric ID Profile)	Metrics (%)				
	Recall	Precision	Specificity	F1-Score	Accuracy
1	29.09	51.61	99.02	37.21	49.27
2	62.50	67.80	98.75	65.04	
3	66.13	38.32	95.66	48.52	
4	76.47	49.52	96.50	60.12	
5	27.42	48.57	98.82	35.05	
6	14.58	70.00	99.80	24.14	
7	70.18	50.63	97.44	58.82	
8	62.50	56.34	97.96	59.26	
9	52.17	46.75	97.29	49.32	
10	40.30	34.18	96.57	36.99	
11	76.56	51.04	96.91	61.25	
12	52.24	61.40	98.55	56.45	
13	66.18	62.50	98.22	64.29	
14	10.29	23.33	98.48	14.29	
15	25.81	45.71	98.75	32.99	
16	59.02	51.43	97.77	54.96	
17	46.67	50.72	97.75	48.61	
18	64.15	38.20	96.41	47.89	
19	24.56	41.18	98.69	30.77	
20	71.43	52.94	97.37	60.81	
21	65.67	59.46	98.02	62.41	
22	66.10	68.42	98.82	67.24	
23	4.55	16.67	99.01	7.14	
24	65.43	46.49	95.94	54.36	
25	16.07	30.00	98.62	20.93	

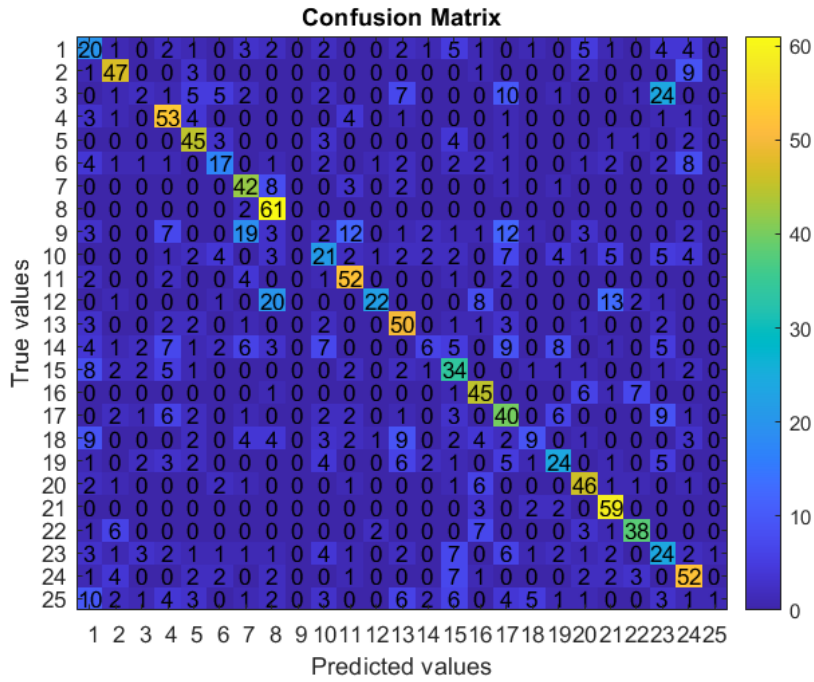


Figure 10E. Confusion Matrix for 162° Camera View Angle, Dataset 3 – Configuration Tag A.

Table 10E. Performance Metrics for 162° Camera View Angle, Dataset 3 – Configuration Tag A.

Class Number (Biometric ID Profile)	Metrics (%)				
	Recall	Precision	Specificity	F1-Score	Accuracy
1	36.36	26.67	96.39	30.77	51.33
2	74.60	66.20	98.42	70.15	
3	3.28	14.29	99.21	5.33	
4	76.81	55.21	97.15	64.24	
5	75.00	59.21	97.96	66.18	
6	35.42	45.95	98.69	40.00	
7	73.68	48.28	97.04	58.33	
8	96.83	54.95	96.70	70.11	
9	0.00	0.00	100.00	0.00	
10	31.82	36.21	97.55	33.87	
11	81.25	63.41	98.02	71.23	
12	32.35	81.48	99.67	46.32	
13	73.53	53.76	97.15	62.11	
14	8.96	37.50	99.34	14.46	
15	53.97	40.96	96.77	46.58	
16	73.77	56.25	97.69	63.83	
17	52.63	38.46	95.74	44.44	
18	16.36	42.86	99.21	23.68	
19	42.11	48.00	98.29	44.86	
20	73.02	62.16	98.15	67.15	
21	89.39	65.56	97.95	75.64	
22	65.52	71.70	99.01	68.47	
23	36.36	27.91	95.90	31.58	
24	65.82	56.52	97.33	60.82	
25	1.79	50.00	99.93	3.45	

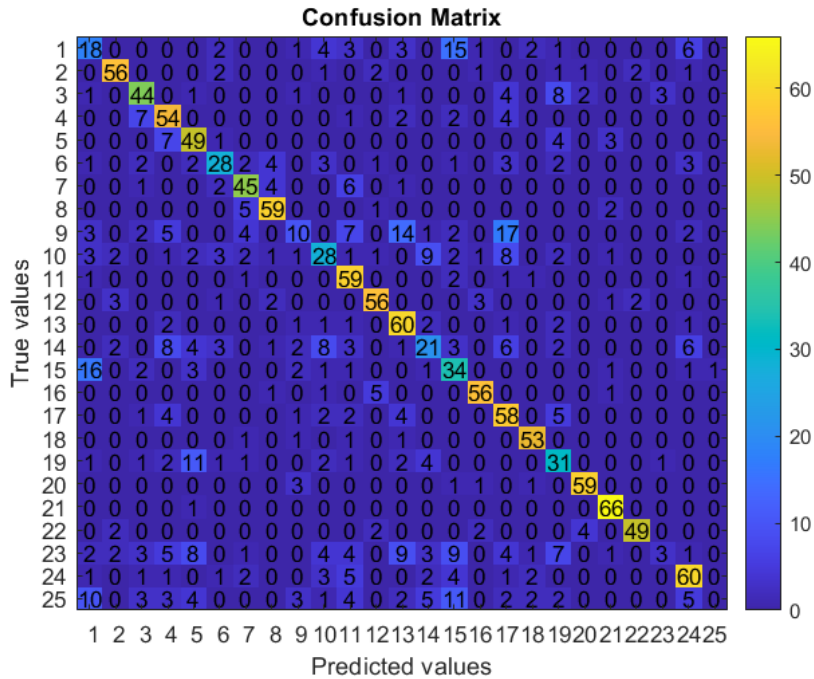


Figure 11D. Confusion Matrix for 180° Camera View Angle, Dataset 3 – Configuration Tag A.

Table 11D. Performance Metrics for 180° Camera View Angle, Dataset 3 – Configuration Tag A.

Class Number (Biometric ID Profile)	Metrics (%)				
	Recall	Precision	Specificity	F1-Score	Accuracy
1	32.14	31.58	97.52	31.86	64.90
2	83.58	83.58	99.29	83.58	
3	67.69	65.67	98.53	66.67	
4	77.14	58.70	97.56	66.67	
5	76.56	57.65	97.70	65.77	
6	53.85	63.64	98.98	58.33	
7	76.27	70.31	98.79	73.17	
8	88.06	81.94	99.17	84.89	
9	14.93	38.46	98.97	21.51	
10	41.18	47.46	98.01	44.09	
11	89.39	59.60	97.44	71.52	
12	82.35	82.35	99.23	82.35	
13	84.51	60.00	97.43	70.18	
14	30.00	43.75	98.27	35.59	
15	53.97	39.53	96.68	45.64	
16	87.50	86.15	99.42	86.82	
17	75.32	53.21	96.71	62.37	
18	92.98	85.48	99.43	89.08	
19	53.45	46.27	97.71	49.60	
20	90.77	89.39	99.55	90.08	
21	98.51	86.84	99.36	92.31	
22	83.05	92.45	99.74	87.50	
23	4.48	42.86	99.74	8.11	
24	72.29	68.97	98.25	70.59	
25	0.00	0.00	99.94	0.00	

Appendix F

Experimental Setup 6 – Confusion Matrices & Metrics Tables

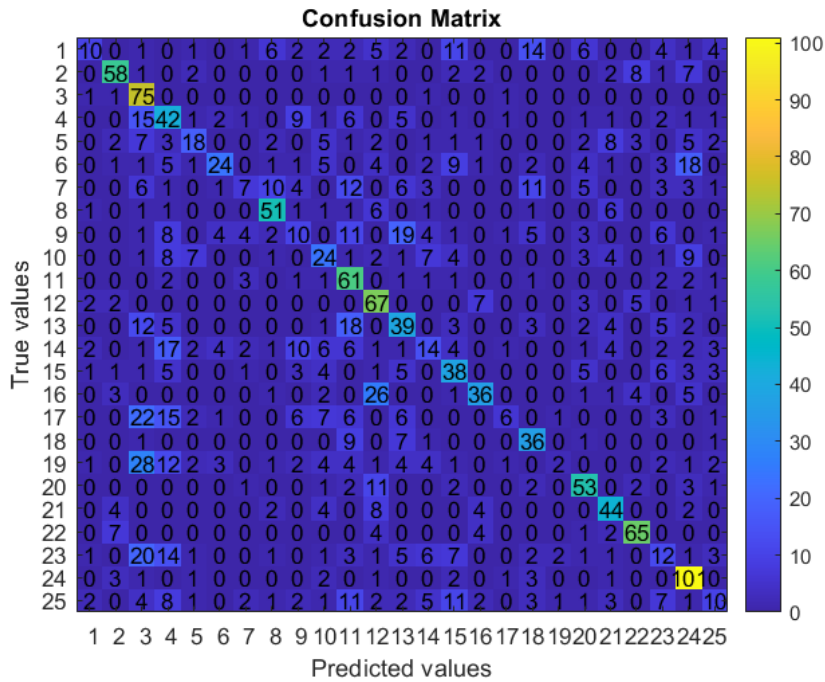


Figure 1F. Confusion Matrix for 0° Camera View Angle, Dataset 3 – Configuration Tag B.

Table 1F. Performance Metrics for 0° Camera View Angle, Dataset 3 – Configuration Tag B.

Class Number (Biometric ID Profile)	Metrics (%)				
	Recall	Precision	Specificity	F1-Score	Accuracy
1	13.89	47.62	99.42	21.51	45.51
2	67.44	70.73	98.74	69.05	
3	94.94	37.69	93.49	53.96	
4	46.67	28.77	94.51	35.59	
5	28.57	46.15	98.91	35.29	
6	28.92	61.54	99.21	39.34	
7	9.59	31.82	99.22	14.74	
8	71.83	63.75	98.48	67.55	
9	12.50	19.61	97.85	15.27	
10	32.88	32.88	97.44	32.88	
11	79.22	39.35	95.07	52.59	
12	76.14	46.85	95.99	58.01	
13	41.49	37.86	96.61	39.59	
14	16.67	28.00	98.11	20.90	
15	49.35	38.38	96.80	43.18	
16	45.00	63.16	98.90	52.55	
17	7.89	50.00	99.69	13.64	
18	64.29	43.37	97.56	51.80	
19	2.67	33.33	99.79	4.94	
20	67.95	56.99	97.90	61.99	
21	64.71	53.66	98.02	58.67	
22	78.31	74.71	98.84	76.47	
23	14.63	20.34	97.53	17.02	
24	87.07	60.12	96.41	71.13	
25	12.50	28.57	98.69	17.39	

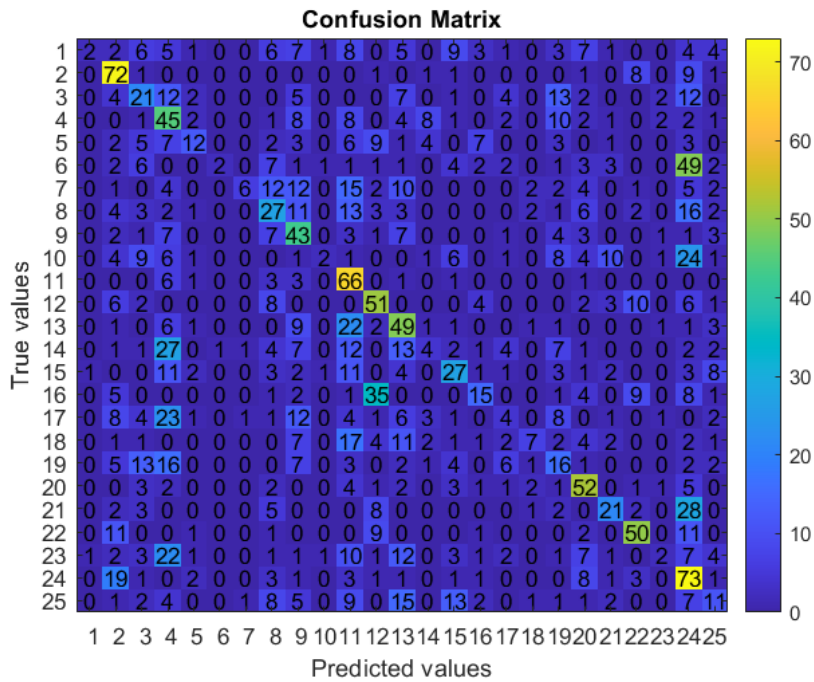


Figure 2F. Confusion Matrix for 18° Camera View Angle, Dataset 3 – Configuration Tag B.

Table 2F. Performance Metrics for 18° Camera View Angle, Dataset 3 – Configuration Tag B.

Class Number (Biometric ID Profile)	Metrics (%)				
	Recall	Precision	Specificity	F1-Score	Accuracy
1	2.67	50.00	99.90	5.06	
2	75.79	46.45	95.90	57.60	
3	24.71	24.42	96.81	24.56	
4	45.92	21.95	92.09	29.70	
5	18.46	42.86	99.22	25.81	
6	2.27	66.67	99.95	4.40	
7	7.69	66.67	99.85	13.79	
8	28.13	26.47	96.29	27.27	
9	51.19	29.25	94.89	37.23	
10	2.50	33.33	99.80	4.65	
11	80.49	30.41	92.59	44.15	
12	54.84	39.23	96.10	45.74	
13	49.49	31.82	94.80	38.74	32.08
14	4.44	16.00	98.97	6.96	
15	33.33	34.18	97.45	33.75	
16	18.29	37.50	98.77	24.59	
17	4.94	12.90	98.68	7.14	
18	10.77	41.18	99.51	17.07	
19	20.25	18.18	96.47	19.16	
20	64.20	44.83	96.86	52.79	
21	29.17	42.86	98.63	34.71	
22	58.14	58.14	98.23	58.14	
23	2.41	18.18	99.56	4.26	
24	61.34	26.07	89.66	36.59	
25	13.25	21.15	97.99	16.30	

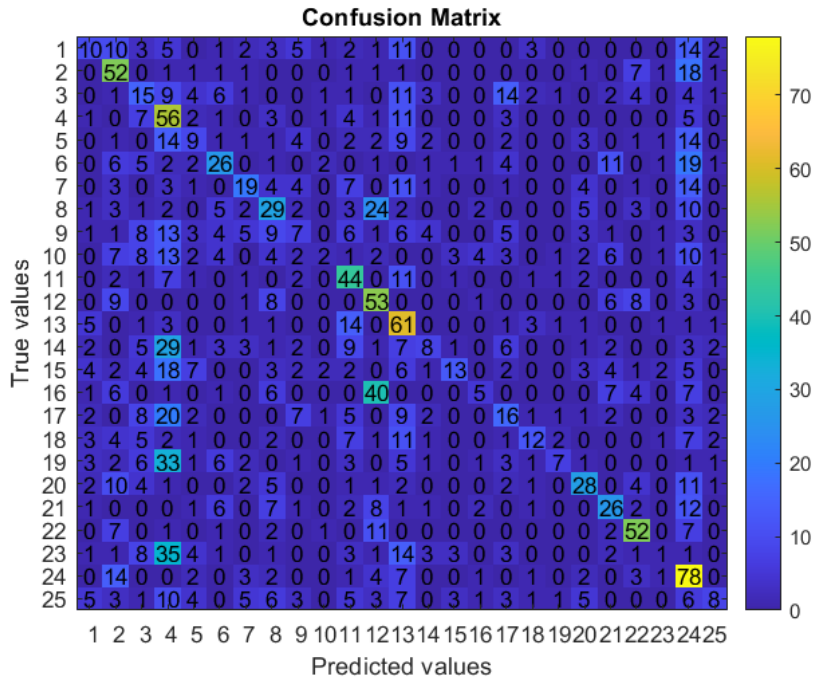


Figure 3F. Confusion Matrix for 36° Camera View Angle, Dataset 3 – Configuration Tag B.

Table 3F. Performance Metrics for 36° Camera View Angle, Dataset 3 – Configuration Tag B.

Class Number (Biometric ID Profile)	Metrics (%)				
	Recall	Precision	Specificity	F1-Score	Accuracy
1	13.70	23.81	98.38	17.39	31.04
2	59.77	36.11	95.32	45.02	
3	18.75	16.67	96.20	17.65	
4	58.95	20.14	88.66	30.03	
5	13.43	18.75	98.04	15.65	
6	30.95	38.81	97.92	34.44	
7	26.03	38.78	98.48	31.15	
8	30.85	29.59	96.48	30.21	
9	8.64	16.67	98.22	11.38	
10	2.63	18.18	99.54	4.60	
11	55.70	35.77	96.00	43.56	
12	59.55	33.97	94.75	43.27	
13	64.21	30.05	92.74	40.94	
14	9.30	28.57	98.98	14.04	
15	16.05	52.00	99.39	24.53	
16	6.41	27.78	99.34	10.42	
17	19.51	23.19	97.31	21.19	
18	19.35	44.44	99.25	26.97	
19	8.97	46.67	99.59	15.05	
20	37.33	45.16	98.28	40.88	
21	36.62	36.62	97.73	36.62	
22	61.90	57.14	98.02	59.43	
23	1.20	9.09	99.49	2.13	
24	65.55	30.00	90.58	41.16	
25	10.00	33.33	99.19	15.38	

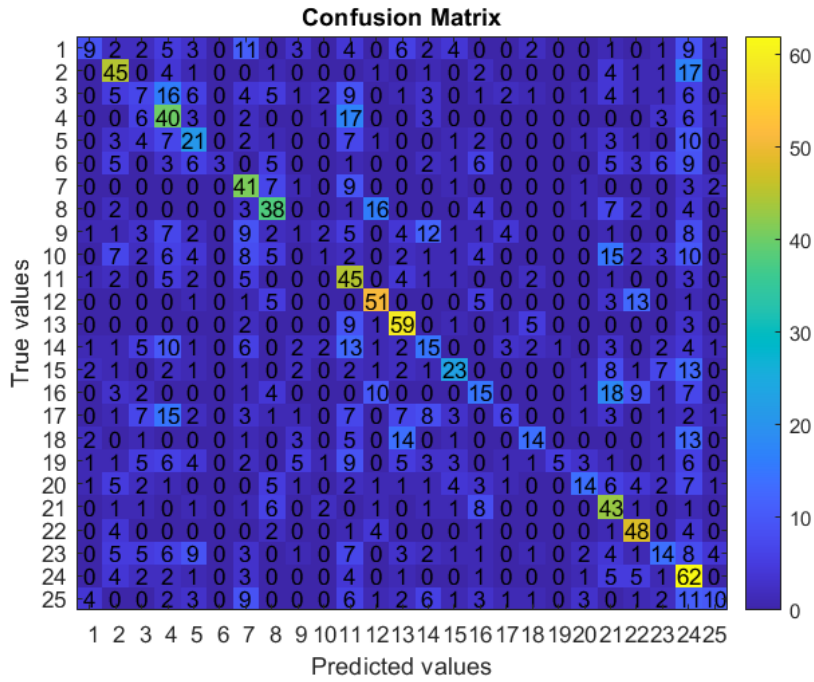


Figure 4F. Confusion Matrix for 54° Camera View Angle, Dataset 3 – Configuration Tag B.

Table 4F. Performance Metrics for 54° Camera View Angle, Dataset 3 – Configuration Tag B.

Class Number (Biometric ID Profile)	Metrics (%)				
	Recall	Precision	Specificity	F1-Score	Accuracy
1	13.85	40.91	99.23	20.69	35.71
2	57.69	45.92	96.86	51.14	
3	9.21	12.96	97.22	10.77	
4	48.78	29.20	94.23	36.53	
5	32.81	29.58	97.06	31.11	
6	5.45	100.00	100.00	10.34	
7	63.08	34.75	95.47	44.81	
8	48.72	43.68	97.09	46.06	
9	1.56	4.76	98.82	2.35	
10	1.37	9.09	99.41	2.38	
11	62.50	27.27	92.91	37.97	
12	63.75	57.30	97.74	60.36	
13	72.84	52.21	96.79	60.82	
14	20.00	24.19	97.22	21.90	
15	33.82	47.92	98.53	39.66	
16	21.13	26.32	97.52	23.44	
17	8.70	31.58	99.23	13.64	
18	25.45	48.28	99.12	33.33	
19	7.94	83.33	99.94	14.49	
20	22.58	46.67	99.06	30.43	
21	63.24	31.62	94.52	42.16	
22	73.85	51.61	97.35	60.76	
23	18.18	29.79	98.04	22.58	
24	67.39	27.31	90.13	38.87	
25	15.15	47.62	99.35	22.99	

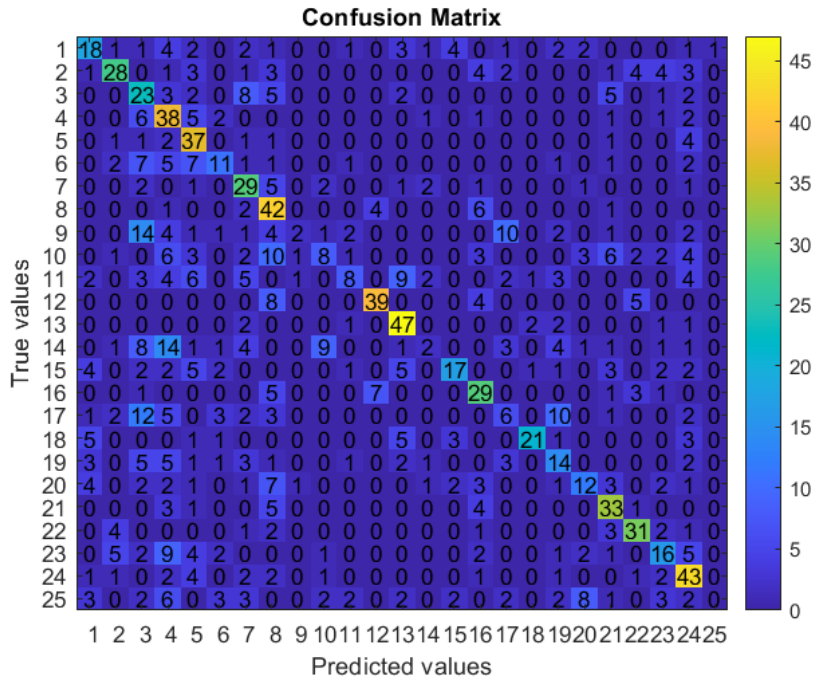


Figure 5F. Confusion Matrix for 72° Camera View Angle, Dataset 3 – Configuration Tag B.

Table 5F. Performance Metrics for 72° Camera View Angle, Dataset 3 – Configuration Tag B.

Class Number (Biometric ID Profile)	Metrics (%)				
	Recall	Precision	Specificity	F1-Score	Accuracy
1	40.00	42.86	97.96	41.38	45.45
2	50.91	60.87	98.45	55.45	
3	45.10	25.27	94.18	32.39	
4	66.67	32.76	93.29	43.93	
5	77.08	43.53	95.90	55.64	
6	28.21	40.74	98.64	33.33	
7	64.44	41.43	96.51	50.43	
8	75.00	40.00	94.58	52.17	
9	4.44	40.00	99.74	8.00	
10	15.38	33.33	98.63	21.05	
11	16.00	44.44	99.14	23.53	
12	69.64	78.00	99.05	73.58	
13	83.93	61.04	97.42	70.68	
14	3.85	20.00	99.31	6.45	
15	36.17	60.71	99.06	45.33	
16	61.70	49.15	97.44	54.72	
17	12.77	20.69	98.04	15.79	
18	52.50	84.00	99.66	64.62	
19	33.33	31.11	97.37	32.18	
20	27.91	41.38	98.55	33.33	
21	70.21	51.56	97.35	59.46	
22	68.89	65.96	98.64	67.39	
23	32.00	42.11	98.12	36.36	
24	70.49	48.86	96.11	57.72	
25	0.00	0.00	99.91	0.00	

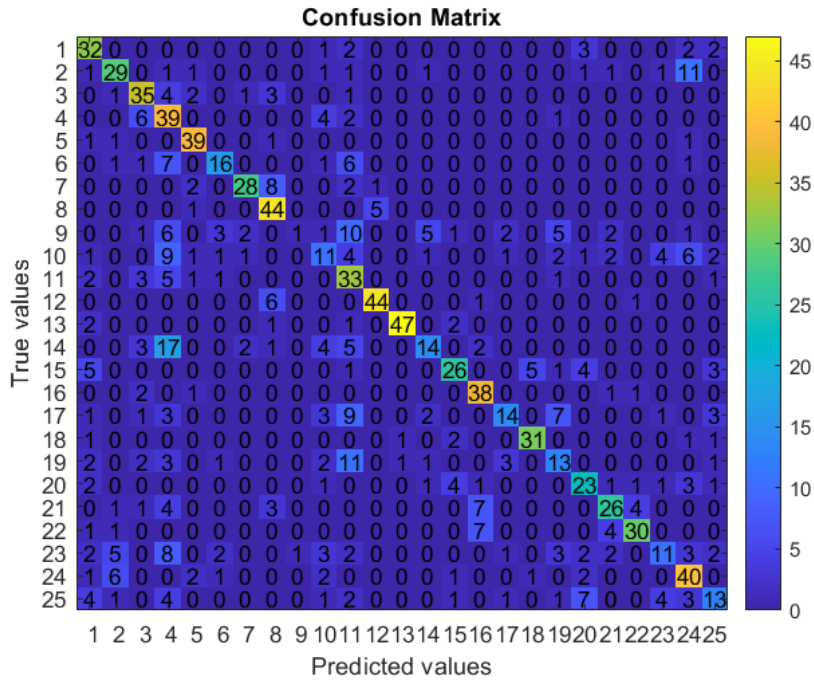


Figure 6F. Confusion Matrix for 90° Camera View Angle, Dataset 3 – Configuration Tag B.

Table 6F. Performance Metrics for 90° Camera View Angle, Dataset 3 – Configuration Tag B.

Class Number (Biometric ID Profile)	Metrics (%)				
	Recall	Precision	Specificity	F1-Score	Accuracy
1	76.19	55.17	97.60	64.00	60.12
2	59.18	63.04	98.42	61.05	
3	74.47	63.64	98.15	68.63	
4	75.00	35.45	93.39	48.15	
5	90.70	78.00	98.98	83.87	
6	48.48	64.00	99.18	55.17	
7	68.29	82.35	99.45	74.67	
8	88.00	65.67	97.86	75.21	
9	2.50	50.00	99.91	4.76	
10	23.40	31.43	97.78	26.83	
11	70.21	35.87	94.53	47.48	
12	84.62	88.00	99.44	86.27	
13	88.68	95.92	99.81	92.16	
14	29.17	56.00	98.98	38.36	
15	57.78	70.27	98.98	63.41	
16	88.37	67.86	98.34	76.77	
17	31.82	63.64	99.26	42.42	
18	83.78	83.78	99.45	83.78	
19	32.50	38.24	98.07	35.14	
20	58.97	53.49	98.16	56.10	
21	56.52	66.67	98.80	61.18	
22	69.77	81.08	99.35	75.00	
23	23.40	50.00	98.98	31.88	
24	71.43	55.56	97.01	62.50	
25	30.95	44.83	98.52	36.62	

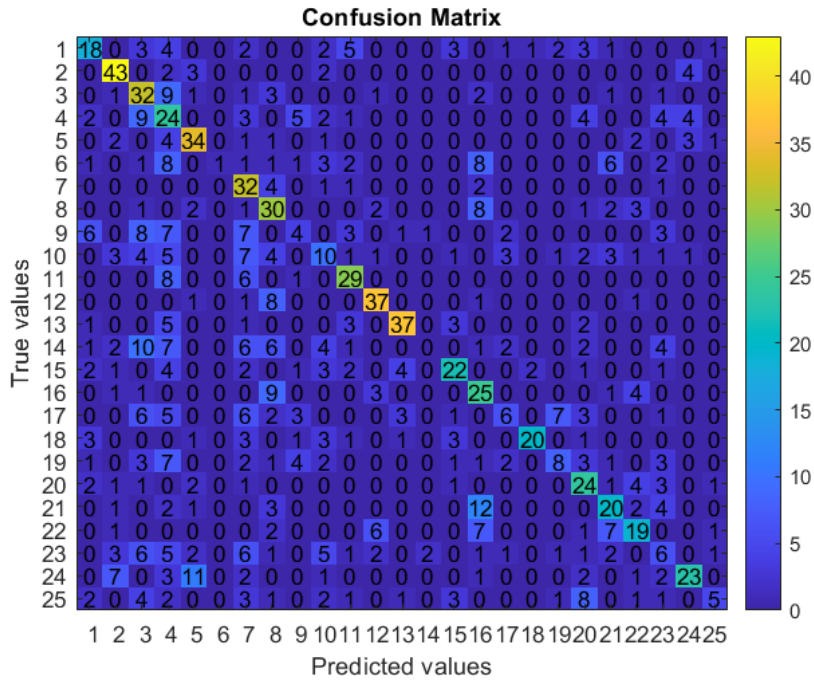


Figure 7F. Confusion Matrix for 108° Camera View Angle, Dataset 3 – Configuration Tag B.

Table 7F. Performance Metrics for 108° Camera View Angle, Dataset 3 – Configuration Tag B.

Class Number (Biometric ID Profile)	Metrics (%)				
	Recall	Precision	Specificity	F1-Score	Accuracy
1	39.13	46.15	98.08	42.35	44.73
2	79.63	65.15	97.88	71.67	
3	61.54	35.96	94.75	45.39	
4	41.38	21.62	91.94	28.40	
5	69.39	58.62	97.80	63.55	
6	2.86	100.00	100.00	5.56	
7	78.05	34.04	94.35	47.41	
8	60.00	39.47	95.77	47.62	
9	9.52	20.00	98.54	12.90	
10	20.83	24.39	97.16	22.47	
11	65.91	56.86	97.99	61.05	
12	75.51	71.15	98.62	73.27	
13	71.15	78.72	99.08	74.75	
14	0.00	0.00	99.73	0.00	
15	48.89	57.89	98.54	53.01	
16	56.82	36.23	95.98	44.25	
17	13.95	35.29	99.00	20.00	
18	54.05	86.96	99.73	66.67	
19	20.51	40.00	98.91	27.12	
20	58.54	41.38	96.90	48.48	
21	44.44	44.44	97.71	44.44	
22	43.18	50.00	98.26	46.34	
23	13.04	16.22	97.16	14.46	
24	43.40	65.71	98.89	52.27	
25	14.29	50.00	99.55	22.22	

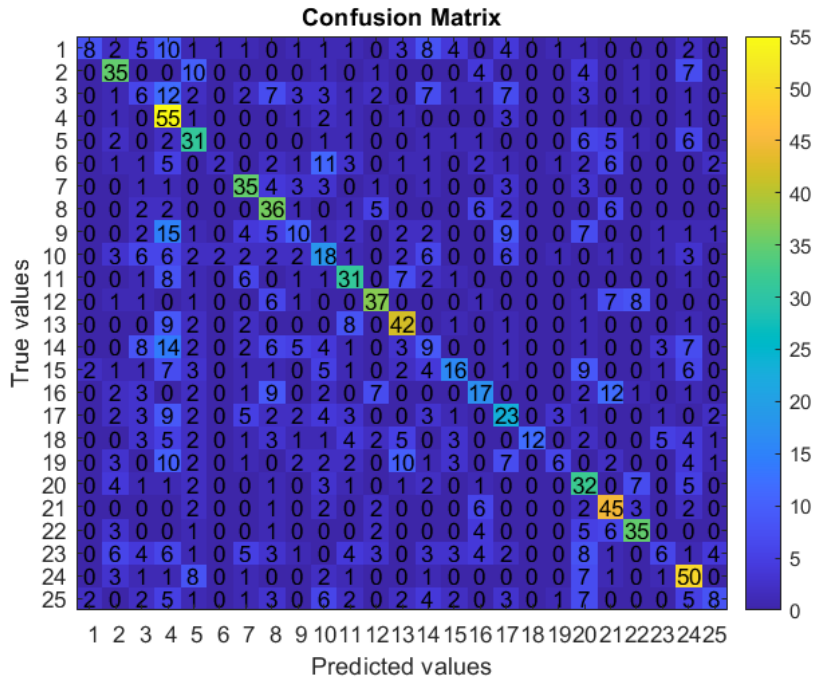


Figure 8F. Confusion Matrix for 126° Camera View Angle, Dataset 3 – Configuration Tag B.

Table 8F. Performance Metrics for 126° Camera View Angle, Dataset 3 – Configuration Tag B.

Class Number (Biometric ID Profile)	Metrics (%)				
	Recall	Precision	Specificity	F1-Score	Accuracy
1	14.81	66.67	99.73	24.24	39.83
2	55.56	50.00	97.60	52.63	
3	10.00	11.76	96.92	10.81	
4	82.09	30.05	91.18	44.00	
5	53.45	38.75	96.65	44.93	
6	4.76	40.00	99.80	8.51	
7	63.64	50.00	97.61	56.00	
8	59.02	39.13	96.16	47.06	
9	15.87	28.57	98.28	20.41	
10	28.13	24.66	96.22	26.28	
11	51.67	44.93	97.40	48.06	
12	57.81	59.68	98.28	58.73	
13	62.69	51.85	97.31	56.76	
14	13.64	16.36	96.83	14.88	
15	26.23	44.44	98.63	32.99	
16	28.81	36.17	97.95	32.08	
17	34.85	31.51	96.56	33.09	
18	22.22	100.00	100.00	36.36	
19	10.71	46.15	99.52	17.39	
20	52.46	30.48	94.99	38.55	
21	69.23	48.91	96.77	57.32	
22	61.40	61.40	98.50	61.40	
23	9.23	31.58	99.11	14.29	
24	64.94	46.30	95.98	54.05	
25	14.81	42.11	99.25	21.92	

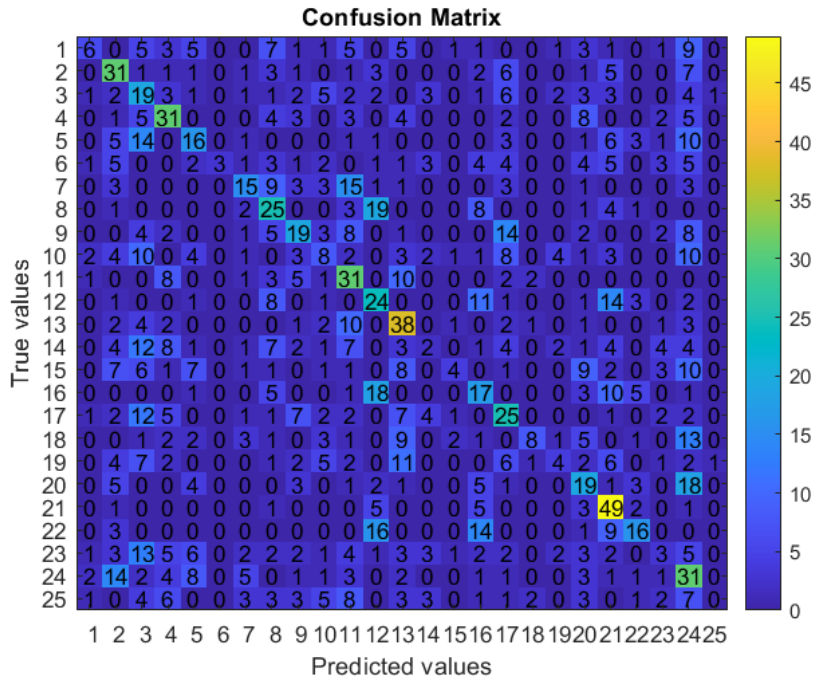


Figure 9F. Confusion Matrix for 144° Camera View Angle, Dataset 3 – Configuration Tag B.

Table 9F. Performance Metrics for 144° Camera View Angle, Dataset 3 – Configuration Tag B.

Class Number (Biometric ID Profile)	Metrics (%)				
	Recall	Precision	Specificity	F1-Score	Accuracy
1	10.91	37.50	99.35	16.90	28.05
2	48.44	31.63	95.59	38.27	
3	30.65	15.97	93.43	20.99	
4	45.59	37.35	96.57	41.06	
5	25.81	27.12	97.17	26.45	
6	6.25	100.00	100.00	11.76	
7	26.32	37.50	98.36	30.93	
8	39.06	27.78	95.72	32.47	
9	27.54	32.20	97.36	29.69	
10	11.94	17.78	97.56	14.29	
11	48.44	27.93	94.73	35.43	
12	35.82	25.81	95.45	30.00	
13	55.88	34.55	95.25	42.70	
14	2.94	10.00	98.81	4.55	
15	6.45	36.36	99.54	10.96	
16	27.87	22.67	96.19	25.00	
17	33.33	27.17	95.56	29.94	
18	15.09	57.14	99.61	23.88	
19	7.02	25.00	99.21	10.96	
20	30.16	24.05	96.05	26.76	
21	73.13	38.89	94.92	50.78	
22	27.12	44.44	98.69	33.68	
23	4.55	11.54	98.48	6.52	
24	38.27	19.38	91.41	25.73	
25	0.00	0.00	99.87	0.00	

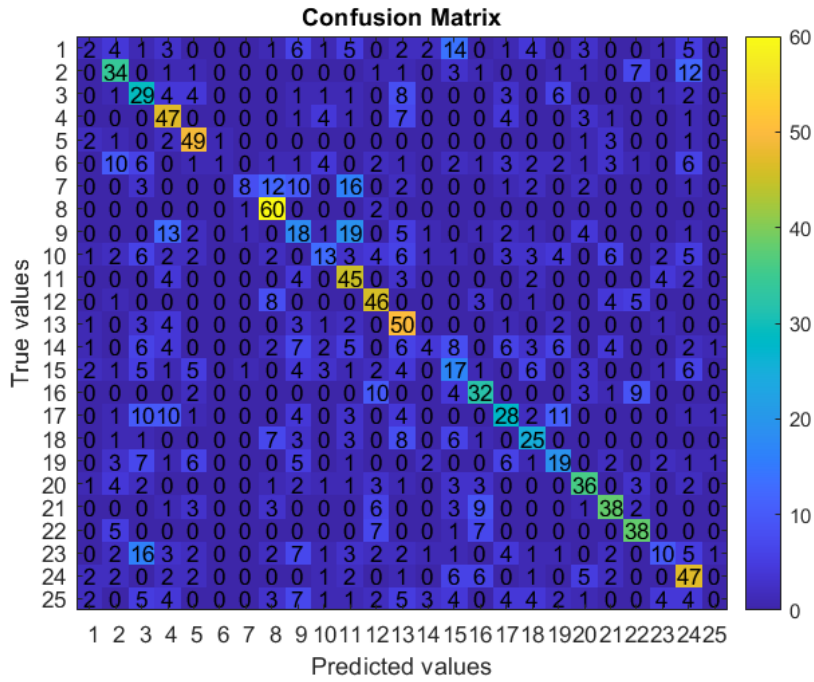


Figure 10F. Confusion Matrix for 162° Camera View Angle, Dataset 3 – Configuration Tag B.

Table 10F. Performance Metrics for 162° Camera View Angle, Dataset 3 – Configuration Tag B.

Class Number (Biometric ID Profile)	Metrics (%)				
	Recall	Precision	Specificity	F1-Score	Accuracy
1	3.64	14.29	99.21	5.80	44.11
2	53.97	47.22	97.49	50.37	
3	47.54	29.00	95.32	36.02	
4	68.12	44.34	96.09	53.71	
5	81.67	61.25	97.96	70.00	
6	2.08	50.00	99.93	4.00	
7	14.04	72.73	99.80	23.53	
8	95.24	58.82	97.23	72.73	
9	26.09	21.69	95.69	23.68	
10	19.70	38.24	98.61	26.00	
11	70.31	40.18	95.57	51.14	
12	67.65	52.87	97.28	59.35	
13	73.53	43.10	95.63	54.35	
14	5.97	28.57	99.34	9.88	
15	26.98	23.29	96.30	25.00	
16	52.46	49.23	97.82	50.79	
17	36.84	42.42	97.47	39.44	
18	45.45	43.10	97.83	44.25	
19	33.33	35.19	97.70	34.23	
20	57.14	56.25	98.15	56.69	
21	57.58	57.58	98.15	57.58	
22	65.52	58.46	98.22	61.79	
23	15.15	38.46	98.94	21.74	
24	59.49	45.19	96.20	51.37	
25	0.00	0.00	99.74	0.00	

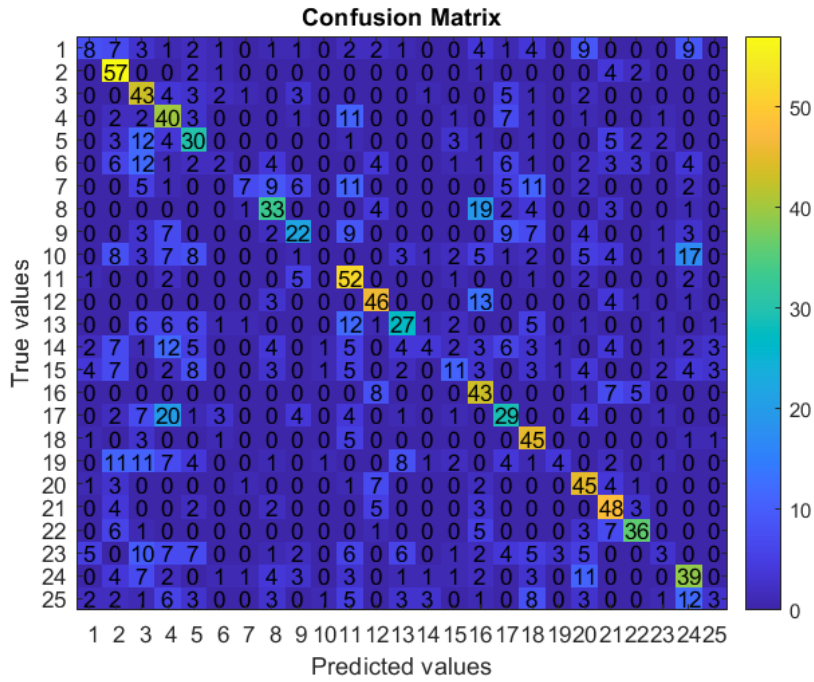


Figure 11F. Confusion Matrix for 180° Camera View Angle, Dataset 3 – Configuration Tag B.

Table 11F. Performance Metrics for 180° Camera View Angle, Dataset 3 – Configuration Tag B.

Class Number (Biometric ID Profile)	Metrics (%)				
	Recall	Precision	Specificity	F1-Score	Accuracy
1	14.29	33.33	98.98	20.00	41.61
2	85.07	44.19	95.38	58.16	
3	66.15	33.08	94.43	44.10	
4	57.14	31.01	94.28	40.20	
5	46.88	34.88	96.42	40.00	
6	3.85	16.67	99.37	6.25	
7	11.86	58.33	99.68	19.72	
8	49.25	47.14	97.63	48.18	
9	32.84	45.83	98.33	38.26	
10	0.00	0.00	99.74	0.00	
11	78.79	39.39	94.88	52.53	
12	67.65	58.97	97.95	63.01	
13	38.03	48.21	98.14	42.52	
14	5.71	33.33	99.49	9.76	
15	17.46	39.29	98.91	24.18	
16	67.19	39.81	95.84	50.00	
17	37.66	36.71	96.77	37.18	
18	78.95	42.45	96.11	55.21	
19	6.90	44.44	99.68	11.94	
20	69.23	43.27	96.22	53.25	
21	71.64	50.53	96.99	59.26	
22	61.02	67.92	98.92	64.29	
23	4.48	20.00	99.23	7.32	
24	46.99	40.21	96.24	43.33	
25	5.26	27.27	99.49	8.82	

